THESE DE DOCTORAT

Présentée par
Rubén PICÓ VILA

Thèse en cotutelle pour obtenir le titre de Docteur de l'Université du Maine (France) et de Doctor de l'Universidad Politécnica de Valencia (Espagne)

VIBROACOUSTIQUE DES CONDUITS CYLINDRIQUES FAIBLEMENT DISTORDUS, ETUDE DE L'INFLUENCE DES VIBRATIONS DE PAROI SUR LES OSCILLATIONS DES INSTRUMENTS DE MUSIQUE A VENT

Soutenance prévue **en septembre 2004**
devant le jury français composé de :

J. LLINARES	Professeur, UPV, Valence (Espagne)	Président
F. GAUTIER	Maitre de Conférence, LAUM, Le Mans	Co-directeur de thèse
J. GILBERT	Chargé de Recherche CNRS (HDR), LAUM, Le Mans	Directeur de thèse
B. LAULAGNET	Maitre de Conférence, LVA, INSA Lyon	Examinateur
J. ALBA	Professeur, EPSG, UPV, Gandia (Espagne)	Examinateur
J. RAMIS	Professeur, EPSG, UPV, Gandia (Espagne)	Examinateur

Sous la direction de François Gautier et Joël Gilbert du Laboratoire d'Acoustique de l'Université du Maine (LAUM)

et le jury espagnol composé de :

J. LLINARES	Professeur, UPV, Valence (Espagne)	Président
R. ARRUDA	Universidade Estadual de Campinas, FEC – DMC, Brésil	Examinateur
B. LAULAGNET	Maitre de Conférence, LVA, INSA Lyon	Examinateur
A. BARJAU	Maitre de conférence, UPC, Barcelone, Espagneº	Examinateur
J. ALBA	Professeur, EPSG, UPV, Gandia (Espagne)	Examinateur

sous la direction de Jaime Ramis Soriano et Javier Redondo Pastor du Departamento de Física Aplicada (DFA) de l'Universidad Politécnica de Valencia (UPV).

Agradecimientos

A mis directores Jaime Ramis y Javier Redondo por su apoyo personal y profesional, además de su paciencia y ayuda.

A mis directores franceses Joel Gilbert y François Gautier por proponerme un trabajo de investigación interesante y por abrirme el camino en el mundo de la acústica musical.

Mis agradecimientos a José Roberto Arruda y Bernard Laulagnet por haber aceptado evaluar mi trabajo como "rapporteurs".

Igualmente, agradezco a Ana Barjau, Jaime Llinares y Jesús Alba por haber aceptado participar en el tribunal de tesis.

A todos mis compañeros de la unidad docente de la Escuela Politécnica Superior de Gandia por haberme apoyado durante estos cuatro años de "convivencia" en la escuela.

A los compañeros del Laboratorio de Acústica de la Université du Maine por haberme acogido durante mis estancias en Francia. En particular, quiero agradecer a Christophe Ayrault su hospitalidad y simpatía.

A mis padres y hermano por saber que siempre puedo contar con ellos.

A toda la gente de Gandia y Oliva que ha estado a mi lado.

Finalmente a Eva, por haberme apoyado, animado y aguantado incondicionalmente desde el primer día hasta el último.

Índice

Capítulo 1

1. Introducción general

El objetivo general de este trabajo, que se presenta para su evaluación como tesis de doctorado, es realizar un estudio del efecto de vibración de las paredes sobre el funcionamiento de los instrumentos de música de viento. Este trabajo se lleva a cabo en el marco de una cotutela dentro del « Programa general del conocimiento » de doctorado en la Universidad Politécnica de Valencia (UPV, Valencia, España) y como tesis doctoral de la Université du Maine (Le Mans, Francia) en la especialidad de acústica. Se trata de una colaboración entre el Laboratoire d'Acoustique de l'Université du Maine (LAUM, UMR CNRS 6613) y el grupo de investigación Dispositivos y Sistemas Acústicos y Ópticos (DISAO) de la UPV.

En la Université du Maine, el trabajo se ha realizado en el marco de las actividades relacionadas con la vibroacústica (grupo "Transfers vibratoires") y con la física de los instrumentos de música de viento (grupo "ondes guidées"). Está dirigido bajo la responsabilidad conjunta de François Gautier (Maitre de conférence), codirector de la tesis y Joël Gilbert (Chargé de Recherche, Habilité à diriger des recherches), director de la tesis.

En la Universidad Politécnica de Valencia este trabajo se sitúa dentro de la línea de investigación "sistemas radiantes", en la cual se realizan actividades relacionadas con el diseño, la caracterización y la optimización de fuentes sonoras que incluyen las fuentes electroacústicas y los instrumentos de viento. Este estudio se ha dirigido bajo la responsabilidad conjunta de Francisco Javier Redondo Pastor (Titular de Escuela Universitaria), como codirector de la tesis y Jaime Ramis Soriano (Catedrático de Escuela Universitaria), como director de la tesis.

1.1. El efecto de vibración de las paredes: estudio bibliográfico

La problemática del efecto de vibración de paredes sobre el funcionamiento de los instrumentos de viento se remonta al siglo XIX. De hecho, Millar en 1909 hace una recopilación de trabajos [Mil09] relacionados con el tema. Los estudios publicados posteriores que abordan el tema están relacionados principalmente con el papel que juega el material que constituye el instrumento y no específicamente con el efecto de

vibración de las paredes. Entre las publicaciones dentro del campo de la acústica musical que tratan el problema, podemos citar por ejemplo:

- Boner y Newman [BN40], Knauss y Yeager [KY41] y Parker [Par47], quienes estudian el efecto del material en diferentes instrumentos de viento. A pesar de que utilizan diferentes técnicas, llegan a la misma conclusión: el efecto de vibración de las paredes debe ser pequeño comparado con el sonido emitido por la columna de aire.
- Backus en [Bac87], fue el primero en medir la contribución del campo acústico emitido por el instrumento relacionado con la radiación de la estructura vibrante. Encontró que el sonido radiado es 48dB más pequeño que el sonido directamente producido por el instrumento.

Coltman [Col71] ha utilizado métodos psicoacústicos para demostrar mediante tests ciegos que varios flautistas no pueden distinguir el material de construcción de instrumentos con la misma geometría. En su trabajo, Coltman concluye que el efecto de la vibración de las paredes no tiene consecuencias perceptibles en el sonido emitido por el instrumento.

Se han publicado también diversos estudios teóricos, de entre los que se destaca el trabajo de Backus y Hundley [BH66] en el que se presenta un modelo local de impedancia de pared que toma en consideración de manera aproximada las vibraciones axisimétricas del tubo. Este modelo predice una pequeña variación de las frecuencias de resonancia debido al fenómeno de vibración de las paredes.

El desarrollo de la acústica de los instrumentos de viento a lo largo de los años 80 y 90 ha posibilitado la mejora de los métodos de medida y la caracterización acústica de estos instrumentos. Como consecuencia de estos progresos, diversos trabajos han abordado la problemática con nuevos métodos:

- Gibiat et al. [GBP97] midieron variaciones en el espectro de un instrumento de viento simplificado de 6dB después de limitar la vibración del tubo.
- Malte Kob [Kob00] realiza experimentos con tubos de órgano barrocos tanto con las paredes amortiguadas como con libres. Los resultados indican que cuando el tubo está emitiendo se excitan varios modos de la estructura y se observan pequeños cambios en el espectro
- Finalmente, Nederveen y Dalmont [ND04] observan un fenómeno espectacular relacionado con el efecto de vibración de las paredes con un tubo de órgano deformado.

El factor común de estos trabajos es que evalúan las consecuencias del efecto de vibración de las paredes en el sonido emitido por el instrumento. El problema propuesto en este trabajo no está relacionado con los efectos, sino con las causas y los fenómenos físicos que engendran el efecto de vibración de las paredes. Estas directrices de trabajo, conducen a la definición de un modelo de instrumento a partir del cual se establecen los mecanismos físicos que permiten describir el fenómeno.

1.2. Enfoque elegido

1.2.1. Un modelo analítico

Para cuantificar o estimar de forma objetiva la importancia de la vibración de las paredes en el sonido producido por el instrumento, optamos por el desarrollo de un modelo analítico de un instrumento con geometría sencilla. Otras orientaciones como las puramente numéricas (utilizando, por ejemplo el método de elementos finitos o elementos de frontera) son también posibles. Sin embargo, en este problema, puesto que el objetivo principal es el análisis de los distintos mecanismos de acoplamiento y la búsqueda de magnitudes pertinentes relacionados con ellos, se ha preferido un método analítico. Este modelo se basa en la resolución exacta de la ecuación de una estructura cilíndrica delgada (teoría de Donnell) acoplada a las ecuaciones que gobiernan las oscilaciones de un fluido interno en el marco de la acústica lineal en un medio homogéneo en reposo (ecuación de Helmholtz). El método de resolución elegido es el método integromodal en régimen forzado en el dominio de frecuencias.

1.2.2. Simulaciones temporales

A partir del modelo físico propuesto se desarrollan simulaciones en el dominio temporal del funcionamiento del instrumento. A partir de ellas se calculan las soluciones auto-oscilantes del problema que se corresponden con los modos de funcionamiento del instrumento. Este modelo incluye, por tanto, una descripción del acoplamiento entre el instrumento y el instrumentista. La escucha comparada de estas simulaciones es una herramienta potente de análisis ya que se pueden a partir de parámetros perfectamente controlados. En particular, se pueden elegir valores característicos del material utilizado para simular condiciones muy precisas, como por ejemplo, la presencia de frecuencias de resonancia de coincidencia mecánica y acústica.

1.2.3. Importancia de los defectos de circularidad

El instrumento simplificado se basa en un tubo cilíndrico acoplado a una lengüeta simple que constituye el mecanismo de excitación del instrumento. El resonador es un cilindro cuya sección es o bien circular, o bien ligeramente deformado por un defecto en la simetría axial (ovalización) que siempre existe en la práctica. Se supone a priori que la asimetría de la estructura induce acoplamientos específicos entre las familias de modos que estarían desacopladas en caso contrario. Dado que buscamos las condiciones que pueden dar lugar a un efecto importante de vibración de las paredes, se investigará la importancia de estos acoplamientos adicionales.

1.2.4. Estructura del trabajo

Tras esta introducción general, la memoria contiene cinco capítulos que pueden agruparse en tres partes. En los capítulos 2 y 3, se presenta un modelo vibroacústico teórico de una estructura cilíndrica vibrante y de una estructura cilíndrica ligeramente

deformada, respectivamente. En el capítulo 4 se muestran diferentes efectos de vibración de paredes mediante simulaciones en el dominio temporal. En el capítulo 5 se comparan las medidas de la impedancia de entrada de un tubo vibrante en caucho con un modelo sencillo basado en la hipótesis de membrana. Estos cinco capítulos están redactados en inglés con la excepción de un complemento en el capítulo 4 que está redactado en español y en francés. Las conclusiones generales del trabajo también están en español y francés. Finalmente, se han incluido dos anexos generales al final de la memoria.

En el capítulo 2 se propone un modelo vibroacústico para comprender y cuantificar el fenómeno de vibración de las paredes en los instrumentos de viento. El enfoque elegido consiste en suponer que la fuente principal de generación de la vibración de las paredes es el acoplamiento entre la columna de aire y la estructura. La presión acústica en la columna de aire hace vibrar las paredes del instrumento que, a su vez, perturba las de este campo de presión por radiación interna. En general, esta perturbación es despreciable, pero en algunos casos particulares, puede ser significativa. El método de resolución consiste en descomponer el campo vibratorio en los modos in vacuo de la estructura y describir el campo de presión interno por medio del método integromodal. Este enfoque proporciona una expresión de la matriz impedancia acústica de entrada de un tubo cilíndrico vibrante. Se realiza un estudio paramétrico con el fin de conocer la influencia de la geometría y los materiales que constituyen la estructura en el acoplamiento vibroacústico.

En el capítulo 3, se utiliza el modelo desarrollado en el capítulo 2 (artículo [PGR04]) para obtener una expresión de la matriz impedancia de entrada de un tubo cilíndrico ligeramente oval. La ovalización complica la resolución de la ecuación de movimiento de la estructura, puesto que el operador de Donnell depende, en este caso, de la coordenada angular. El modelo teórico propuesto para abordar este problema se basa en el método desarrollado por Yousri y Fahy en [YF77]. En este método, se supone que las bases modales acústica y mecánica de la estructura deformada son muy similares a las bases acústica y mecánica de un cilindro de sección perfectamente circular. Estas últimas se utilizan para expresar los campos acústico y vibratorio que verifican las ecuaciones acopladas de Helmholtz y del movimiento de la estructura. Al final del capítulo se presentan diversas aplicaciones numéricas que muestran el efecto de la deformación de la estructura en el comportamiento acústico del tubo sonoro. Se estudia el rol de diferentes materiales, así como la influencia del parámetro de deformación.

En el capítulo 4, se propone un modelo sencillo de instrumento de tipo clarinete con el que se simulan las oscilaciones periódicas del régimen principal de oscilación del mismo. Se utiliza la técnica propuesta por Schumacher [Sch81] para estudiar las auto-oscilaciones de un instrumento de viento de lengüeta simple. La respuesta acústica del resonador en este modelo toma en consideración los efectos de vibración de las paredes definido por el modelo vibroacústico propuesto en el capítulo 2 (artículo [PGR04]). Las simulaciones muestran que el acoplamiento entre la estructura y el fluido interno puede influir en el comportamiento acústico del instrumento. Se analizan las señales simuladas para los instrumentos con las paredes vibrantes respecto de la referencia de un instrumento rígido (con las paredes no vibrantes). Se observan cambios en el tiempo de ataque, cambios de timbre y de régimen de oscilación (notas multifónicas). Las simulaciones realizadas con instrumentos deformados muestran que la deformación de

la estructura induce el acoplamiento del modo acústico plano con el primer modo oval que presenta una frecuencia propia menor que el primer modo de respiración.

Finalmente, en el capítulo 5, se mide la impedancia acústica de entrada de un tubo de caucho con el objetivo de medir los efectos de vibración de las paredes e interpretar los fenómenos vibroacústicos observados. Se introduce un método tipo « desarrollo en ondas » ya que, en este caso, el número de modos en el método multimodal es demasiado elevado. En este método el operador de Donnell ha sido remplazado por el operador de membrana en la ecuación de movimiento de la estructura, y el campo de presión se obtiene a partir de una ecuación de ondas planas inhomogénea. El campo acústico se representa como la suma de tres ondas: la onda de Korteweg, que está asociada a una onda acústica plana que se propaga en el fluido y está fuertemente acoplada con las vibraciones de las paredes; las otras dos ondas que se propagan principalmente en la estructura. Se define y obtiene una velocidad de onda equivalente con el objetivo de comparar los cálculos teóricos y los resultados experimentales de la impedancia acústica de entrada del tubo.

Introduction générale

L'objectif général de ce travail qui est présenté pour son évaluation en tant que thèse de doctorat, est de réaliser une étude de l'effet des vibrations de paroi sur le fonctionnement des instruments de musique à vent. Ce travail est mené dans le cadre d'une cotutelle dans le cadre "Programa general del conocimiento" de l'Universidad Politécnica de Valencia (UPV, Valence, Espagne) et thèse de doctorat de l'Université du Maine (Le Mans, France), spécialité « acoustique ». Il s'agit d'une collaboration entre le Laboratoire d'Acoustique de l'Université du Maine (LAUM, UMR CNRS 6613) et le groupe de recherche Dispositivos y Sistemas Acústicos y Ópticos (DISAO) de l'UPV.

Coté français, le travail est effectué dans le cadre des activités relatives à la vibroacoustique (groupe « Transferts vibratoires») et à la physique des instruments de musique à vent (groupe « ondes guidées »). Il est mené sous la responsabilité conjointe de François Gautier (Maitre de conférence) codirecteur de thèse et Joël Gilbert (Chargé de Recherche, Habilité à diriger des recherches) directeur de thèse.

Coté espagnol, ce travail se situe dans l'axe de recherche de "sistemas radiantes" dans laquelle se réalisent des activités liées au design, à la caractérisation et à l'optimisation de sources sonores, qui incluent les sources electroacoustiques et les instruments à vent. Ce travail a été réalisé sous la responsabilité conjointe de Francisco Javier Redondo Pastor (Titular de Escuela Universitaria) codirecteur de thèse et Jaime Ramis Soriano (Catedrático de Escuela Universitaria) directeur de thèse.

1.1 L'effet de vibration de paroi: étude bibliographique

La problématique de l'effet de vibration de parois sur le fonctionnement des instruments de musique à vent remonte au 19ème siècle. En fait Miller en 1909 a fait une compilation de travaux [Mil09] liés à ce problème. Ensuite d'autres travaux se sont développés. Les études publiées qui abordent ce sujet concernent principalement le rôle du matériau constituant l'instrument et non spécifiquement le rôle des vibrations de parois. Parmi les publications dans le domaine de l'acoustique musicale qui traitent le problème, on peut citer par exemple :

- Boner et Newman [BN40], Knauss et Yeager [KY41] et Parker [Par47] étudient l'effet du matériau de différents instruments à vent. Ils emploient des techniques différentes mais ils ont la même conclusion, l'effet des vibrations de parois doit être très petit comparé au son émis par la colonne d'air.
- Backus en [Bac87], a été le premier a mesurer la contribution au champ acoustique émis par l'instrument lié au rayonnement de la struture vibrante. Il a trouvé que le son rayonné est 48dB plus petit que le son directement produit par l'instrument.

Des méthodes psychoacoustiques ont été employées par Coltman [Col 71] pour montrer au moyen de tests de reconnaissance en aveugle, que des flûtistes ne peuvent pas distinguer le matériau de construction d'instruments ayant la même géométrie. Il confirme donc que l'effet des vibrations de parois n'a pas de conséquences perceptibles dans le son émis par l'instrument.

Des études théoriques ont été publiées : Backus et Hundley [BH66] présentent un modèle local d'impédance de paroi qui permet de prendre en compte de manière approchée les vibrations axisymétriques du tube, modèle qui prédit un décalage des fréquences de résonance.

Le développement de l'acoustique des instruments à vent au cours des années 80 et 90 a permis d'améliorer les méthodes de mesure et de caractérisation acoustique de ces instruments. Comme suite à ces avancées, certains travaux ont abordé la problématique avec de nouvelles méthodes :

- Gibiat et al. [GBP97] ont mesuré des variations de spectre de 6 dB d'un instrument à vent simplifié, lorsque le tube est tenu ou bloqué.
- Malte Kob [Kob00] a mené des expériences avec des tuyaux d'orgue baroques avec et sans amortissement de paroi. Les résultats indiquent que lorsque le tuyau est en situation de jeu, quelques mode structuraux sont excités et des petits changements du spectre sont observés.
- Finalement, un phénomène spectaculaire liée à l'effet des vibrations de paroi est observé par Nederveen et Dalmolt [ND04] avec un tuyau d'orgue de géométrie distordue.

Le facteur commun de tous ces travaux, est qu'ils évaluent les conséquences de l'effet des vibrations des parois dans le son généré par l'instrument. La problématique proposée dans ce travail n'est pas ciblée sur les effets, mais sur les causes et phénomènes physiques qui engendrent l'effet de vibrations de paroi. Ces directions de travail impliquent la définition d'un modèle d'instrument à partir duquel s'établissent les mécanismes physiques qui permettent de décrire et de comprendre l'effet des vibrations de parois.

1.2 L'approche envisagée

1.2.1 Un modèle analytique

Pour quantifier ou estimer de façon objective l'importance des vibrations de parois sur le son musical produit par l'instrument, nous faisons le choix de développer un modèle analytique portant sur un instrument de géométrie simplifiée. D'autres approches, purement numériques (utilisant les méthodes d'éléments finis ou de frontière par exemple) ou expérimentales seraient possibles. Cependant, dans ce problème comprenant de multiples paramètres, l'analyse des différents mécanismes de couplages et la recherche des grandeurs pertinentes dont dépend l'importance de ce couplage étant l'un de nos objectifs, nous préférons l'emploi d'une méthode analytique. Ce modèle analytique est basé sur la résolution exacte des équations de coque mince (théorie de Donnell) couplées à celle régissant les oscillations d'un fluide interne dans le cadre de l'acoustique linéaire relative à un milieu homogène au repos (équation de Helmholtz). La méthode de résolution choisie est la méthode intégro-modale, mise en œuvre en régime forcé dans le domaine fréquentiel.

1.2 Des simulations temporelles

Le modèle physique envisagé pour l'instrument permet de développer des simulations dans le domaine temporel de son fonctionnement en situation de jeu. Ceci autorise le calcul des solutions auto-oscillantes du problème, correspondant aux modes de jeu possibles de l'instrument. Ce modèle comprend donc une description du couplage instrument / instrumentiste. L'écoute comparative de telles simulations est un moyen puissant d'analyse. En effet les simulations peuvent être réalisées avec des jeux de paramètres parfaitement maîtrisés et quelconques. En particulier, les valeurs caractéristiques du matériau utilisé peuvent être choisis pour réaliser des conditions très précises relatives par exemple à des coïncidences de fréquences de résonances acoustique et mécanique. Cette possibilité intéressante motive notre choix.

1.3 L'importance des défauts de circularité

L'instrument simplifié est constitué d'un tube cylindrique couplé à une anche simple, qui constitue le mécanisme excitateur de l'instrument. Le résonateur est un cylindre dont la section est soit circulaire, soit légèrement distordue du fait de défaut d'axisymétrie (ovalisation) qui existent toujours en pratique. Il est naturel de supposer a priori que la non symétrie de la structure induit des couplages particuliers entre des familles de modes qui seraient découplés dans le cas contraire. Comme nous recherchons les conditions qui peuvent donner lieu à un effet important des vibrations de parois, l'intérêt et l'importance de ces couplages additionnels sont à examiner et nous faisons de cet élément un axe central de notre approche.

1.4 Articulation de l'étude

A la suite de cette introduction générale ce mémoire contient cinq chapitres, qui peuvent être regroupés en trois parties. Aux chapitres 2 et 3, un modèle théorique vibroacoustique est présenté pour une structure cylindrique vibrante et pour une structure cylindrique légèrement distordue, respectivement. Le chapitre 4 montre

plusieurs effets des vibrations de paroi au moyen de simulations dans le domaine temporel. On propose dans le chapitre 5 une comparaison de mesures de l'impédance d'entrée d'un tuyau vibrant en caoutchouc avec un modèle simplifié basé sur l'hypothèse de membrane. Ces cinq chapitres sont rédigés en anglais à l'exception d'un complément au chapitre 4 qui est rédigé en espagnol et en français. Les conclusions générales du travail sont présentées en espagnol et en français. Deux annexes générales sont ajoutées à la fin du mémoire.

Dans le chapitre 2, un modèle vibroacoustique permettant de comprendre et de quantifier le phénomène de vibration de parois dans les instruments à vent est proposé. L'approche retenue consiste à supposer que la source principale de génération de vibration des parois est le couplage entre la colonne d'air et la structure. La pression acoustique dans la colonne d'air fait vibrer les parois de l'instrument qui, en retour perturbe ce champ de pression par rayonnement interne. En général, cette perturbation est négligeable, mais dans certains cas particuliers, elle peut devenir significative. La méthode de résolution consiste à décomposer le champ vibratoire sur les modes *in vacuo* de la coque et à décrire le champ de pression interne au moyen de la méthode intégro-modale. Cette approche est utilisée pour fournir une expression de la matrice impédance acoustique d'entrée d'un tuyau cylindrique vibrant. Une étude paramétrique est réalisée pour étudier l'influence de la géométrie et les matériaux constituant la coque dans le couplage vibroacoustique.

Dans le chapitre 3, l'approche retenue dans le chapitre précédent (chapitre 2, [PGR04]) est utilisée pour obtenir une expression de la matrice impédance d'entrée d'un tuyau cylindrique faiblement ovalisé. L'ovalisation (appelée encore distorsion) complique la résolution de l'équation de mouvement de la structure puisque l'opérateur de Donnell dépend dans ce cas de la coordonnée angulaire. L'approche retenue se base sur la méthode proposée par Yousri et Fahy en [YF77]. Dans cette méthode, les bases modales acoustique et mécanique de la structure déformée sont supposées très proches des bases acoustique et mécanique du cylindre de section parfaitement circulaire. Ces dernières sont utilisées pour exprimer les champs acoustique et vibratoire, vérifiant les équations couplées de Helmholtz et du mouvement de la coque. A la fin du chapitre, plusieurs applications numériques sont présentées qui montrent l'effet de la distorsion du tube sur le comportement acoustique du tuyau sonore. Le rôle de différent matériaux, ainsi que l'influence du paramètre de distorsion sont étudiés.

Dans le chapitre 4, un modèle simple d'instrument type clarinette permet de simuler les oscillations périodiques qui correspondent au régime principal d'oscillation de l'instrument. La technique proposée par Schumacher [Sch81] est utilisée pour étudier les auto-oscillations d'un instrument à vent à anche simple. La réponse acoustique du résonateur dans ce modèle prend en compte les effets de vibration de parois donnés par le modèle vibroacoustique proposé dans le chapitre 2 (article [PGR04]). Les simulations montrent que le couplage coque/fluide interne peut agir sur le comportement acoustique de l'instrument. Les signaux simulés pour les instruments à parois vibrantes sont analysés par rapport à la référence d'un instrument rigide (parois non vibrantes). Des changements du temps d'attaque, des changements de timbre et des changements de régime d'oscillation (notes multiphoniques) sont observés. Des simulations réalisées avec des instruments distordus montrent que la distorsion de la coque induit le couplage du mode acoustique plan avec le premier mode ovalisant qui a lieu à fréquence plus basse que le premier mode de respiration.

Finalement, dans le chapitre 5, l'impédance acoustique d'entrée d'un tuyau en caoutchouc a été mesurée dans le but de mesurer des effets de vibration de paroi et d'interpréter les phénomènes vibroacoustiques observés. Une méthode de type 'développement en ondes' est introduite puisque, dans ce cas, le nombre de modes dans la méthode multimodal est trop important. Dans cette méthode, l'opérateur de Donnell a été remplacé par l'opérateur de membrane à l'équation de mouvement de la coque et le champ de pression est obtenu à partir d'une équation d'ondes planes inhomogène. Le champ acoustique est représenté comme la somme de l'onde de Korteweg qui correspond à l'onde acoustique plane se propageant dans le fluide fortement couplée aux vibrations de parois et deux autres ondes se propagent principalement dans la structure. Une vitesse d'onde équivalente est définie et obtenue afin de comparer les calculs théoriques et les résultats expérimentaux à partir de l'impédance acoustique d'entrée.

Capítulo 2

Acoustic input impedance of a vibrating cylindrical tube

Este capítulo reproduce un artículo redactado en inglés enviado para su publicación[1]*. En este trabajo se propone un modelo vibroacústico que permite cuantificar y comprender el fenómeno de vibración de las paredes en los instrumentos de viento. El enfoque elegido consiste en suponer que la fuente principal de generación de vibración de las paredes es el acoplamiento entre la columna de aire y la estructura. La presión interna de la columna de aire hace vibrar las paredes del instrumento que, a su vez, radia presión. En general, esta contribución es despreciable, pero en ciertos casos particulares, puede ser significativa.*

La sección 2 presenta el método de resolución que consiste en descomponer el campo vibratorio en los modos in vacuo de la estructura y describir el campo de presión interna mediante el método integromodal. Este método ha sido utilizado principalmente por [Lau95] para calcular las impedancias de radiación externa y por [Gau97] para determinar las impedancias de radiación interna de una estructura con diferentes condiciones en los límites de la columna de aire. Este método proporciona una expresión de la matriz de impedancia acústica de entrada del tubo cilíndrico vibrante. En la solución del problema, se imponen unas condiciones límite mecánicas y acústicas a la estructura: la estructura mecánica se apoya simplemente, se impone una fuente excitadora acústica plana en un extremo del instrumento y la presión es nula en el otro extremo.

En la sección 3 se analiza la influencia de la vibración de las paredes en la impedancia del modo acústico plano. La formulación se trunca en el modo plano, puesto que los modos acústicos de orden superior tienen una frecuencia propia demasiado elevada y no influyen en el régimen de oscilación del instrumento. En general, el efecto de vibración de paredes puede ser interpretado como una pequeña corrección (factor de corrección) de la impedancia acústica de entrada de un tubo rígido con la misma geometría. El acoplamiento entre el modo acústico plano y los modos de respiración de la estructura se traduce en tres efectos: una resonancia estructural, una coincidencia espacial y un efecto de "refuerzo" de las resonancias acústicas. El análisis del factor de corrección de la impedancia debido a la vibración pone en evidencia que si dos efectos se superponen, pueden ocurrir fenómenos importantes de vibración de paredes.

Finalmente, se ha realizado un estudio paramétrico con el objetivo de estudiar la influencia de la geometría y los materiales que constituyen la estructura en el acoplamiento vibroacústico. Los resultados muestran que cuando se consideran las

[1] *Enviado para su publicación a la revista* Journal of Sound and Vibration *en febrero de 2004*

dimensiones típicas de un instrumento de viento y los materiales habituales de construcción, no se observa ningún efecto significativo relacionado con el acoplamiento fluido/estructura en el comportamiento acústico del tubo. Sin embargo, para ciertas estructuras, la impedancia acústica de entrada del tubo está muy alterada, y, por tanto, el fenómeno de vibración de paredes es significativo. En efecto, sólo si el módulo de Young y la densidad de los materiales que constituyen el cuerpo del instrumento son suficientemente pequeños, se pueden producir acoplamientos fluido/estructura importantes.

Ce chapitre reproduit un article rédigé en anglais soumis à la revue Journal of Sound and Vibration. Dans ce travail nous proposons un modèle vibroacoustique permettant de comprendre et de quantifier le phénomène de vibration de parois dans les instruments à vent. L'approche retenue consiste à supposer que la source principale de génération de vibration des parois soit le couplage entre la colonne d'air et la structure. La pression acoustique dans la colonne d'air fait vibrer les parois de l'instrument qui, en retour perturbe ce champ de pression par rayonnement interne.. En général, cette perturbation est négligeable, mais dans certains cas particuliers, elle peut devenir significative.
Après une introduction qui fait l'objet de la partie 1, la partie 2 présente la méthode de résolution qui consiste à décomposer le champ vibratoire sur les modes in vacuo de la coque et à décrire le champ de pression interne au moyen de la méthode intégro-modale. Cette méthode a été utilisée notamment par [Lau95] pour calculer les impédances de rayonnement externe et en [Gau97] pour déterminer les impédances de rayonnement interne d'une coque avec différentes conditions aux limites imposées à la colonne d'air. Cette approche est utilisée pour fournir une expression de la matrice impédance acoustique d'entrée d'un tuyau cylindrique vibrant. Dans la résolution du problème, des conditions aux limites mécaniques et acoustiques sont imposées à la coque: la structure mécanique est simplement appuyée. Une source acoustique plane excitatrice est imposée à une extrémité de l'instrument, la pression étant supposée nulle à l'autre extrémité.

Dans la partie 3, l'influence de la vibration des parois dans l'impédance du mode acoustique plan est analysée. La formulation est tronquée au mode plan puisque les modes acoustiques d'ordre supérieur n'ont d'influence notable qu'a des fréquences élevées et ne jouent pas sur le régime d'auto-oscillation de l'instrument. De façon générale, l'effet de vibration de parois peut être interprété comme une petite correction (facteur de correction) de l'impédance acoustique d'entrée d'un tuyau rigide avec la même géométrie. Le couplage entre le mode acoustique plan et les modes de respiration de la coque se traduit par trois effets : une résonance de structure, une coïncidence spatiale et un effet de 'renforcement' des résonances acoustiques. L'analyse du facteur de correction de l'impédance du à la vibration des parois met en évidence que si deux effets se superposent, des perturbations importantes peuvent alors avoir lieu. Finalement, une étude paramétrique est réalisée pour étudier l'influence de la géométrie et les matériaux constituant la coque dans le couplage vibroacoustique. Les résultats montrent que quand on considère les dimensions typiques d'un instrument à vent et les matériaux habituels de construction, aucun effet significatif lié au couplage fluide/parois n'est observé sur le comportement acoustique du tuyau. Pourtant, pour des coques

présentant des conditions très particulières, l'impédance acoustique d'entrée du tuyau est fortement altérée et donc, le phénomène de vibration de parois s'avère alors important. Ces conditions particulières se traduisent par des valeurs du module de Young et de la masse volumique du matériau particulièrement faibles.

2.1. Introduction

Many applications in mechanical engineering are related to the vibroacoustics of cylindrical shells. Such elastic ducts are generally filled and surrounded with fluid, leading to complex couplings between the structure and the internal and external fluids. This is the case of cylindrical shells, which constitute models of structures, such as the fuselages of aircrafts or the hulls of submarines. Industrial pipes, which generate noise because of fluid-borne sound or wind music instruments, which produce musical sounds are other examples of this configuration. Considering such cylindrical tubes as vibroacoustic wave-guides, they can be characterized by their input impedance matrix, which in this case depends on the fluid/structure interaction. The aim of this paper is to develop a model of the input impedance of a vibrating elastic cylindrical shell of finite length simply supported at both ends and filled with fluid. This model allows us to determine in which conditions shell vibrations can significantly affect the acoustic input impedance. The final application of this study is related to musical acoustics as explained below.

Vibroacoustics of pipes have been extensively studied in the literature. Wave propagation into infinite cylindrical elastic shells containing fluid has been studied in [FF82]. Dispersion curves and energy distribution of free waves of the system are investigated and interpreted. In the case of light fluid, the dispersion curves of the coupled system are found to be close to the ones of the uncoupled systems. For heavy fluids, fluid-loading term has an important effect on the dispersion curves and leads to complex interpretation of the various branches [Trd95], [BF93], [Fen94]. For applications related to active control of pipes' vibrations, the determination of the response of an infinite elastic fluid-filled shell excited by elementary sources is often needed, and is possible using free waves expansions: the case of a harmonic point force excitation (see [Ful83]), and the case of an interior monopole source (see [Ful84]) are presented in [FEN96].

The previously mentioned studies are related to wave propagation into infinite systems. Since the propagation modes of the fluid/structure coupled system are not orthogonal, they are not easy to use to describe the behavior of finite systems. A convenient way to do that is to represent fluid/shell system oscillations using functions associated to the uncoupled systems [JF93], [GL94], [Lau95]: the shell's displacement field is expanded over the *in vacuo* structural modes and the inner acoustic field is written as a multimodal expansion using transverse modes of the rigid wave-guide. For given excitation conditions, the integro-modal method provides the acoustic and vibratory fields [Les88], [Bru98], [MI86]. This approach is retained in this paper to describe the interaction between wall vibrations and the air column. This method has been used in [LG89] to compute external radiation impedances, which are useful to describe external acoustic radiation of the cylinder into light or heavy fluid. In addition, the method has been used in [GT98b] to determine the internal radiation impedances of a shell of finite length with various acoustic boundary conditions imposed at both ends of the air column. The influence of the mean flow on internal radiation impedances of a finite cylindrical shell with infinite rigid extensions has been studied in [OLG94].

Wind musical instruments are particular acoustic wave-guides, in which vibroacoustic couplings between the air column and the instrument's body occur. The walls of the instruments are able to vibrate, leading to internal and external acoustic radiations. The

evaluation of the importance of the role played by these vibrations on the musical sound produced by the instrument is an open question (see [Gau97] for a bibliography review). In [GT98a], a vibroacoustic model of a simplified instrument has been proposed in order to quantify the wall vibrations effect of its body on tone. This simplified instrument consists in a simply supported cylindrical elastic shell filled and surrounded with fluid. Such a model enables the calculation in the frequency domain of the forced response of the system taking into account 3 kinds of couplings: the shell/internal fluid coupling, the shell/lateral external fluid coupling and the inter-modal coupling induced by acoustic radiation at the end of the tube. Since musical instruments do not work in forced regime, time domain simulations of the self-induced oscillation have been developed for rigid-walled instruments [GGA95]. For these simulations, only its acoustic input impedance characterizes the instrument. The input impedance model presented in this paper is developed in order to be used as input data for time domain simulations of sounds of clarinet-like instruments. Since the vibrations of the walls can be taken into account or disregarded by these, comparisons between these two cases allow us to determine in which case the wall vibration effect is audible. The first results related to these comparisons are available in [PGG04a].

The structure of the paper is as follows: in Sec. 2.2 and 2.3, the governing equations of the shell/internal fluid coupled problem are presented. The input impedance matrix is obtained using projections of the vibratory and acoustic fields on appropriated functional bases: the *in vacuo* shell modes for the structural displacement field and acoustical transverse modes for the acoustic field. The general form of the acoustic impedance matrix at the entrance of the vibrating wave-guide is presented: the effect of wall vibrations is expressed as a correction term of the well-known impedance matrix of a rigid pipe. In Sec 2.4, attention was focused on the acoustic impedance of the plane mode. Since the cross-section of the shell is supposed to be perfectly circular, this kind of acoustic mode is coupled only with axisymmetric structural vibrations (breathing modes). Interaction with the first breathing mode is analysed in detail: the structure of the correction term is presented and the effects of structural resonances and the coincidence effects on the acoustic impedance are discussed. Strong vibroacoustic coupling is found in two conditions: when structural and acoustic resonance frequencies are close, and when the coincidence frequency and the mechanical resonance frequency are the same. These conditions are satisfied for particular sets of material parameters. For these cases, illustrating examples are given. Considering the effect of several breathing modes on the correction term, the input impedance of the plane mode is finally given taking into account interaction with N breathing modes. To conclude, a summary of the results is presented.

2.2. Vibroacoustic model

2.2.1. Formulation of the problem

We consider a homogeneous, isotropic, thin-walled circular cylindrical shell of length L, mean radius a, and thickness h. The shell material has a Young's modulus E, a Poisson's ration ν and a density ρ_s. The internal cylindrical cavity is filled with a fluid characterized by its density ρ_0, and its sound speed c. Surfaces S_0, S, S_L described on figure 2.1 correspond to the circular top surface of the cylinder at coordinate z = 0, the lateral surface of the cylinder (r = a), and the circular bottom surface at coordinate z = L,

respectively. Let D_i be the fluid domain inside the cylinder, delimited by S_0, S, S_L, and let **n** be the unitary normal vector to the cylinder in the outward direction.

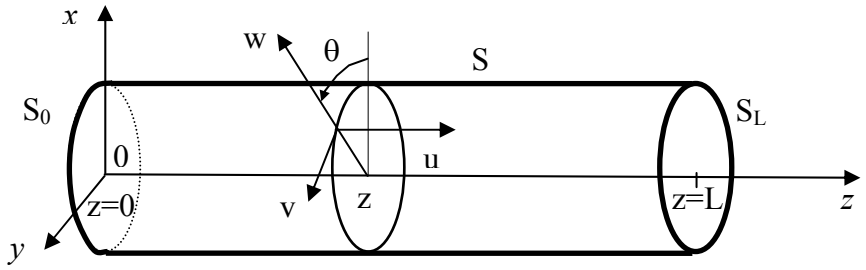

Figure 2.1: Notations for the vibrating cylinder

The presence of external fluid, which surrounds the shell, is ignored in this study. The external fluid/structure coupling leads to added mass and added damping effects for the shell, and also to intermodal coupling effect [LG89], [Gau97], [GT98a]. In the case of light external fluid, these effects can be neglected for the calculation of the shell response and their influence on the acoustic input impedance can be considered as negligible compared to the influence of inner fluid/shell coupling. Thus, we consider only the inner fluid/shell interaction.

The acoustic pressure inside the cylindrical cavity and the normal particle velocities related to the surfaces S_0, S, S_L are denoted p, v_{S0}, v_S and v_{SL} respectively. In harmonic regime, (the factor $e^{-j\omega t}$ is omitted) two equations are governing the problem: The first one is the Helmholtz equation,

$$\left(\Delta + k^2\right) p(M) = 0, \qquad \text{for } M \in D_i, \tag{2.1.}$$

where k=ω/c is the acoustic wave number. Dissipative visco-thermal effects induced by acoustic boundary layer are taken into account by means of the complex sound velocity c (see appendix E for details). The Helmholtz equation is associated to appropriate acoustic boundary conditions on surfaces S_0, S, and S_L. On the surface s_0, the acoustic normal velocity v_{S0} is supposed to be equal to a known value denoted $\bar{v}_{S_0}(M)$:

$$v_{S0}(M) = \bar{v}_{S_0}(M), \qquad \text{for } M \in S_0. \tag{2.2}$$

The acoustic velocity distribution $\bar{v}_{S_0}(M)$ is considered as the excitation source of the system. On the lateral surface S, continuity of the normal velocities of the fluid and of the shell is expressed as

$$v_s(M) = \dot{w}(M), \qquad \text{for } M \in S. \tag{2.3}$$

On the surface S_L, the tube is supposed to be open. Acoustic radiation into the external fluid through S_L is occurring and can be described using appropriated impedance matrix condition on surface S_L [Zor73]. Such a radiation induces additional acoustic intermodal

coupling [18]. Since this study is focused on inner fluid / shell interaction, we do not take into account the phenomenon and we consider that the acoustic pressure is equal to zero on S_L:

$$p(M) = 0 \qquad \text{for} \qquad M \in S_L . \tag{2.4}$$

The second governing equation is the shell motion equation. The motion of the middle surface of the cylindrical shell is described by displacement vector **X**, whose components *u*, *v* and *w* denote the longitudinal, circumferential, and radial displacements, respectively (see figure 2.1). Using usual cylindrical coordinates, the dynamic behaviour of the shell is described by the Donnell operator denoted by $\mathcal{L}$ [Lei73]

$$\mathcal{L} = \begin{bmatrix} a^2 \dfrac{\partial^2 \cdot}{\partial z^2} + \dfrac{1-\nu}{2} \dfrac{\partial^2 \cdot}{\partial \theta^2} & \dfrac{1+\nu}{2} a \dfrac{\partial^2 \cdot}{\partial z \partial \theta} & \nu\, a \dfrac{\partial \cdot}{\partial z} \\ \dfrac{1+\nu}{2} a \dfrac{\partial^2 \cdot}{\partial z \partial \theta} & \dfrac{\partial^2 \cdot}{\partial \theta^2} + \dfrac{1-\nu}{2} a^2 \dfrac{\partial^2 \cdot}{\partial z^2} & \dfrac{\partial \cdot}{\partial \theta} \\ -\nu\, a \dfrac{\partial \cdot}{\partial z} & -\dfrac{\partial \cdot}{\partial \theta} & -1 - \beta \left(a^2 \dfrac{\partial^2 \cdot}{\partial z^2} + \dfrac{\partial^2 \cdot}{\partial \theta^2} \right)^2 \end{bmatrix}, \tag{2.5}$$

where $\beta = \dfrac{h^2}{12a^2}$ is a non-dimensional thickness parameter. Using shell operator, the motion equation of the loaded by the air shell can be written in the following form [Lei73]:

$$\rho_s h \left(\omega_a^2 \mathcal{L} + \omega^2 \right) \mathbf{X}(M) = -p(M)\mathbf{n} \qquad \text{for} \qquad M \in S , \tag{2.6}$$

where

$$\omega_a = \frac{1}{a} \sqrt{\frac{E}{\rho_S \left(1-\nu^2\right)}} \tag{2.7}$$

is the shell ring frequency. Equation (2.6) is associated to mechanical boundary conditions: the shell is supposed to be simply supported boundary at both ends (z = 0, *l)*. This set of particular boundary conditions leads to an analytical tractable solution for the normal *in vacuo* modes of the shell [Lei73].

This work aims to evaluate the wall vibration effect of a cylinder in its acoustic behaviour. To achieve this objective, the input acoustic impedance of the wall-vibrating cylinder will be calculated by solving coupled equations (2.1) and (2.6), associated to boundary conditions (2.3), (2.4) for the acoustic cavity and simply supported conditions for the shell. The acoustic impedance is deduced from the calculation of the coupled system response to the known excitation condition (2.2).

2.2.2. Resolution method

An *in vacuo* modal expansion of the shell displacement field and a multimodal expansion of the inner acoustic pressure field are used in this part to formulate two coupled equations from governing equations of the system (2.1) and (2.6).

2.2.2.1. Modal expansion of the displacement field

The *in vacuo* simply supported modes of the shell, denoted $\mathbf{\Phi}_\mu$ are used as a functional basis to express the shell displacement field. Their expression is obtained using Donnell shell theory [22]. Notations and useful results are presented in appendix A. The problem of the representation of the shell displacement field is expressed as a linear combination of shell modes, involving the unknown modal amplitudes A_μ

$$\mathbf{X}(M) = \sum_\mu A_\mu \mathbf{\Phi}_\mu(M)\,, \tag{2.8}$$

where M is a point located on the middle surface of the shell. Inserting modal expansion (2.8) into the shell motion equation and making use of the homogeneous relation (A3, see Appendix A) leads to the following form for the shell motion equation:

$$\rho_s h \sum_\mu \left(-\omega^2 + \omega_\mu^2\right) A_\mu \mathbf{\Phi}_\mu(M) = -\mathrm{p}(M)\cdot\mathbf{n}\,, \tag{2.9}$$

Projecting equation (2.9) on a particular mode $\mathbf{\Phi_\mu}$ and using orthogonal properties of modal basis functions (A4), the motion equation takes the generalized form containing the modal mass m_μ

$$m_\mu\left(-\omega^2 + \omega_\mu^2\right)A_\mu = -\left\langle p(M)\cdot\mathbf{n}\,\middle|\,\mathbf{\Phi}_\mu\right\rangle \tag{2.10}$$

We take into account shell mechanical damping by introducing structural damping term (involving η_μ parameter) into the equation (2.11):

$$m_\mu\left(-\omega^2 + \omega_\mu^2\cdot\left(1 - j\eta_\mu\right)\right)A_\mu = -\left\langle p(M)\cdot\mathbf{n}\,\middle|\,\mathbf{\Phi_\mu}\right\rangle \tag{2.11}$$

From expression (2.11) it can be concluded that if the inner acoustic pressure field is known, the shell modal amplitudes can be calculated. In this case, the shell response is known. Equation (2.11) is the first coupled equation of the problem.

2.2.2.2. Description of the inner acoustic field using the integro-modal approach

To obtain the inner pressure field, the starting point is its integral formulation [Bru98], [MI86]:

$$p(M) = \int_{S_0,S,S_l} \left[G(M,M_0)\partial_n P(M) - p(M)\partial_n G(M,M_0) \right] dS_0 . \tag{2.12}$$

The choice of an appropriated Green function $G(M,M_0)$ is required to solve the problem. The Green's function of the infinite cylinder whose form is recalled in appendix B, leads to multimodal expansion for the acoustic pressure field and allows expressing the boundary conditions imposed to this field in a simple way. Acoustical basis is composed of the orthonormal eigenfunctions functions Ψ_α, which are the solutions of the two-dimensional transverse Neumann problem. The Green's function (Appendix B) is replaced in the integral representation (2.12). Using the boundary conditions (2.2), (2.3) and (2.4), we obtain:

$$p(M) = \sum_{\alpha=(m,n,s)} \left[\left\{ B_\alpha^+ + D_\alpha^+(z) \right\} e^{jk_{mn}z} + \left\{ B_\alpha^- + D_\alpha^-(z) \right\} e^{jk_{mn}(l-z)} \right] \Psi_\alpha(r,\theta), \ \textit{for} \ M \in S_0 \ \textit{or} \ M \in S_L \tag{2.13}$$

Thus, the pressure field can be interpreted as the superposition of two travelling waves in opposite directions with amplitudes depending on z. Both amplitudes are defined by

$$D_\alpha^+(z) = \frac{-\rho}{2k_{mn}} \left\langle \dot{w}(z,\theta) e^{-jk_{mn}z_0} \,\middle|\, \Psi_\alpha(a,\theta) \right\rangle_{S_{0,z}} = \frac{-\rho}{2k_{mn}} \int_0^z \dot{w}(z,\theta) e^{-jk_{mn}z_0} \Psi_\alpha(a,\theta) a \, d\theta \tag{2.14}$$

$$D_\alpha^-(z) = \frac{-\rho}{2k_{mn}} \left\langle \dot{w}(z,\theta) e^{-jk_{mn}(z_0-l)} \,\middle|\, \Psi_\alpha(a,\theta) \right\rangle_{S_{z,l}} = \frac{-\rho}{2k_{mn}} \int_z^l \dot{w}(z,\theta) e^{-jk_{mn}(z_0-l)} \Psi_\alpha(a,\theta) a \, d\theta \tag{2.15}$$

and

$$B_\alpha^+ = \frac{1}{1+e^{2jk_{mn}l}} \left[\left\langle V_{So} \,\middle|\, \Psi_\alpha(r,\theta) \right\rangle_{S_0} + D_\alpha^-(0) e^{jk_{mn}l} - D_\alpha^+(l) e^{2jk_{mn}l} \right] \tag{2.16}$$

$$B_\alpha^- = \frac{1}{1+e^{2jk_{mn}l}} \left[-\left\langle V_{So} \,\middle|\, \Psi_\alpha(r,\theta) \right\rangle_{S_0} - D_\alpha^-(0) e^{2jk_{mn}l} - D_\alpha^+(l) e^{jk_{mn}l} \right] \tag{2.17}$$

The coefficients $D_\alpha^+(z)$ and $D_\alpha^-(z)$ are obtained making use of the projections of the wall normal velocity on the lateral cylinder surfaces $S_{0,z}$ and $S_{z,L}$, defined from 0 to z and from z to L respectively (see figure 2.2).

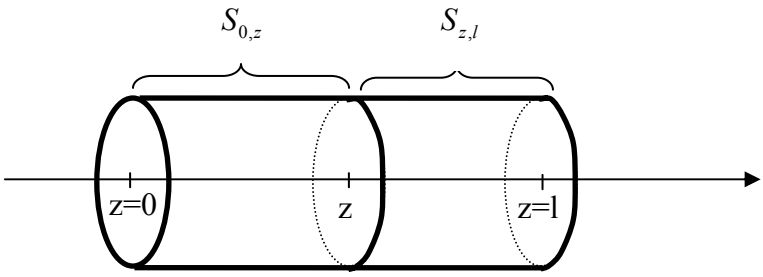

Figure 2.2: Integration of cylindrical surfaces $S_{0,z}$ and $S_{L,z}$ for the calculation of coefficients $D_\alpha^+(z)$ and $D_\alpha^-(z)$

From expressions (2.14) and (2.15) it can be deduced that whenever the cylinder walls do not vibrate $\dot{w}=0$, then coefficients $D_\alpha^+(z)$ and $D_\alpha^-(z)$ are null. In that case, as expected, the only source of the pressure field within the cylinder is the input velocity excitation represented by the term $\left\langle V_{S_0} \middle| \Psi_\alpha \right\rangle_{S_0}$ in expressions (2.16) and (2.17). In the case of a vibrating wall cylinder, it can be concluded that if the vibratory field $\dot{w}$ is known on the shell surface, the inner acoustic pressure can be calculated. Equation (2.13) is the second coupled equation of the problem.

2.3. Acoustic impedances

Acoustic input impedance matrix connects the projections of acoustic pressure and acoustic velocity on the transverse modes of the tube. Expressions of these projections can be deduced from coupled equations (2.11) and (2.13) as it is shown in this section. It can be seen that this vibrating cylinder impedance is the sum of two terms. The first one corresponds to the rigid cylinder impedance (subsection 2.3.1). The second is a complementary term, which depends on the vibration on the walls of the cylinder (subsection 2.3.3) and whose calculation needs previously the determination of internal radiation impedances of the vibrating tube (subsection 2.3.2).

2.3.1. Acoustic impedance of the rigid tube

For a particular pattern of wall vibration amplitude, inner acoustic pressure radiated by the cylindrical shell is known in the form of the multimodal acoustic expansion (2.13). Projecting the inner pressure on a particular mode Ψ_α, of the acoustic basis on the surface S_0 we obtain

$$\left\langle p(M) \middle| \Psi_\alpha \right\rangle_{S_0} = B_\alpha^+ + D_\alpha^+(0) + \left[B_\alpha^- + D_\alpha^-(0)\right] e^{jk_{mn}l} \qquad (2.18)$$

.

A convenient way to solve (2.18), taking into account the boundary conditions (2.2), (2.3) and (2.4) is to use a matrix representation as presented for example in [PAK96].

Using equations (2.14), (2.15), (2.16), (2.17), equation (2.18) can be written as matrix equations as

$$\mathbf{P} = \mathbf{Z}^r \cdot \mathbf{V} + \mathbf{Q} \cdot \mathbf{A}, \tag{2.19}$$

where vectors **P** and **V** are the projections of the inner pressure and the input velocity on the acoustic modes Ψ_α , with α = *(m,n,s)* (see appendix D for matrix notations). The first term on the right hand side of the equation (2.19) is due to acoustic excitation inside the cylinder. It involves the input acoustic impedance matrix $\mathbf{Z}^{\mathbf{r}}$ which corresponds to a rigid cylinder with non-vibrating walls. This is the diagonal matrix given in appendix 2.D, whose terms are the scalar impedances

$$Z_{mn} = -j\rho c \frac{k}{k_{mn}} \tan\left(k_{mn} \cdot l\right), \tag{2.20}$$

of the modes α = *(m,n,s)*. The axial wave number associated to the mode α is denoted k_{mn}. The second term **Q·A** in equation (2.19) describes the wall vibration effect. It involves the modal amplitudes A_μ that are included in vector **A** and a coupling matrix **Q** defined as

$$\mathbf{Q} = -j\omega \cdot \mathbf{H} \cdot \mathbf{Z}^{\mathbf{r}} \tag{2.21}$$

where $\mathbf{Z}^{\mathbf{r}}$ is the acoustic input impedance of the rigid cylindrical shell and each term of matrix **H** is defined by

$$H_{\mu\alpha} = \left(1 - \delta_{m0}\delta_{s0}\right)\delta_{mm'}\delta_{ss'} \cdot 2\sqrt{\frac{\pi}{\varepsilon_m}} \cdot \frac{1}{\sqrt{1-\gamma_{mn}^2}} \cdot \frac{q\pi}{l} \cdot \frac{1}{k_{mn}^2 - \left(q\pi/l\right)^2} \tag{2.22}$$

subscripted by μ = *(m',q,s',j)* and α = *(m,n,s)*. In equation (2.22), ε_m and the normalization factor γ_{mn} are defined on appendix B. Factor $\left(1-\delta_{m0}\delta_{s0}\right)$ imposes a restriction on the acoustic indeces of the modal basis. The circumferential index *m* and the symmetry index *s* cannot be null simultaneously, because none of the acoustic modes corresponds to this couple of indeces.

Because of the form of the coupling term given by (2.22), expression (2.19) outlines the coupling by families among acoustic and shell modes. Indeed, the presence of the Kronecker Delta $\delta_{m,m'}$ in equation (2.22) implies that coupling between acoustic and shell modes exists only for modes having the same circumferential index *m*. As a consequence, the plane mode, of null circumferential index (m=0), is exclusively coupled to the shell modes that present revolution symmetry (m'=0) (these modes are usually called the shell breathing modes). The other Kronecker Delta $\delta_{ss'}$ imposes a restriction on the coupling between acoustic and shell modes: only the modes with the same symmetry index *s* are coupled.

2.3.2. Internal radiation impedances of the shell

Expression (2.19) provides the projections vector **P** for the acoustic pressure as a function of the unknown modal amplitude vector **A**. This amplitude vector **A** is obtained from motion equation (2.11), using the multimodal expansion of acoustic pressure field (2.18). Projecting the internal acoustic field on the structural modal basis (and not on the acoustic modal basis as done in 2.3.1), we obtain:

$$\left\langle p(M)\mathbf{n}\middle|\mathbf{\Phi}_{\mu}\right\rangle_{S} = -\sum_{\alpha=(m,n,s)} H_{\mu\alpha} Z_{mn} V_{\alpha} + j\omega\cdot\sum_{\mu'} Z^{i}_{\mu\mu'}\mathbf{A}_{\mu'}, \qquad (2.23)$$

In expression (2.23), $Z^{i}_{\mu\mu'}$ are the internal radiation impedances of the shell. They constitute the terms of an impedance matrix $\mathbf{Z^i}$, as described in appendix 2.D. The expressions of $Z^{i}_{\mu\mu'}$ are derived in [OLG94] and useful relations are recalled in appendix 2.C. Each term $Z^{i}_{\mu\mu'}$ of the internal radiation impedance matrix $\mathbf{Z^i}$ refers to interaction of modes $\mu = (m,q,s,j)$ and $\mu' = (m',q',s',j')$ via the fluid, when Neumann and Dirichlet boundary conditions are applied to the surfaces S_0 and S_l respectively.

Off-diagonal terms of matrix $\mathbf{Z^i}$ are called internal impedances or mutual-impedances. They describe intermodal coupling between different shell modes due to internal acoustic radiation. Diagonal terms are called direct impedances. Their real and imaginary parts describe resistive and reactive effects induced by the inner fluid on the structural mode.

Substituting expression (2.23) into the shell's motion equation (2.11), we obtain

$$m_{\mu}\rho_{c}h\left(-\omega^{2}+\omega_{\mu}^{2}\cdot\left(1-j\eta_{\mu}\right)\right)A_{\mu} = -\sum_{\alpha=(m,n,s)} H_{\mu\alpha} Z_{mn} V_{\alpha} + j\omega\cdot\sum_{\mu'} Z^{i}_{\mu\mu'} A_{\mu'}, \qquad (2.24)$$

which can be written in matrix form as

$$\mathbf{M}\cdot\mathbf{A} = \mathbf{E}\cdot\mathbf{V}, \qquad (2.25)$$

where the coupling matrix term **E** is defined as

$$\mathbf{E} = -\mathbf{H}\cdot\mathbf{Z^r}. \qquad (2.26)$$

and where matrix **M** is

$$\mathbf{M} = \mathrm{diag}\left[m_{\mu}\left(-\omega^{2}+\omega_{\mu}^{2}\cdot\left(1-j\eta_{\mu}\right)\right)\right] - j\omega\cdot\mathbf{Z^i}. \qquad (2.27)$$

The first term of equation (2.27) is a diagonal matrix whose elements consist of the expression $m_{\mu}\left(-\omega^{2}+\omega_{\mu}^{2}\cdot\left(1-j\eta_{\mu}\right)\right)$ calculated for each modal index of the structural modal basis. In equation (2.25), the amplitude vector **V** for the acoustic velocity is given

since the velocity is prescribed on the input surface S_0. Thus, inverting matrix **M** in (2.27) provides the amplitude vector **A**.

For light fluids like air, the structure is not significantly affected by the fluid loading. A simple approximation involves neglecting acoustic and mechanical modes are not affected by the structural shell intermodal coupling. Light inner fluid approximation implies disregarding the coupling terms contained in the mutual-impedances on equation (2.27). In this particular problem, a greater approximation than that of light fluid, which consist in disregarding the inner radiation impedances ($\mathbf{Z}^{\mathbf{i}}$) in relation to the shell terms of matrix **M** in equation (2.27) will be carried out.

2.3.3. Acoustic input impedance matrix of the vibrating tube

Equations (2.19) and (2.25) are matrix forms of the coupled equations of the system (2.11) and (2.13). Eliminating the amplitude mode vector **A** from these equations, we obtain a matricial relationship between **P** and **V**, which defines the acoustic input impedance matrix at the entrance of the cylinder:

$$\mathbf{P} = \left\{\mathbf{Z}^{\mathbf{r}} + \mathbf{Q}\cdot\mathbf{M}^{-1}\cdot\mathbf{E}\right\}\cdot\mathbf{V} = \mathbf{Z}\cdot\mathbf{V}\,. \tag{2.28}$$

Thus, the following expression can be written

$$\mathbf{Z} = \mathbf{Z}^{\mathbf{r}} + \mathbf{Z}^{\mathbf{c}} \tag{2.29}$$

The matrix $\mathbf{Z}^{\mathbf{r}}$ represents the contribution of the rigid acoustic input impedance for modes α and α'. Each scalar term of $\mathbf{Z}^{\mathbf{r}}$ is defined on equation (2.20). The second term can be interpreted as an impedance correction caused by wall vibrations. Using equations (2.21) and (2.26), we obtain a symmetric expression for the acoustic input impedance correction induced by wall vibration, where

$$\mathbf{Z}^{\mathbf{c}} = \overline{\mathbf{Z}}^{\mathbf{r}}\cdot\mathbf{H}\cdot\overline{\mathbf{M}}^{-1}\cdot\mathbf{H}\cdot\mathbf{Z}^{\mathbf{r}}\,, \tag{2.30}$$

and where matrix $\mathbf{M}^{-1}$ has been normalized by factor $j\omega$:

$$\overline{\mathbf{M}}^{-1} = \frac{\mathbf{M}^{-1}}{j\omega} \tag{2.31}$$

and $\mathbf{Z}^{\mathbf{r}}$ has been normalized by

$$\overline{\mathbf{Z}}^{\mathbf{r}} = \frac{\mathbf{Z}^{\mathbf{r}}}{\rho\cdot c}\,. \tag{2.32}$$

Finally, the vibrating acoustic impedance of the cylinder can be written as

$$\mathbf{Z} = \mathbf{Z}^{\mathbf{r}}\cdot\left(\mathbf{I} + \mathbf{C}\right) \tag{2.33}$$

where **I** is the identity matrix and

$$\mathbf{C} = \mathbf{H}\cdot\overline{\mathbf{M}}^{-1}\cdot\mathbf{H}\cdot\mathbf{Z}^{\mathbf{r}} \qquad (2.34)$$

is a non-dimensional correction factor taking into account the effect of the inner wall vibration on acoustic input impedance of the vibrating cylinder.

2.4. Wall vibration influence on the plane mode impedance

The vibroacoustic model developed in section 2 provides an expression able to quantify the influence of the inner wall vibration effect on the acoustic input impedance matrix of the tube cylinder for all circumferential orders. This effect can be understood as a correction factor of the rigid acoustic input impedance. In this section, the analytical expression of *C* is obtained and particular conditions determining the importance of wall vibration effect are studied.

2.4.1. Simplified model: interaction between plane acoustic mode and first shell breathing mode

Below the first cut-off frequency of the tube, the plane mode (α=(0,0,1)) is the only propagating acoustic mode. In this frequency range, the influence on the acoustic response of the shell of the higher order modes can be neglected. Because of its practical importance in many applications, we focus our attention on plane mode impedance. The amplitude vector **P** is reduced to the scalar term $P_{(0,0,1)}$ (for the notation, see the relation D2 in appendix 2.D). Note that this scalar plane mode impedance is the (1,1) term of the input impedance matrix **Z** defined by equation (2.33). As a consequence of this truncation, the correction factor and the rigid input impedance are no more matrices but scalars:

$$Z = Z^r \cdot (1+C). \qquad (2.35)$$

The scalar correction factor takes the form:

$$C = \mathbf{H}\cdot\overline{\mathbf{M}}^{-1}\cdot\mathbf{H}\cdot Z^r . \qquad (2.36)$$

In order, to understand the wall vibrations influence, we study firstly, the effect of the first breathing mode in an isolated way. For this purpose, a shell modal basis truncation is achieved to the first shell breathing mode (m=0, q=1). For this particular case, shell matrix **M** in the previous equation is equal to a scalar and we have

$$C = H\cdot\overline{M}^{-1}\cdot H\cdot Z^r . \qquad (2.37)$$

Replacing the equation (2.37) into equation (2.35), we obtain a simple expression for the acoustic input impedance of the plane mode, when only the first breathing mode is taken into account:

$$Z = Z^r \cdot \left(1 + H^2 \overline{M}^{-1} Z^r\right). \tag{2.38}$$

Note that, in this particular case, H, M and Z^r are scalars so Z also is. Using equations (2.22) and (2.37), we obtain the following form of the correction term

$$C(\omega) = \frac{4\pi\rho \cdot c}{m_\mu}\left(\frac{\pi}{l}\right)^2 \frac{\omega \tan(\omega l/c)}{\left[(\omega/c)^2 - (\pi/l)^2\right]^2\left[\omega^2 - \omega_\mu^2 \cdot (1 - j\eta_\mu)\right]}, \tag{2.39}$$

where ω_μ is the eigenpulsation of the shell motion equation associated to the mode μ=(m,q)=(1,0) and m_μ is its modal mass defined by equation (A5). If this correction term C is small compared to unity (C<<1), the wall vibration effect can be understood as a length correction of the cylinder. In this case

$$Z = j\tan(kl) \cdot (1 + C) = j\tan(kl'), \tag{2.40}$$

where $\delta = l'-l$ is the length correction of the cylinder. Assuming that δ is very small, a series expansion of tan(kl') can be computed and it can be deduced as a function of the factor correction:

$$\delta = \frac{C \cdot \tan(kl)}{k\left(1 + \tan^2(kl)\right)(1 + C)}. \tag{2.41}$$

2.4.2. Description of main wall vibration effects

2.4.2.1. Structure of the impedance correction term

Considering only the first breathing shell mode, it can be seen from equation (2.35) that the input acoustic impedance of the plane mode can be drastically perturbed by the wall vibration if the correction factor C is significant compared to unity. As can be seen in equation (2.39), the correction factor is inversely proportional to the modal mass m_μ. The modal mass is proportional to the density of the shell's material. This means that, generally speaking, the smaller the density of the material is, the bigger the wall vibration effect is.

The correction factor is also proportional to the factors $\left[\omega^2 - \omega_\mu^2 \cdot (1 - j\eta_\mu)\right]^{-1}$, $\left[(\omega/c)^2 - (\pi/l)^2\right]^{-2}$, and $\tan(kl)$. When at least one of these factors takes high values, the correction term takes high values too and the wall vibration effect is important. The conditions $\left[\omega^2 - \omega_\mu^2 \cdot (1 - j\eta_\mu)\right] \cong 0$ and $\left[(\omega/c)^2 - (\pi/l)^2\right] \cong 0$ correspond to structural resonance effect and spatial coincidence effect respectively. The condition $\left[\tan(kl)\right]^{-1} = 0$ is the acoustic resonance condition of the rigid system associated. In the case of a conservative system, the condition can be written as $k_n l = \pi(n + 1/2)$. When these effects are produced at similar frequencies, the wall vibration effect becomes important. In order to understand the nature of the effects induced by these three conditions, they will be analysed separately.

2.4.2.2. *Structural resonance effect*

The condition $\omega^2 - \omega_\mu^2 \cdot (1 - j\eta_\mu) \cong 0$ leads to a great value of correction factor C and corresponds to a mechanical resonance condition. For a conservative system ($\eta_\mu = 0$), this condition is satisfied when the frequency is strictly equal to a eigenfrequency of the shell. These eigenfrequencies are defined by the equation (A7). They strongly depend on the Young's modulus and the density of the material of the shell. The smaller the Young's modulus is, the smaller the shell eigenfrequency is. The variation of the eigenfrequency of the first breathing shell mode on the density is opposite as the previous case: The bigger the material density is, the smaller the shell eigenfrequency. In fact, the eigenfrequency of the first breathing mode depends on the ratio of the Young's modulus and the density (E/ρ_S) of the shell material.

Thus, the physical properties of the material determine the resonant behaviour of the cylindrical shell. It is therefore interesting to carry out a parametric study to know better the relationship between the vibration of the structure and the characteristics of the material it is made of. The mechanical behaviour of four structures made of different materials; steel, aluminium, wood A and polymer A is studied below. The mechanical properties of these materials are shown in table 2.2. Figure 2.3 represents in a contour map, the first breathing eigenfrequency of the shell as a function of the Young's modulus and the density of the material it is made of. Each material has been placed in this plot at its corresponding physical values.

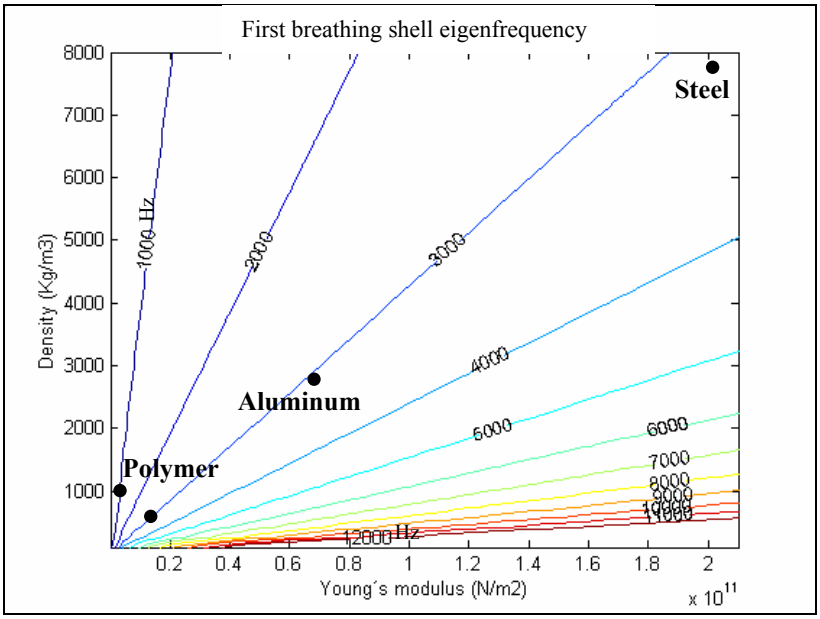

Figure 2.3: Eigenfrequency (Hz) of the first breathing mode of the shell as function of the density and the Young's modulus of the material. Geometry of the shell is given in table 2.1. Dots represent 4 shells made of steel, aluminium, wood and polymer.

It must be pointed out that, despite the fact that wood is less dense than steel, the wooden structure presents a first breathing eigenfrequency similar to that of steel. This is because its Young's modulus is almost two orders of magnitude smaller

The frequency at which the resonance effect of the structure is produced, is strongly related to the mechanical properties of the material the cylindrical structure is made of. According to this, structures built with different materials can present different acoustic behaviours due to the mechanical resonance effect. This effect is purely mechanical, which implies that it is completely independent of the internal acoustic field.

2.4.2.3. Spatial coincidence effect

As it has been explained previously, the correction factor defined on equation (2.39) depends inversely on the factor $(\omega/c)^2-(q\pi/l)^2$. The condition $(\omega/c)^2-(q\pi/l)^2=0$ can strictly be satisfied only if fluid damping is ignored. In this case the celerity c is real and the condition is satisfied when the acoustic wavenumber $k=\frac{\omega}{c}$ is equal to one of values $\frac{q\pi}{l}=k_q$. Such a condition is a coincidence condition. This wavenumber condition can be read in the frequency domain: each coincidence wavenumber k_q is related to a particular coincidence pulsation $\omega_q=k_q\cdot c$ and a coincidence frequency $f_q=\omega_q/2\pi$. These coincidence frequencies correspond to acoustic antiresonances of the tube.

In other words, each shell mode q produces an alteration of the q-th antiresonance of the input acoustic impedance. For these antiresonance frequencies, the axial profile of the acoustic pressure along the tube fits well with one of the breathing mode shapes of the shell. Indeed, for these frequencies, the acoustic pressure is equal to zero at both ends. The spatial coincidence effect is related to the spatial coincidence between the acoustic profile and structural modes.

In order to understand the behaviour of the wall vibration effect at these coincidence frequencies, the correction factor is studied for values of k close to a coincident wavenumber of the correction factor will be developed. In the vicinity of k_q, the correction factor takes the following form.

$$\text{if } k=\frac{q\pi}{l}+\varepsilon,\ \text{with } |\varepsilon|<<1,\qquad C(k)\propto\frac{\tan(kl)}{\left[(k)^2-(q\pi/l)^2\right]^2}\approx\frac{\varepsilon\cdot l}{(2q\pi\varepsilon/l)^2}=\frac{l^3}{4\cdot q^2\pi^2\varepsilon}\qquad(2.42)$$

In the expression (2.42), losses have been neglected with the intention of simplifying the calculation and ε has been supposed very small. The wavenumber being closer to the coincidence one, ε is close to zero. In this case, expression (2.42) shows that the correction factor diverges and tends to infinite value.

For a lossless system, the coincident condition is satisfied at each acoustic antiresonance and induces a divergence of the input acoustic impedance for these values completely determine the response of the input acoustic impedance at the antiresonances. The effect of losses consists on reducing the influence of this effect on the global response of the system.

2.4.2.4. Effect of the acoustic resonances

The correction factor is proportional to Z^r (see equation (2.38)). That means that for frequencies for which impedance Z^r is maximum (that is, for acoustic resonances frequencies of the rigid tube), the correction factor takes also great values. Thus, the wall vibrations can reinforce the resonance of the acoustic input impedance. It will be seen in paragraph 3.4.5 on that this phenomenon must be added to those explained before in order to be significant.

2.4.3. Typical numerical applications

With the purpose of illustrating and quantifying the wall vibration effect on the input acoustic impedance, the impedance correction factor C defined by (2.39) is calculated numerically in this section for some particular shells. Table 2.1 contains the shell's geometrical fixed values for all the calculations carried out from now on. For these calculations, the structural damping coefficient has been fixed at η_μ=0.01 and the acoustical losses model used, which includes visco-thermal dissipation is described on appendix 2.E.

Radius (a)	14.25mm
Length (l)	0.5m
Thickness (h)	0.5mm

Table 2.1: Geometrical parameters of the shell

2.4.3.1. Case of a steel shell

Figure 2.6 shows the correction factor of the input acoustic impedance, induced by the wall vibration effect, when only interaction between the plane acoustic mode and the first breathing mode are considered. For this numerical application, shell material is steel (density and Young's modulus have been fixed at ρ_S=7800kg/m^3 and E=210N/m^2 respectively). In order to evaluate the importance of wall vibrations, the magnitude of the non-dimensional coefficient C must be compared to unity (dashed line).

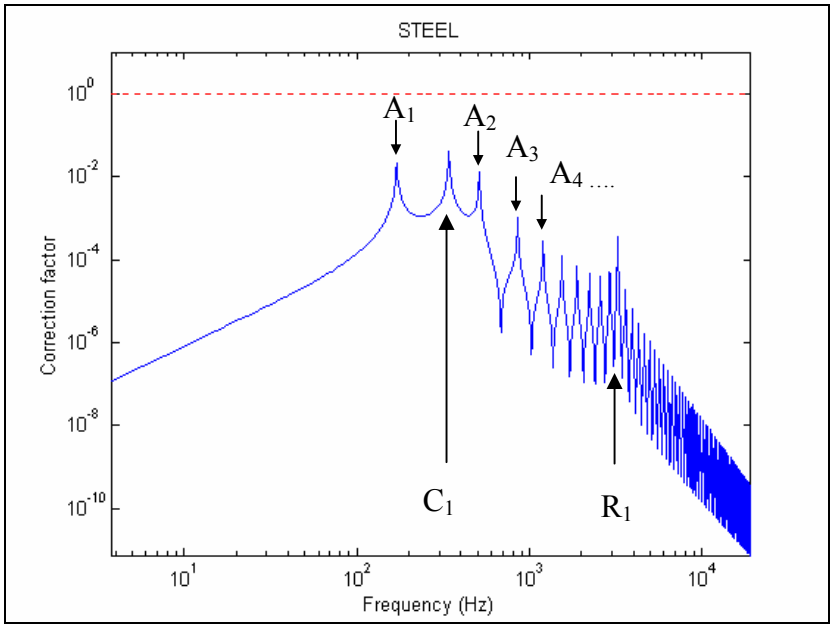

Figure 2.4: Correction factor of the acoustic input impedance induced by wall vibration. Steel is the material of the shell: Its Young's modulus is $E=210\cdot10^9 N/m^2$ and its density $\rho_S=7800kg/m^3$. Only the breathing mode (eigenfrequency $f_{R1}=3200Hz$) has been considered. Peaks C_1 and R_1 correspond to the coincident condition and the mechanical resonance respectively.

For the values of the parameters, the wall vibrations have very small influence on the input impedance since the correction factor C is always less than 10^{-1}. However, C has some local maximums as discussed previously. Three kinds of peaks, corresponding to the 3 conditions described in subsections 3.2.2, 3.2.3 and 3.2.4 are observed. Mechanical resonance frequency of the first breathing mode (referred as R_1 on figure 2.6) is $f_{R1}=3200Hz$. Spatial coincidence effect (C_1) is reached for $f_{C1}=342Hz$. As expected (see subsection 3.2.4), local maximums for C are observed for each acoustic resonance frequency. These are denoted by A_i (i=1,…N) on figure 2.6. Except for these local maximums R_1, C_1 and A_i, the correction factor is negligible for all frequencies for the steel pipe.

2.4.3.2. Case of a polymer shell

Correction factor C has been computed for a polymer cylinder with the same geometrical features as the previous one (see figure 2.5). This material is lighter than steel and its Young's modulus is much smaller (see polymer A in table 2.2: $\rho_S=1050kg/m^3$ and $E=3\cdot10^9 N/m^2$). The correction factor for this shell has been calculated and represented as a function of frequency in figure 2.5. It can be seen that the global resonance pattern of the function is the same as that of steel. However, two main differences can be pointed out: The first is that, in the entire frequency range, the correction factor is bigger for polymer than for steel. As explained in section 3.2.1., the correction factor is inversely proportional to the wall density of the shell. And so, the wall vibration effect is more important in light materials like polymers than in heavy materials like steel. The second difference is that the mechanical resonance R_1 is much smaller for the polymer $f_{R1}\approx1000Hz$ than for steel. The frequency of mechanical resonance is proportional to the ratio E/ρ_S. As a result, the smaller this ratio, the smaller will be the frequency of the mechanical resonance of the shell.

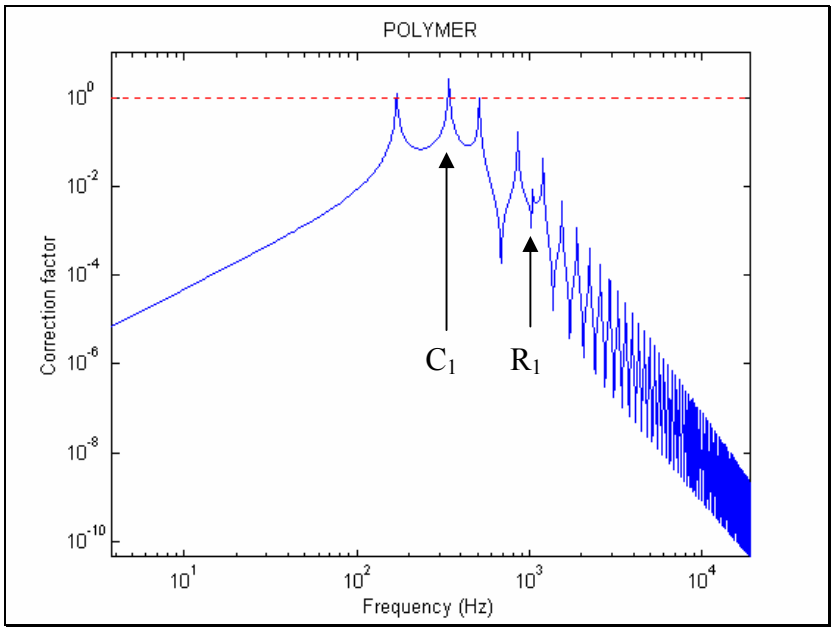

Figure 2.5: Correction factor of the acoustic input impedance induced by wall vibration of a cylindrical shell conformed by polymer. Only the breathing mode has been considered. Polymer A is the material of the shell: Its Young's modulus is $E=3\cdot109N/m^2$ and its density $\rho_S=1050kg/m^3$ ($f_{R1}=1048Hz$)

As deduced on equation (2.43), if the correction factor is sufficiently small, the wall vibration effect can be interpreted as a correction of the cylinder length. In figure 2.6, the length correction of a vibrating cylinder, only considering the breathing mode, has been represented against frequency. It can be seen that this correction is very small for all the frequencies (<0.02% for the studied case).

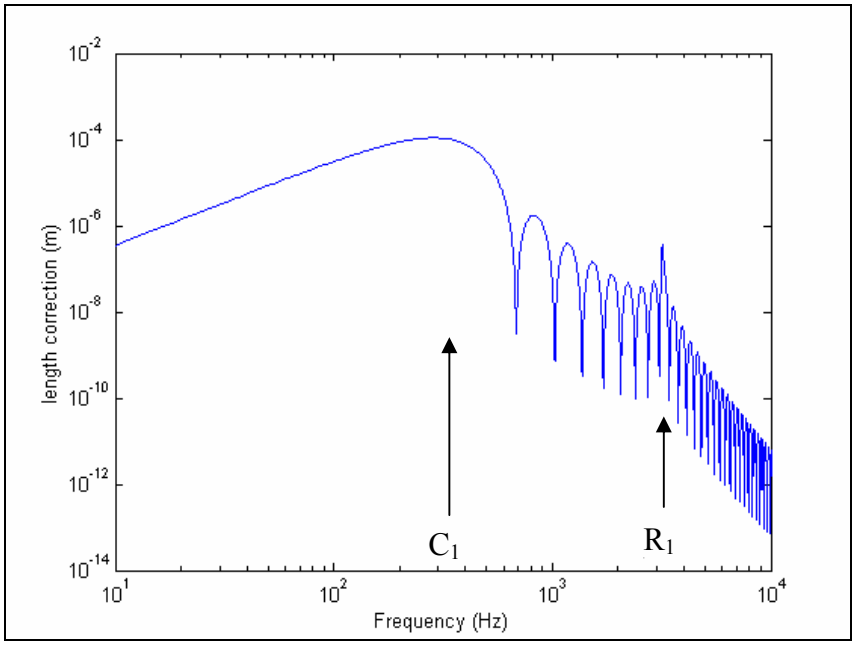

Figure 2.6: Length correction of the shell due to the wall vibration effect. Only the breathing mode has been considered. The Young's modulus of the material of the structure is $E=210\cdot10^9 N/m^2$ and the density $\rho_S=7800kg/m^3$

For this particular shell made of a shell with $\rho_S=7800kg/m^3$ and $E=210\cdot10^9 N/m^2$, the length correction at the first acoustic resonance is $\delta(f_1)\approx10^{-4}m$. Considering that the whole length of this shell is L=0.5m, the length correction due to wall vibration effect is very small. This change of the effective length, can be understood as a shift of the acoustic resonance frequencies of the tube

$$\Delta f(f_i) = f_i \frac{\delta(f_i)}{L} \text{ where i=1,2,3,…,} \tag{2.43}$$

and f_i are the acoustic resonance frequencies of the tube. Next, the change of the first acoustic resonance frequency is analysed as an example of application for the particular shell under study. At the first acoustic resonance, the relative shift in frequency is $\Delta f(f_1)/f_1\approx2\cdot10^{-4}$ which corresponds to 0.3 cents. This means that the first acoustic resonance of the tube is shifted by only $\Delta f(f_1)\approx0.03Hz$.

In figure 2.7, the vibrating acoustic input impedances of four cylinders made of different materials have been plotted: steel, aluminium, wood A and polymer A. The Young's modulus and density of these materials are shown in table 2.2.

Material	Density ρ_S (kg/m^3)	Young's modulus E (10^9 N/m^2)	Poisson's modulus
Steel	**7800**	**210**	**0.29**
Aluminum	**2710**	**70**	**0.33**
Wood A	**525**	**13**	**0.3**
Polymer A	**1050**	**3**	**0.33**
Polymer B	**1050**	**0.09**	**0.3**
Polymer C	**1500**	**0.47**	**0.3**
Wood B	**300**	**0.212**	**0.3**

Table 2.2: Density, Young's modulus and Poisson's modulus of materials used in the numerical applications studied.

No differences can be seen except for a small shift of frequency for the case of the polymer shell.

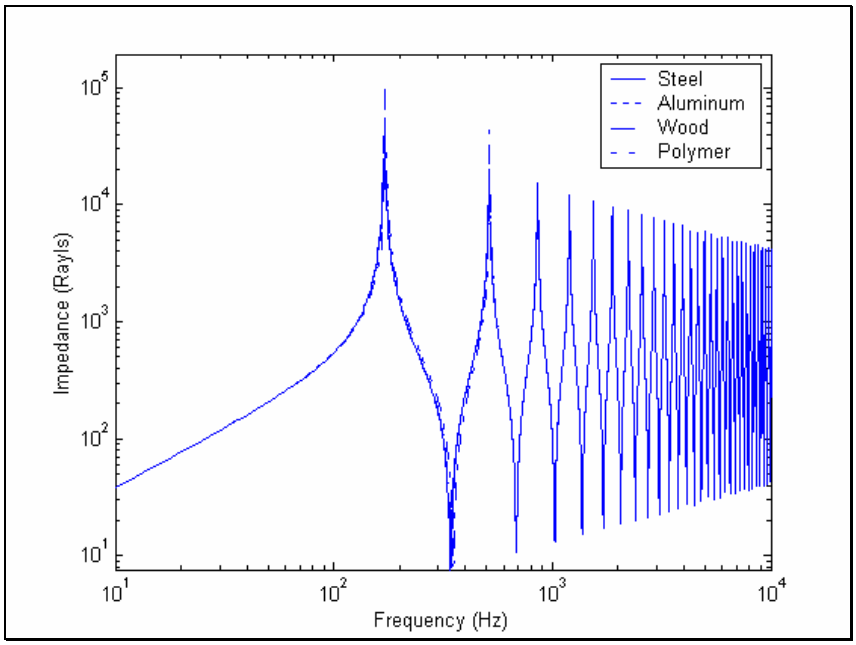

Figure 2.7: Acoustic input impedance of 4 vibrating shells made of steel, aluminum, wood A, and polymer A. Only the breathing mode has been considered. Differences are very small.

The representation is focused on the first antiresonance of the shells on figure 2.8, which corresponds to the coincident condition of the first breathing mode. It can be seen that the lower the density of the material the shell is made of (that is, polymer A, wood A, aluminum and steel), the more important the wall vibration effect. However, this effect is very small in any case.

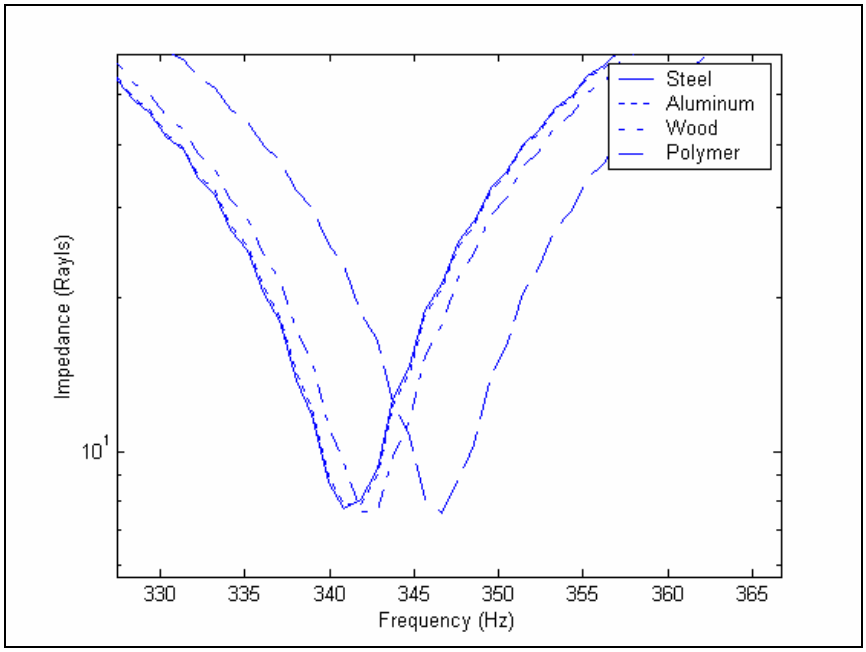

Figure 2.8: Zoom at the first antiresonance of the acoustic input impedance of 4 vibrating shells made of steel, aluminium, wood A and polymer A. It is distorted by the spatial coincidence effect induced by wall vibration effect. Only the breathing mode has been considered.

2.4.4. Special material parameters leading to strong vibroacoustic coupling

It has been shown that a shell made of polymer is more sensible vibroacoustic phenomena, and so, to be coupled to the air column of the tube, than a shell made of steel. Polymer is lighter and its Young's modulus is smaller than steel and both conditions favour the importance of the influence of the wall vibrations effect on the input acoustic impedance. In both cases (steel and polymer A), the coupling is very small and the acoustic input impedance is not distorted by the effect of wall vibrations.

For some specific frequency matching conditions detailed in the following, shell modes interact strongly with acoustic modes, leading to important changes on the acoustic response of the tube. These conditions are satisfied for special material parameters, given for each case. In this part, several special phenomena linked to shell/fluid coupling are studied.

2.4.4.1. Splitting of the fundamental acoustic resonance

If eigenfrequency of the first breathing shell mode is close to the first acoustic resonance, a splitting of the first acoustic impedance peak can be observed. In this case, the correction factor takes actually great values when frequency is in the vicinity of the first resonance frequency because in the expression of C (see (2.39)), both terms $\tan(kl)$ and $\left[\omega^2 - \omega_\mu^2 \cdot (1 - j\eta_\mu)\right]^{-1}$ take high values.

Numerical application has been carried out in the case of a polymer shell (see polymer B in table 2.2) having a Young's modulus $E=0.33\cdot10^9$ N/m^2 and a density ρ_S=1050kg/m^3 and for values of the geometrical parameters given in table 1. The modal

damping factor is set to $\eta_\mu = 0.01$. The frequency of the first breathing mode is $f_{R1}(m=0,q=1)=179Hz$ and the first acoustic resonance occurs for $f_1=171Hz$. In these conditions, the first mechanical resonance is next to the first acoustical resonance ($f_{R1} \approx f_1$) of the tube as shown in figure 2.9.

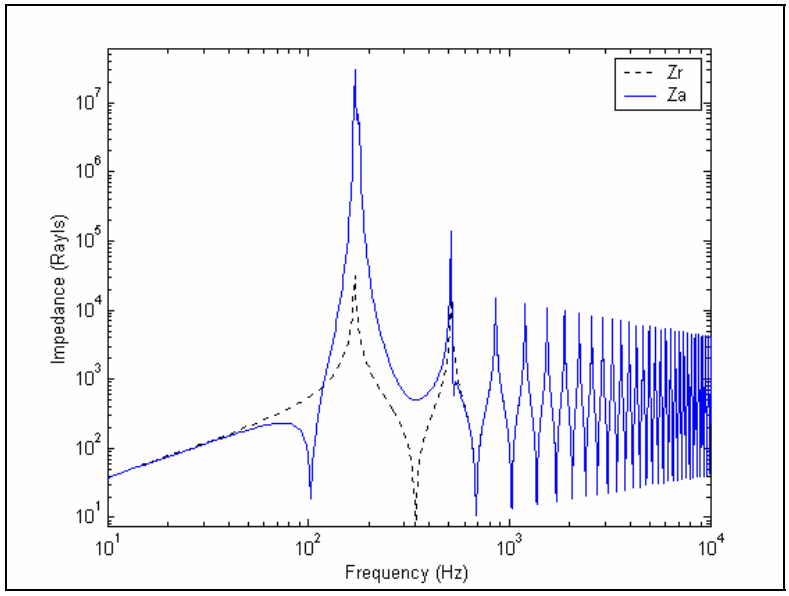

Figure 2.9: Acoustic input impedance of a rigid cylinder (Zr) and a wall vibrating cylinder (Za). The Young's modulus of polymer B is E= 0.09·109N/m2 and the density ρS=1050kg/m3 (f1=171Hz, fR1=179Hz). Only the breathing mode has been considered. An unfolding of the first acoustic resonance is produced.

Figure 2.10 zooms the splitting of the fundamental acoustic resonance produced in these circumstances. A difference of $|f_{R1}-f_1| \approx 8Hz$ between both peaks can be observed.

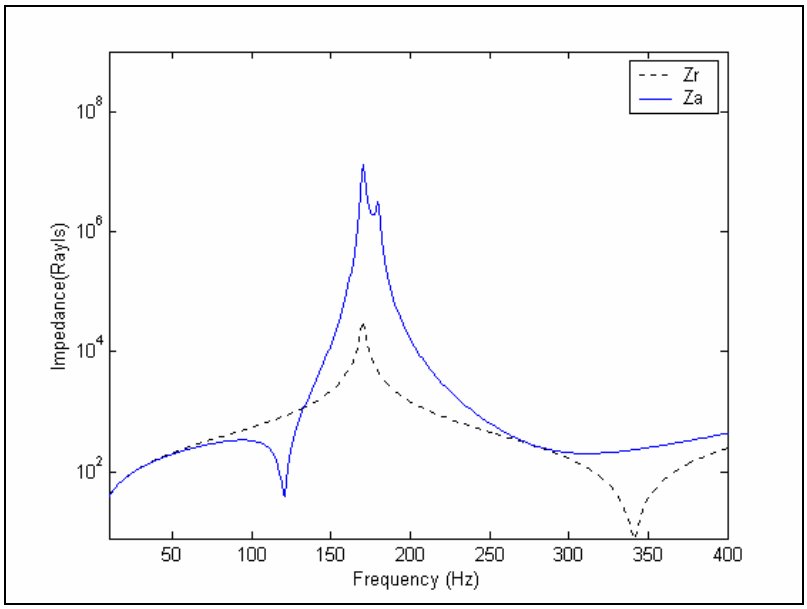

Figure 2.10: Acoustic input impedance of a rigid cylinder (Zr) and a wall-vibrating cylinder (Za) zoomed on the first acoustic resonance unfolded. The Young's modulus of polymer B is E= 0.09·109N/m^2 and the density ρ_S=1050kg/m^3. Only the breathing mode has been considered.

2.4.4.2. Mechanical Resonance and spatial coincidence effects satisfied simultaneously

When the mechanical resonance and the coincident condition are produced at near frequencies, the wall vibration effect becomes drastically important. This situation is satisfied if the Young's modulus and the density of the material of the shell's wall are appropriated. Young's modulus of the shell material has been chosen in a way that the shell resonance is produced at the coincidence frequency of the shell's first mode ($f_{R1}=f_{C1}=342$Hz). The correction factor for this frequency presents a significant peak much higher than unity. For a fixed value of the density of $\rho_S=1500$kg/m^3, the superposition of both effects is satisfied if the Young's modulus of the material of the shell is $E=0.47\cdot10^9$N/m^2. This couple of values (ρ_S,, E) refers to a polymer (see polymer C in table 2.2) and is of high interest because the vibration effect of the wall becomes very important. As it can be seen in figure 2.11, the acoustic input impedance of the vibrating cylindrical shell changes severely. Wall vibration effect becomes so important that the acoustic behaviour of the shell is no more comparable to the equivalent rigid shell.

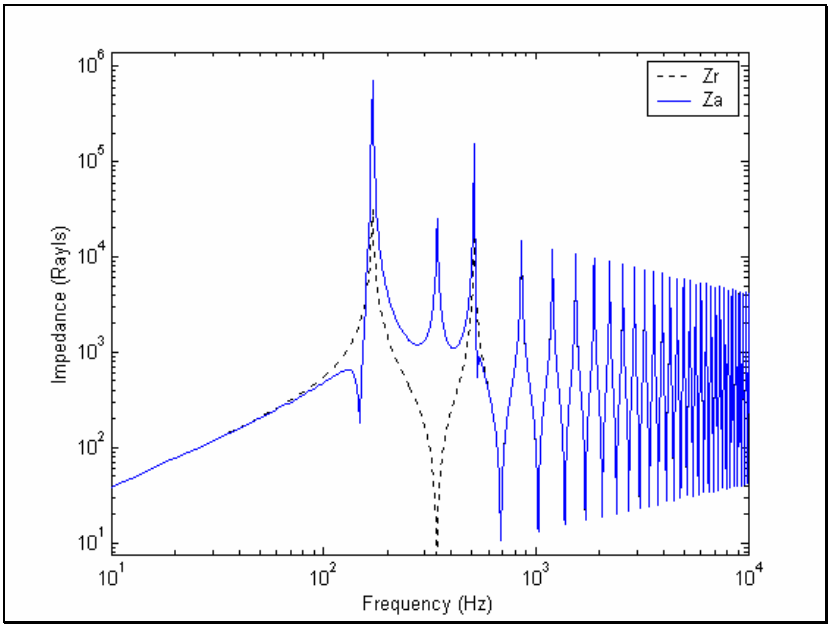

Figure 2.11: Acoustic input impedance of a rigid cylinder (Z^r) and a wall vibrating cylinder (Z^a). Only the breathing mode has been considered. The superposition of the first coincident condition and the first mechanical resonance is produced ($f_{C1}=f_{R1}=343$Hz). The Young's modulus of polymer C is E= 0.47·109N/m^2 and density $\rho_S=1500$kg/m^3.

2.4.4.3. Perturbation of the second acoustic resonance

Another special phenomenon can take place if the first mechanical resonance (f_{R1}) is produced at an acoustic resonance (f_1, f_2, f_3, …). As before, the wall vibration effect becomes very important. At this frequency, the correction factor is much greater than unity, and the superposition of both effects (structural and acoustical resonances) changes the input acoustic impedance of the cylinder. Figure 2.12 corresponds to the input acoustic impedance of a shell made of wood with $E=0.212\cdot10^9$N/m^2 and $\rho_S=300$kg/m^3 (see wood B in table 2.2). For this shell, the superposition of the first mechanical resonance and the second acoustic resonance of the cylinder ($f_{R1}=f_2=512$Hz) is produced.

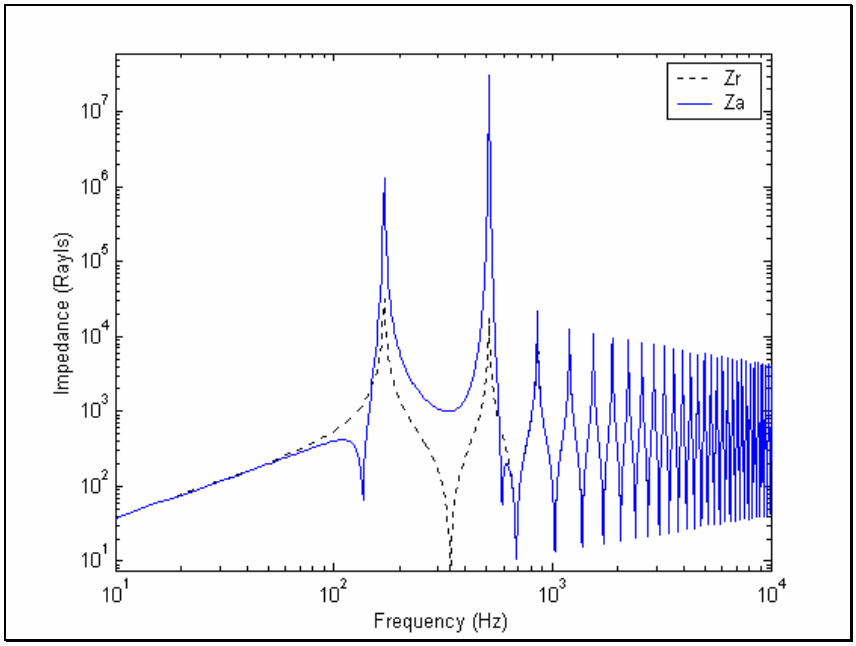

Figure 2.12: Acoustic input impedance of a rigid cylinder (Z^r) and a wall vibrating cylinder (Z^a). Only the breathing mode has been considered. The superposition of the second acoustic resonance and the first mechanical resonance is produced ($f_2=f_{R1}=512$). The Young's modulus of wood B is $E= 0.212\cdot10^9 N/m^2$ and density $\rho_S=300kg/m^3$.

2.4.5. Multimodal model analysis

In paragraph 2.4.1, the shell modal expansion has been restricted to the first shell breathing mode, allowing to identify and to understand main coupling effects. In this section, the effect of several breathing modes on the tube input acoustic impedance is considered. The cases of 2 and 10 modes are presented and generalized the conclusions of previous section.

Preliminary numerical simulations show that internal radiation impedances Z_i can be ignored in expression (2.27). As already mentioned in 3.1, this approximation is usual for light fluid and correspond to the fact that the response of the shell can be calculated ignoring fluid loading on it. If $\mathbf{Z_i}$ is set to zero in (2.27), it is seen that matrix **M** becomes diagonal and the correction factor can be expressed as

$$C = \mathbf{H}\cdot\overline{\mathbf{M}}^{-1}\cdot\mathbf{H}\cdot\overline{Z^r} = \sum_{\substack{q=1 \\ \mu=(0,q,1,1)}}^{Q} H_{\mu,(0,0,1)}\,\overline{M}^{-1}_{\mu\mu}\,H_{\mu,(0,0,1)}\,\overline{Z^r}\,, \qquad (2.44)$$

where $H_{\mu 1}$ and $M_{\mu\mu}$ are the terms contained on matrices **H** and **M** respectively (see (2.22), (2.27) and appendix 2.D for the notations). The terms of the sum in equation (2.44) correspond to the contributions of each shell breathing mode (defined by the q modal number) to the correction factor of the input acoustic impedance. Factor C can be expressed as

$$C(\omega) = 4\pi\rho \cdot c \sum_{\substack{q=1 \\ \mu=(0,q,1,1)}}^{Q} \frac{1}{m_\mu}\left(\frac{q\pi}{l}\right)^2 \frac{\omega \cdot \tan(\omega l/c)}{\left[(\omega/c)^2 - (q\pi/l)^2\right]^2 \left(\omega^2 - \omega_\mu^2 \cdot (1 - j\eta_\mu)\right)} \qquad (2.45)$$

The correction factor is shown on figure 2.13 for two shell modes (q=1 and q=2) of a shell made of steel. The consequence of considering two shell modes is that two coincidences and two resonances exist and lead to local maximums on the correction factor. Both spatial coincidence effects are satisfied at frequencies f_{C1}=342Hz and f_{C2}=684Hz. The two resonance effects are satisfied at frequencies f_{R1}=6344Hz and f_{R2}=3185Hz.

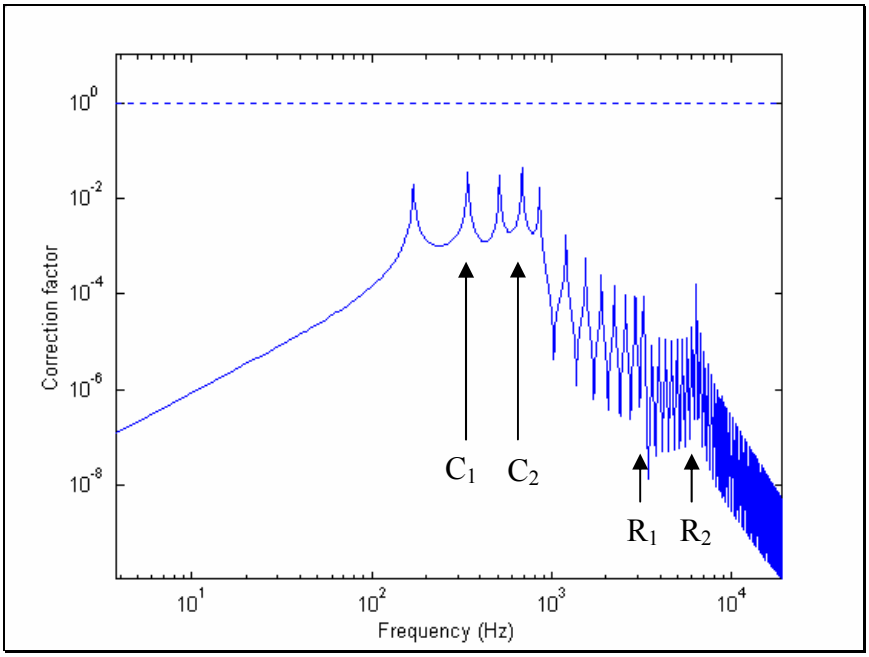

Figure 2.13: Correction factor of the acoustic input impedance induced by wall vibration of a steel shell. Two shell modes have been considered: The breathing (q=1) and the bending (q=2) modes. Peaks C_2 and R_2 correspond to the coincidence condition and the mechanical resonance of the bending mode, respectively. The Young's modulus of steel is E= 210·10⁹N/m² and the density ρ_S=7800kg/m³ (f_{C1}=342Hz, f_{C2}=684,f_{R1}=3218, f_{R2}=6436)

The wall vibration effect of a great number of mechanical modes is now considered. The truncation of the structural bases is fixed on 10 mechanical modes. Figure 2.14 shows the correction factor of the rigid input acoustic impedance.

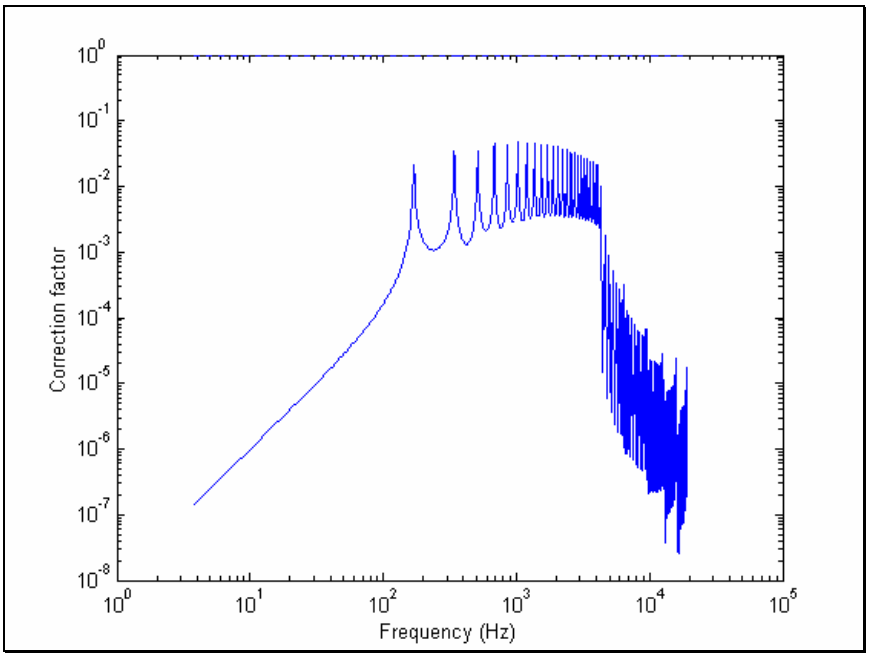

Figure 2.14: Correction factor of the acoustic input impedance induced by wall vibration. The structural modal basis has been truncated at 12 modes. The Young's modulus of the material of the structure is $E = 210 \cdot 10^9 N/m^2$ *and the density* $\rho_S = 7800 kg/m^3$

2.5. Conclusions

A vibroacoustic model of a simply-supported thin cylindrical shell is developed in order to evaluate the inner fluid/shell coupling and quantify the wall vibration effect on its acoustic behaviour. The input acoustic impedance matrix of the tube has been obtained. The plane acoustic mode interacts with the shell modes that have its same symmetry, and therefore, it is only coupled to the shell breathing modes. In general, vibroacoustic coupling is negligible and can be understood as a very small variation of the plane mode impedance of an equivalent rigid cylinder. However, for some special materials, the wall vibration effect becomes very important. Three phenomena underlay this singular behaviour: A mechanical resonance, a spatial coincidence effect and an acoustic resonance. If two of these phenomena take place simultaneously, the perturbation effect becomes significant and the acoustic resonances and antiresonances of the tube can be significantly altered.

Appendix 2.A: Structural modal basis

The aim of this appendix is to recall main results, allowing us to define the *in vacuo* modes of the shell $\mathbf{\Phi}_\mu$. These modes are used as a functional basis to express the shell displacement field. They can be written as [Lei73]

$$\mathbf{\Phi}_\mu = \begin{bmatrix} \Phi_{1\mu} \\ \Phi_{2\mu} \\ \Phi_{3\mu} \end{bmatrix} = \begin{bmatrix} U_\mu \cos(q\pi z/l)\cdot\sin(m\theta + s\pi/2) \\ V_\mu \sin(q\pi z/l)\cdot\cos(m\theta + s\pi/2) \\ \sin(q\pi z/l)\cdot\sin(m\theta + s\pi/2) \end{bmatrix}, \tag{A1}$$

where the subscript μ denotes the four indeces

$$\mu=(m, q, s, j), \tag{A2}$$

in which *m* denotes the circumferential index (m ≥ 0), *q* denotes the axial index (q ≥ 0), s is the index of symmetry (s=0,1), and j is the mode type index (j = 1 for bending modes, j = 2 for extension/compression modes, j =3 for twisting modes). The modal amplitudes U_μ, V_μ and the natural angular frequency ω_μ can be found by solving a 3 x 3 linear system as shown below.

The mode $\mathbf{\Phi}_\mu$, associated to the eigenpulsation ω_μ is the solution of the conservative homogeneous problem

$$\rho_s h\left(\omega_a^2 \mathcal{L} + \omega_\mu^2\right)\mathbf{\Phi}_\mu = 0\,. \tag{A3}$$

Note that it can be verified that the modes $\mathbf{\Phi}_\mu$ satisfy the useful a mass weighted orthogonality relationship [24]:

$$\rho_s h\left\langle \mathbf{\Phi}_\mu \middle| \mathbf{\Phi}_{\mu'} \right\rangle = \rho_s h \int_S \mathbf{\Phi}_\mu \mathbf{\Phi}_{\mu'}\, dS = \rho_s h \sum_{i=1}^{3} \left\langle \Phi_{i\mu}, \Phi_{i\mu'} \right\rangle_S = m_\mu \cdot \delta_{\mu\mu'}, \tag{A4}$$

where the generalized mass or modal mass m_μ, associated to the mode μ is defined by:

$$m_\mu = \frac{h\rho_S \pi\, al}{\varepsilon_m}\left(U_\mu^2 + V_\mu^2 + 1\right), \tag{A5}$$

and where ε_m is the Neumann factor (ε_m = 1 if m=0, ε_m = 2 if m>0), $\delta_{\mu\mu'}$ is the Kronecker notation, $\Phi_{i\mu}$ (i = 1, 2, 3) are the components of the vector $\mathbf{\Phi}_\mu$, and where the inner product $\langle\cdot|\cdot\rangle_s$ is defined by $\langle g | h\rangle_s = \int_s g h^* ds$.

Inserting the equation A1 into the homogeneous motion equation (A3), it can be seen that the condition $\left|\omega_a^2 \mathcal{L} + \omega_\mu^2\right| = 0$ provides the dispersion relationship of the *in vacuo* which can be written as:

$$\Omega^6 - K_4\Omega^4 + K_2\Omega^2 - K_0 = 0\,, \tag{A6}$$

where $\Omega = \dfrac{\omega}{\omega_a}$ is an non-dimensional angular frequency normalized to the ring frequency ω_a (7). Coefficients K_4, K_2, and K_0 depend on the geometrical and material parameters of the shell [22]. Eigenpulsations can be obtained numerically by solving equation (A7), or by using Cardan's relations, which give analytical expressions of the roots of a third order polynomial [25].

For each modal indices values *m* and *q,* the three roots of (A7) are indexed by the integer j (j = 1, 2 or 3). For each roots, the amplitudes U_μ, V_μ can be calculated from (A3). For thin shells, usually only the smaller solution, corresponding to j=1 produces a radial predominant mode. For this study, only this mode will be taken into account and we disregard the other two because their eigenfrequencies are in the ultrasound-range frequency.

Appendix 2.B: Acoustic modal basis

The Green's function of an infinite cylindrical tube can be written as a modal expansion [26], [12]:

$$G(M,M_0)=G\big(M(r,\theta,z),M_0(r_0,\theta_0,z_0)\big)=\frac{j}{2}\sum_{\alpha}\frac{\Psi_\alpha(M,\theta)\Psi_\alpha^*(M_0,\theta)}{k_{mn}}\cdot e^{jk_{mn}|z-z_0|}, \quad \text{(B1)}$$

where Ψ_α is the solution of the two-dimensional Neumann problem orthonormal eigenfunctions

$$\Psi_\alpha(r,\theta)=J_m(k_{Wmn}r)\cdot\sin(m\theta+s\pi/2)/\Lambda_\alpha \quad \text{(B2)}$$

where the normalization factor Λ_α is

$$\Lambda_\alpha^2=\frac{\pi a^2}{\varepsilon_m}\left(1-\gamma_{mn}^2\right)J_m^2(k_{Wmn}a),\ \text{with}\ \gamma_{mn}^2=\begin{cases}0 & m=0,\\ m^2/(k_{Wmn}a)^2 & m>0.\end{cases} \quad \text{(B3,B4)}$$

The longitudinal eigenvalues k_{mn} are given by $k_{mn}^2=k^2-k_{Wmn}^2$ $(\mathrm{Re}(k_{mn})\geq 0,$ $\mathrm{Im}(k_{mn})\geq 0)$ and the radial eigenvalue k_{Wmn} by $J_m'(k_{Wmn}a)=0$ $(k_{Wmn}\geq 0, n\geq 0)$. The subscript α is the triplet of integers α=(m, n, s), here m is the circumferential index ($m\geq 0$), n the radial index ($n\geq 0$), and s the index of symmetry (s = 0,1)

Appendix 2.C: Internal radiation impedances

The internal radiation impedances are defined by relation (24). If the excitation terms V_α are null, this relation reduces to

$$\left\langle p(M)\mathbf{n}\middle|\mathbf{\Phi}_\mu\right\rangle_S = j\omega\cdot\sum_{\mu'} Z^i_{\mu\mu'}A_{\mu'}\,, \tag{24}$$

Thus, impedances $Z^i_{\mu\mu'}$ (μ=(m,q,j,s) and μ'=(m',q',j,s')) describes the interactions between the shell and the internal fluid when Neumann and Dirichlet boundary conditions are applied on S_0 and S_L. The expressions of $Z^i_{\mu\mu'}$ have been obtained in [15]. Their normalized form is recalled with adapted notation:

For mutual-impedances ($\mu \neq \mu'$):

$$\frac{Z^i_{\mu\mu'}}{\rho c 2\pi l} = -j\frac{2}{\varepsilon_m}\frac{a}{l}ka\frac{q\pi a}{l}\frac{q'\pi a}{l}\sum_n \frac{\tan(k_{mn}l)}{k_{mn}a\left[1-\gamma^2_{mn}\right]\left[(k_{mn}a)^2-(q\pi a/l)^2\right]\left[(k_{mn}a)^2-(q'\pi a/l)^2\right]}.$$

For direct impedances ($\mu = \mu'$):

$$\frac{Z^i_{\mu\mu}}{\rho c 2\pi l} = -j\frac{2}{\varepsilon_m}\frac{a}{l}ka\left(\frac{q\pi a}{l}\right)^2\sum_n \frac{\tan(k_{mn}l)}{k_{mn}a\left[1-\gamma^2_{mn}\right]\left[(k_{mn}a)^2-(q\pi a/l)^2\right]^2} - \frac{j}{2\varepsilon_m}\frac{k}{k_q}\frac{J_m(k_q a)}{J'_m(k_q a)}$$

with

$$k_q = \sqrt{k^2-(q\pi/l)^2}\ ,\ \ \mathrm{Re}(k_q)\geq 0\,,\ \mathrm{Im}(k_q)\geq 0\,. \tag{C5}$$

Appendix 2.D: Matrix notations

For the shell considered, the resonance frequencies of the extension/compression (type index j=2) and twisting modes (type index j=3) have high values compared to those of the bending modes (j=1). Thus, only the bending modes are of interest and are taken into account. In order to simplify notations and without loss in generality, we consider the case where the acoustic excitation source (the acoustic velocity distribution on S_0) are symmetrical with respect to the plane (X,0,Z). Thus, the acoustic and vibratory responses are also symmetrical, which implies the symmetry index s being equal to 1 (s is present in relations A1 and B2). In the following, indeces s and j are set to 1. Vectors

$$\mathbf{A}_m = \begin{bmatrix} A_{(m,1,s,j)} \\ \vdots \\ A_{(m,Q,s,j)} \end{bmatrix}, \quad \mathbf{P}_m = \begin{bmatrix} P_{(m,0,s)} = \left\langle p \middle| \Psi_{(m,0,s)} \right\rangle \\ \vdots \\ P_{(m,N,s)} = \left\langle p \middle| \Psi_{(m,N,s)} \right\rangle \end{bmatrix}, \quad \mathbf{V}_m = \begin{bmatrix} V_{(m,0,s)} = \left\langle V_{S_0} \middle| \Psi_{(m,0,s)} \right\rangle \\ \vdots \\ V_{(m,N,s)} = \left\langle V_{S_0} \middle| \Psi_{(m,N,s)} \right\rangle \end{bmatrix} \tag{D1,D2,D3}$$

describe the unknown modal amplitudes for a given circumferential index m. For each m, the mechanical basis is truncated to Q modes and the acoustic basis is reduced to N modes. Grouping these amplitudes vectors as

$$\mathbf{A} = \begin{bmatrix} \mathbf{A}_1 \\ \vdots \\ \mathbf{A}_m \\ \vdots \\ \mathbf{A}_M \end{bmatrix}, \quad \mathbf{P} = \begin{bmatrix} \mathbf{P}_1 \\ \vdots \\ \mathbf{P}_m \\ \vdots \\ \mathbf{P}_M \end{bmatrix}, \quad \mathbf{V} = \begin{bmatrix} \mathbf{V}_1 \\ \vdots \\ \mathbf{V}_m \\ \vdots \\ \mathbf{V}_M \end{bmatrix}, \tag{D4,D5,D6}$$

we obtain modal amplitude vectors for the shell displacement **A**, the acoustic pressure **P** and the velocity **V**.

The rigid impedance matrix $\mathbf{Z}^{\mathbf{r}}$ corresponds to the input acoustic impedance of the cylinder with rigid walls, and therefore, it does not take into account wall vibration effect. It is built using the matrix impedances $\mathbf{Z}^r_{mm}$ associated to each circumferential index *m*

$$\mathbf{Z}^{\mathbf{r}} = \begin{bmatrix} \mathbf{Z}^r_{11} & 0 & 0 & 0 & 0 \\ 0 & \ddots & 0 & 0 & 0 \\ 0 & 0 & \mathbf{Z}^r_{mm} & 0 & 0 \\ 0 & 0 & 0 & \ddots & 0 \\ 0 & 0 & 0 & 0 & \mathbf{Z}^r_{MM} \end{bmatrix}, \tag{D9}$$

Matrices $\mathbf{Z}^r_{mm}$ correspond to the rigid impedance of each circumferential modal family m.

$$\mathbf{Z}^{r}_{mm} = \begin{bmatrix} Z^{r}_{(m,0,s),(m,0,s)} & 0 & 0 & 0 & 0 \\ 0 & \ddots & 0 & 0 & 0 \\ 0 & 0 & Z^{r}_{(m,n,s),(m,n,s)} & 0 & 0 \\ 0 & 0 & 0 & \ddots & 0 \\ 0 & 0 & 0 & 0 & Z^{r}_{(m,N,s),(m,N,s)} \end{bmatrix} \tag{D10}$$

The Boldtype of $\mathbf{Z}^{r}_{mm}$ represents the matricial character of the rigid impedance and each element write in italics $Z^{r}_{(m,n,s),(m,n,s)}$ represents a scalar.

The radiation impedance matrix $\mathbf{Z}^{\mathbf{i}}$ is given by

$$\mathbf{Z}^{\mathbf{i}} = \begin{bmatrix} \mathbf{Z}^{i}_{11} & 0 & 0 & 0 & 0 \\ 0 & \ddots & 0 & 0 & 0 \\ 0 & 0 & \mathbf{Z}^{i}_{mm} & 0 & 0 \\ 0 & 0 & 0 & \ddots & 0 \\ 0 & 0 & 0 & 0 & \mathbf{Z}^{i}_{MM} \end{bmatrix}, \tag{D11}$$

with

$$\mathbf{Z}^{i}_{mm} = \begin{bmatrix} Z^{i}_{(m,1,s,j),(m,1,s,j)} & \cdots & Z^{i}_{(m,Q,s,j),(m,1,s,j)} \\ \vdots & & \vdots \\ Z^{i}_{(m,Q,s,j),(m,1,s,j)} & \cdots & Z^{i}_{(m,Q,s,j),(m,Q,s,j)} \end{bmatrix}. \tag{D12}$$

Matrix

$$\mathbf{M} = \begin{bmatrix} \mathbf{M}_{11} & 0 & 0 & 0 & 0 \\ 0 & \ddots & 0 & 0 & 0 \\ 0 & 0 & \mathbf{M}_{mm} & 0 & 0 \\ 0 & 0 & 0 & \ddots & 0 \\ 0 & 0 & 0 & 0 & \mathbf{M}_{MM} \end{bmatrix}, \tag{D13}$$

with

$$\mathbf{M}_{mm} = \begin{bmatrix} M_{(m,1,s,j),(m,1,s,j)} & 0 & 0 & 0 & 0 \\ 0 & \ddots & 0 & 0 & 0 \\ 0 & 0 & M_{(m,q,s,j),(m,q,s,j)} & 0 & 0 \\ 0 & 0 & 0 & \ddots & 0 \\ 0 & 0 & 0 & 0 & M_{(m,Q,s,j),(m,Q,s,j)} \end{bmatrix} \tag{D14}$$

describes the mechanical behaviour of the shell. Finally, matrix **H** is given by:

$$\mathbf{H} = \begin{bmatrix} \mathbf{H}_{11} & 0 & 0 & 0 & 0 \\ 0 & \ddots & 0 & 0 & 0 \\ 0 & 0 & \mathbf{H}_{mm} & 0 & 0 \\ 0 & 0 & 0 & \ddots & 0 \\ 0 & 0 & 0 & 0 & \mathbf{H}_{MM} \end{bmatrix}, \tag{D15}$$

with

$$\mathbf{H}_{mm} = \begin{bmatrix} \mathbf{H}_{(m,1,s,j),(m,n,s)} & 0 & 0 & 0 & 0 \\ 0 & \ddots & 0 & 0 & 0 \\ 0 & 0 & \mathbf{H}_{(m,q,s,j),(m,n,s)} & 0 & 0 \\ 0 & 0 & 0 & \ddots & 0 \\ 0 & 0 & 0 & 0 & \mathbf{H}_{(m,Q,s,j),(m,n,s)} \end{bmatrix}, \tag{D16}$$

and with

$$\mathbf{H}_{(m,q,s,j),(m,n,s)} = \begin{bmatrix} H_{(m,q,s,j),(m,0,s)} & 0 & 0 & 0 & 0 \\ 0 & \ddots & 0 & 0 & 0 \\ 0 & 0 & H_{(m,q,s,j),(m,n,s)} & 0 & 0 \\ 0 & 0 & 0 & \ddots & 0 \\ 0 & 0 & 0 & 0 & H_{(m,Q,s,j),(m,N,s)} \end{bmatrix} \tag{D17}$$

Appendix 2.E: Viscothermal dissipative effects

Dissipative effects on the inner fluid can be taken into consideration by means of the complex sound velocity. An extended study of the propagation of harmonic plane waves in a cylindrical tube with perfectly rigid walls considering viscothermal dissipative effects can be found at [Bru98]. In this appendix, the expression of the complex sound velocity is presented. For an in-depth understanding of the matter, consultation to the aforementioned reference is recommended.

The complex speed c taken into account the viscothermal losses can be obtained

$$c = c_0\left[1+(1+j)\frac{\sqrt{2}}{a}k^{-1/2}\left[\left(1-\frac{k_{Wmn}^2-m^2/a^2}{k^2}\right)\sqrt{l_v'}+(\gamma-1)\sqrt{l_h}\right]\frac{1}{1-\gamma_{mn}^2}\right]^{-1/2}. \qquad \text{(E1)}$$

In this expression, γ is the ratio of heat capacities C_p/C_v (C_p at constant pressure, C_v at constant volume), k is the wavenumber given by $k=\omega/c_0$, being the speed of sound c_0 a real number. The characteristic lengths l_v' and l_h are defined by

$$l_v' = \frac{\mu}{\rho \cdot c_0} \qquad \text{(E2)}$$

and

$$l_h = \frac{\lambda M}{\rho \cdot c_0 C_p}, \qquad \text{(E3)}$$

where μ is the viscosity coefficient of the fluid, M is the molar mass and λ is the thermal conductivity coefficient. The radial wavenumber k_{Wmn} and the axial wavenumber k_{mn} are related by

$$k_{mn}^2 = \frac{\omega^2}{c^2} - k_{Wmn}^2. \qquad \text{(E4)}$$

Capítulo 3

Vibroacoustics of slightly distorted cylindrical shells: model of the acoustic input impedance

Este capítulo reproduce un artículo enviado para su publicación[1]*. En este trabajo se utiliza el mismo enfoque que en el capítulo 2 (artículo [PGR04]) con el objetivo de obtener una expresión matricial de la impedancia acústica de entrada de un tubo cilíndrico ligeramente deformado. La deformación del cilindro complica la resolución de la ecuación del movimiento de la estructura ya que el operador de Donell depende de las coordenadas angulares. El enfoque considerado para la resolución del problema se basa en el método propuesto por Yousri y Fahy [YF77]. En este método de resolución se asume que las bases modales acústica y mecánica de la estructura deformada son muy similares a las bases de la estructura no deformada y se utilizan para integrar la ecuación del movimiento.*

Suponiendo que la estructura esta poco deformada, se deduce que los defectos de la sección del tubo inducen un acoplamiento entre el modo acústico plano y los modos no axisimétricos. En particular, para un tubo cilíndrico de sección ligeramente elíptica, el primer modo plano está acoplado con el primer modo de ovalización de la estructura (m=2). A pesar de que este modo tenga un índice circuferencial mayor, su frecuencia propia es menor que la del primer modo de respiración (m=0). Por consiguiente, el comportamiento acústico del tubo que está gobernado por las frecuencias de resonancia acústicas, se ve fuertemente alterado por este acoplamiento vibroacustico adicional.

Al final del capítulo, se presentan varios resultados numéricos que muestran el efecto de la deformación de la estructura en el comportamiento acústico del tubo sonoro. Se consideran diferentes materiales y distintos grados de deformación.

[1] *Enviado para su publicación a la revista* Acta Acustica *en junio de 2004*

Ce chapitre reproduit un article soumis à la revue Acta Acustica. L'approche retenue dans le chapitre précédent (chapitre 2, [PGR04]) est utilisée ici pour obtenir une expression de la matrice impédance d'entrée d'un tuyau cylindrique faiblement ovalisé. L'ovalisation (appelée encore distorsion) complique la résolution de l'équation de mouvement de la structure puisque l'opérateur de Donnell dépend dans ce cas de la coordonnée angulaire. L'approche retenue se base sur la méthode proposée par Yousri et Fahy en [YF77]. Dans cette méthode, les bases modales acoustique et mécanique de la structure déformées sont supposées très proches des bases du cylindre de section parfaitement circulaire et, ces dernières sont utilisées pour intégrer l'équation de mouvement de la coque.

Après l'introduction qui fait l'objet de la première partie, on montre dans la seconde partie que pour un tube cylindrique faiblement distordu, les défauts de section du tuyau induisent un couplage entre le mode acoustique plan et les modes non axisymétriques. En particulier, dans le cas d'un tuyau cylindrique de section elliptique, dont l'étude fait l'objet de la partie 3, le mode acoustique plan est couplé au premier mode d'ovalisation de la coque (mode correspondant à un indice circonférenciel m=2). La fréquence propre de ce dernier est plus faible que celle du premier mode de respiration (correspondant à m=0), et ce bien que son indice circonférenciel soit plus grand. Ce mode d'ovalisation est le premier mode de coque ou mode fondamental. Il est en conséquence le premier à interagir avec le mode acoustique plan. Cette interaction s'effectue via le défaut d'ovalisation et induit un couplage additionnel par rapport au cas où la section est parfaitement circulaire. Le comportement acoustique du tuyau, qui est régit par les fréquences de résonance acoustiques, est alors fortement altéré par ce couplage vibroacoustique additionnel. En fin du chapitre, plusieurs applications numériques sont présentées qui montrent l'effet de la distorsion du tube sur le comportement acoustique du tuyau sonore. Le rôle de différents matériaux, ainsi que l'influence du paramètre d'ovalisation sont étudiés.

3.1. Introduction

Vibracoustics of cylindrical ducts is widely developed for applications in mechanical engineering such as noise induced by industrial pipes for example. As a first approach, the interactions between the acoustic oscillations of the internal fluid and the vibrations of the duct can be described considering that the cross-section of the duct is perfectly circular. In practice, small defaults of the circularity of the cross section always exist and such an out of roundness induces couplings between structural and acoustic modes, which do not exist in the case where the cross-section is perfectly circular. The aim of this study is to present a model allowing taking into account these additional couplings induced by geometrical defects of the shell.

The final application of this study is related to musical acoustics. It concerns the problem of quantifying the effect of the wall vibrations of the body of a wind instrument on sound which is emitted [Smi86]. In order to quantify this effect, a generic model of a simplified clarinet-like instrument has been developed [GT98a], [PGR04] and constitute the support of the investigation presented in this paper. This simplified instrument is a cylindrical vibrating duct, excited acoustically by a particle velocity distribution at the input cross section. It has been shown in [GT98a] that the wall vibrations induce several vibroacoustic couplings: inner fluid/shell coupling, external fluid/shell coupling, coupling induced by acoustic radiation at the open end of the tube. Description of such couplings is generally complex and lead to the conclusion that these effects are generally very small and can be neglected since they do not induce audible contribution. However for some particular characteristics of the duct (that is particular choice of material and geometry), wall vibration can play a significant role: in a recent study [PGR04], where the same notations and formalism as in this paper have been used, acoustic input impedance of a vibrating cylindrical shell whose cross section is perfectly circular has been studied. It has been shown that the coupling between the first breathing shell mode and the plane acoustic mode can have a strong influence on the input impedance of the plane mode if spatial coincidence and resonance condition take place at the same frequency. These conditions can be satisfied only if the eigenfrequency of the first breathing mode is equal to the one of the first acoustic antiresonance of the duct. Moreover, if the eigenfrequency of the first breathing mode is equal to the one of the first acoustic resonance, a splitting of the resonance peak of the impedance curve can be observed. For fixed geometrical parameters (shell length, thickness and radius), this kind of condition is only satisfied if the Young's modulus and the density of the wall material are low enough, reaching unrealistic values for the body of a wind instrument. Note that the model of the impedance of a vibrating tube can be used to compute time domain simulations of clarinet's sounds (see [GGA95] for a presentation of the method and [PGG04] for an application to a vibrating tube). Hearing tests on the musical sound allow determining when the wall vibration effect becomes audible.

Models of non-circular cylindrical shells have been developed in the literature. A thin shell operator is a differential operator connecting the displacement field of the mean surface of the shell to the external loads applied to the shell. A presentation of shell theories is given in [Lei73]. Such operator is local and thus, depends on the local curvatures of the medium. For a perfect cylinder, the curvatures are equal to the shell's radius in one direction and to infinity in the other direction. If the curvatures are dependent on the point chosen on the shell, the operator has spatial-dependant

coefficients. Motion equation takes in this case a complicated form, but can be solved using appropriated series expansions: [Ele93]. The radiation of such distorted shells have been studied using this approach [Max95], [Lau93]. In a more general way, the description of complicating effects such as the influence of shell stiffening or defects on the shell introduced by added masses, is discussed in [GL94].

The state vector method constitutes another way to compute the vibratory field of a distorted shell. This method can be applied if the shell vibratory field can be described using separated variables and if the axial dependence of the field is known. This is the case for infinite or simply supported shells, in which the axial dependence of the displacement field can be assumed to be proportional to *sin* (mπx/L). Thus, the motion equation can be written as a first order differential equation, depending on the circumferential coordinate. This kind of equation is called state equation. A presentation of such equations to model beam, plate and shell vibrations is given for example in [Pes63], [WN95], [Mou03]. A numerical integration of the state equation whose parameters depend on the circumferential direction provides the solution of the problem. This method has been applied to shell having different types of circumferential profiles in [YIT84], [IYK84], [SM82].

In this paper, we consider that the shell is slightly distorted, which corresponds to a small ovalisation of the cross-section of the shell. In this case, it is possible to assume that the mode shapes and the eigenfrequencies are close to their values when the distortion parameter is equal to zero. Following [YF77], such a hypothesis allows describing the coupling between acoustic and structural modes of different circumferential orders in a distorted shell. The main objective of this paper is to determine the influence of the vibration of the distorted shell on its input impedance matrix.

The structure of the paper is as follows: after this introduction, in section II, a model of the acoustic impedance matrix of a vibrating slightly distorted shell is presented. Governing equations of the shell/internal fluid coupled problem fluid equation are given and solved in the framework of the light fluid approximation. The forced response of the system to a prescribed acoustic excitation is obtained using projections of the vibratory and acoustic fields on appropriated functional bases: the *in vacuo* shell modes for the structural displacement field and acoustical transverse modes for the acoustic field. The *in vacuo* shell modes are those of a shell having a perfectly circular cross section. The input impedance matrix is determined from the forced response of the system. In section III, attention is focused on the interaction of the plane acoustic mode with the first structural modes. Appropriate truncation of the functional bases is presented and coupling between the plane acoustic mode and the first structural modes (ovaling mode and breathing mode) is studied and illustrating examples are given. To conclude, a summary of the results is presented.

3.2. Vibroacoustic model

3.2.1. Statement of the problem

3.2.1.1. Equation of motion for a distorted shell

We consider a thin-walled cylindrical shell of length *l,* and thickness *h*. This shell is supposed to be slightly distorted: its mean radius is a, and the variation of its radius is supposed to be on the form:

$$r(\theta) = a\cdot(1 + \varepsilon\cdot\cos(t\cdot\theta)), \tag{3.1}$$

where ε <<1 is the non-dimensional magnitude of the distortion, t is an integer number describing the type of distortion along the length of the shell (for an elliptical shell t=2) and θ is the angular coordinate in the cylindrical system axis (see figure 3.1).

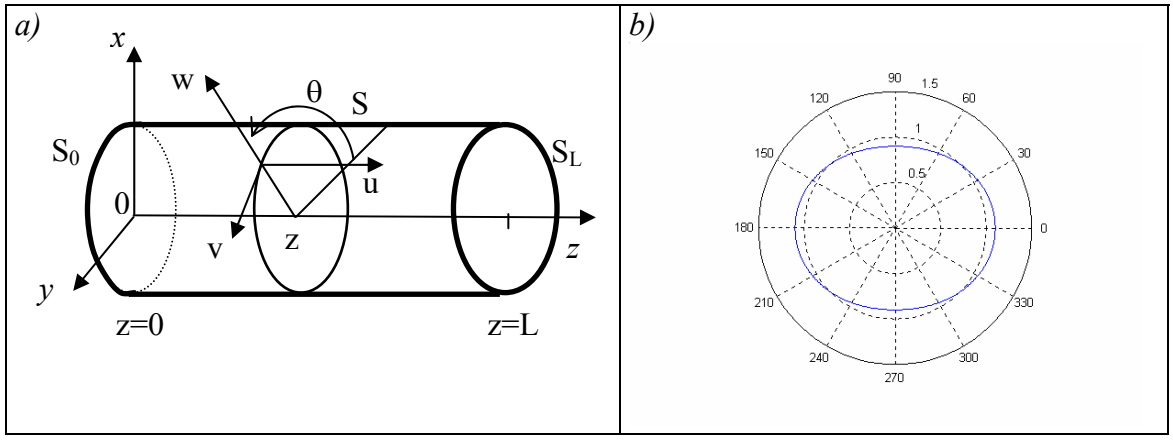

Figure 3.1: Representation of the distorted shell. a) Axial profile and notations and b) cross-section

The shell is made from a homogeneous, isotropic material whose Young's modulus is E, density is ρ_s and Poisson's ratio is σ. The shell is supposed to be simply supported at both ends (z = 0, *l)*.

For a perfectly circular shell (non distorted case $\varepsilon = 0$), the shell's motion equations in harmonic regime can be put on the following form (convention $e^{-j\omega t}$ is adopted, ω being the driving frequency):

$$\rho_s h\left(\omega_a{}^2 \mathcal{L} + \omega^2\right)\mathbf{X}(M) = -p(M)\mathbf{n} \quad \text{for} \quad M \in S, \tag{3.2}$$

where ω_a is the shell ring frequency, $\mathcal{L}$ is the Donnell operator, *X(M)* is the displacement vector of the point *M* belonging to the neutral surface *S* of the shell, *p(M)* is the inner acoustic pressure and **n** denotes a unitary vector normal to the *S* surface. The displacement vector X(M) has the form

$$X(M) = \left[u(M) \quad v(M) \quad w(M)\right]^t \tag{3.3}$$

where *u(M), v(M), w(M)* denote longitudinal, orthoradial and radial displacements of the shell (see figure 3.1).

For a distorted shell, the motion equation is written in the form:

$$\rho_s h\left(\tilde{\omega}_a{}^2 \tilde{\mathcal{L}} + \omega^2\right)\mathbf{X}\left(\tilde{M}\right) = -\tilde{p}\left(\tilde{M}\right)\mathbf{n} \quad \text{for} \quad \tilde{M} \in \tilde{S}\,, \tag{3.4}$$

where symbol ~ refers to elements related to the distorted shell. Parameter $\tilde{\omega}_a$ is defined by

$$\tilde{\omega}_a(\theta) = \frac{1}{r(\theta)}\sqrt{\frac{E}{\rho_S\left(1-\nu^2\right)}}\,. \tag{3.5}$$

and coincide with the ring frequency in the case of a non distorted shell (r(θ)=*a*). $\tilde{\mathcal{L}}$ is the Donnell operator of the distorted shell given by

$$\tilde{\mathcal{L}} = r(\theta)^2 \begin{bmatrix} \dfrac{\partial^2 \cdot}{\partial z^2} + \dfrac{1-\nu}{2}\dfrac{\partial^2 \cdot}{\partial s^2} & \dfrac{1+\nu}{2}\dfrac{\partial^2 \cdot}{\partial z \partial s} & \nu\dfrac{\partial \cdot}{\partial z} \\ \dfrac{1+\nu}{2}\dfrac{\partial^2 \cdot}{\partial z \partial s} & \dfrac{\partial^2 \cdot}{\partial s^2} + \dfrac{1-\nu}{2}\dfrac{\partial^2 \cdot}{\partial z^2} & \dfrac{\partial \cdot}{\partial s} \\ -\nu\dfrac{\partial \cdot}{\partial z} & -\dfrac{\partial \cdot}{\partial s} & -1-\beta\left(\dfrac{\partial^2 \cdot}{\partial z^2} + \dfrac{\partial^2 \cdot}{\partial s^2}\right) \end{bmatrix}, \tag{3.6}$$

in which *z* is the axial co-ordinate, *s* is the curvilinear co-ordinate in the circumferential direction, and where adimensional thickness parameter is defined by $\beta = \dfrac{h^2}{12r^2}$. For a non-distorted shell, the curvilinear co-ordinate *s* is given by $s=a\theta$ and expression (3.6) coincides with the Donnell operator [Lei73]. For a distorted shell, derivatives according to variable of *s* in (3.6) can be expressed as function of the circumferential co-ordinate θ. Such calculations are presented in detail in [Ele93] and lead to complex expressions of the operator. In order to avoid having to use them, we choose the simplified method proposed by [YF77], as we present next.

Note that in relation (3.4), $\tilde{S}$ is the surface of the distorted shell, $\tilde{p}\left(\tilde{M}\right)$ is the inner acoustic pressure at point $\tilde{M}$ belonging to $\tilde{S}$ and $\tilde{X}\left(\tilde{M}\right)$ is the shell displacement vector.

3.2.1.2. Helmholtz equation

Inside the cylindrical cavity, the acoustic pressure obeys the Helmholtz equation,

$$\left(\Delta + k^2\right)\tilde{p}\left(\tilde{M}\right) = 0\,, \tag{3.7}$$

where $k=\omega/c$ is the acoustic wave number. Dissipative visco-thermal effects induced by acoustic boundary layers can be taken into account by means of the complex sound velocity c (see [GT98a]).

Equation (3.7) is associated to appropriate acoustic boundary conditions on the shell surface $\widetilde{S}$ and the cross sections $\widetilde{S}_0$ (at z=0) and $\widetilde{S}_L$ (at z=L) (see figure 1 for definition of these surfaces*)*. On the surface $\widetilde{S}_0$, the acoustic normal velocity $\widetilde{v}(\widetilde{M})$ is supposed to be equal to a known value denoted $\overline{v}_{S_0}(\widetilde{M})$:

$$\widetilde{v}\left(\widetilde{M}\right)=\overline{v}_{S_0}\left(\widetilde{M}\right), \qquad \text{for } \widetilde{M}\in\widetilde{S}_0 . \tag{3.8}$$

The acoustic velocity distribution $\overline{v}_{S_0}(\widetilde{M})$ is considered as the excitation source of the system. On the lateral surface $\widetilde{S}$, continuity of the normal velocities of the fluid $\widetilde{v}_a(\widetilde{M})$ and of the shell $\dot{\widetilde{w}}\left(\widetilde{M}\right)$ is expressed as

$$\widetilde{v}_a(\widetilde{M})=\dot{\widetilde{w}}\left(\widetilde{M}\right), \qquad \text{for } \widetilde{M}\in\widetilde{S} . \tag{3.9}$$

On the surface $\widetilde{S}_L$, the tube is supposed to be open and we consider that the acoustic pressure is equal to zero:

$$\widetilde{p}(\widetilde{M})=0 \qquad \text{for} \qquad \widetilde{M}\in\widetilde{S}_L . \tag{3.10}$$

3.2.1.3. The coupled problem

The inner acoustic field $\widetilde{p}\left(\widetilde{M}\right)$ and the wall displacement field $\widetilde{X}\left(\widetilde{M}\right)$ are the solutions of the coupled problem described by (3.4) and (3.7), associated to the simply supported boundary conditions for the shell and to acoustic boundary conditions (3.8), (3.9), (3.10). Both acoustic and mechanical equations underlay the vibroacoustic nature of the coupled problem. The method of resolution consists in determining the forced response of the problem to the known velocity distribution $\overline{v}_{S_0}(\widetilde{M})$. This response provides the input acoustic impedance of the wall vibrating distorted cylinder which is the searched quantity.

3.2.2. Resolution method

3.2.2.1. Expansion of the shell displacement field on a functional basis

The distorted shell displacement field is expanded on the *in vacuo* shell modes of a shell having a perfectly circular cross section. These modes have the form

$$\mathbf{\Phi}_\mu=\begin{bmatrix}\Phi_{1\mu}\\ \Phi_{2\mu}\\ \Phi_{3\mu}\end{bmatrix}=\begin{bmatrix}U_\mu\cos(q\pi z/l)\cdot\sin(m\theta+s\pi/2)\\ V_\mu\sin(q\pi z/l)\cdot\cos(m\theta+s\pi/2)\\ \sin(q\pi z/l)\cdot\sin(m\theta+s\pi/2)\end{bmatrix}, \tag{3.11}$$

where μ= (m,q,j,s) is a set of 4 modal indices: m is the circumferential index, q is the axial index, j is the type index and s is the symmetry index. For thin shells, usually only the smaller solution, corresponding to j=1 produces a radial predominant mode. For this study, only this mode will be taken into account and we disregard the other two because their eigenfrequencies are in the ultrasound-range frequency. Thus, from now on, the structural modal indeces are considered as the triplet: μ= (m,q,s).

The modal amplitudes U_μ and V_μ are determined using the shell motion equation. The modes $\mathbf{\Phi}_\mu$ constitute a functional basis on which the vibratory field can be expanded [GL94]. We assume that

$$\widetilde{\mathbf{X}}(\widetilde{M}) = \sum_{\mu} \widetilde{A}_\mu \mathbf{\Phi}_\mu(\widetilde{M}), \tag{3.12}$$

where $\widetilde{A}_\mu$ are the unknown modal amplitudes. Such a choice allows us to avoid the computation of the *in vacuo* modes of the distorted shell. Moreover, since the ovalisation parameter ε is small compared to 1, it seems also reasonable to suppose that the modes shapes of the non-distorted shell $\widetilde{\mathbf{\Phi}}_\mu$ (associated to the eigenfrequency $\widetilde{\omega}_\mu$) are similar to the modes shapes of the non-distorted shell $\mathbf{\Phi}_\mu$ (associated to the eigenfrequency ω_μ). The first important assumption of the model is expressed as

$$\widetilde{\mathbf{\Phi}}_\mu \cong \mathbf{\Phi}_\mu . \tag{3.13}$$

For a non distorted shell, the mode defined by μ=(m,q,0), (having the modal symmetry index s=0) has the same axial dependence as the mode μ=(m,q,1),), (having the modal symmetry index s=1))) but it is rotated by the angle 2π/m. These two types of modes are degenerated since their eigenfrequencies are the same. The main difference between the modal basis of the distorted and the non-distorted shell remains in the fact that the eigenfrequencies of the circular shell are split by the shell's defect. However, because the frequency shift induced by this splitting is supposed to be small and do not introduce any additional coupling effect, this frequency shift is ignored and we have:

$$\widetilde{\omega}_\mu \cong \omega_\mu . \tag{3.14}$$

3.2.2.2. Projection of the motion equation

Dividing equation (3.4) by $\widetilde{\omega}^2{}_a$ and projecting it on mode $\mathbf{\Phi_\mu}$, leads to

$$\sum_{\mu} \widetilde{A}_\mu \left\{ \int_S \rho \cdot h \mathbf{\Phi}_\mu \widetilde{\mathbf{L}} \mathbf{\Phi}_{\mu'} dS + \int_S \rho \cdot h \mathbf{\Phi}_\mu \mathbf{\Phi}_{\mu'} \frac{\omega^2}{\widetilde{\omega}_a^2} dS \right\} = -\int_S \frac{\widetilde{p} \mathbf{n} \mathbf{\Phi}_{\mu'}}{\widetilde{\omega}_a^2} \tag{3.15}$$

The modes of the distorted shell $\widetilde{\mathbf{\Phi}}_\mu$ associated to the eigenfrequency $\widetilde{\omega}_\mu$ obeys the homogeneous equation of motion:

$$\widetilde{\omega}_a^2 \widetilde{\boldsymbol{L}} \widetilde{\mathbf{\Phi}}_\mu + \widetilde{\omega}_\mu^2 \widetilde{\mathbf{\Phi}}_\mu = 0 \tag{3.16}$$

Considering assumptions (3.13) and (3.14), equation (3.15) leads to

$$\widetilde{\boldsymbol{L}} \mathbf{\Phi}_\mu \cong -\frac{\omega_\mu^2}{\widetilde{\omega}_a^2} \mathbf{\Phi}_\mu \tag{3.17}$$

With this approximation, the shell motion equation (3.15) can be written as:

$$\sum_\mu \widetilde{A}_\mu \left\{ \int_S \rho \cdot h \mathbf{\Phi}_\mu \frac{\omega^2 - \omega_\mu^2}{\widetilde{\omega}_a^2} \mathbf{\Phi}_{\mu'} dS \right\} \cong -\int_S \frac{\widetilde{p} \mathbf{n} \mathbf{\Phi}_{\mu'}}{\widetilde{\omega}_a^2} dS \tag{3.18}$$

It must be pointed out that the dependency of $\widetilde{\omega}_a = \widetilde{\omega}_a(\theta)$ is linked to the distortion of the shell. As a second important assumption, we neglect this dependency in the left hand term of (3.18) which is written as

$$\sum_\mu \widetilde{A}_\mu \frac{\omega^2 - \omega_\mu^2}{\omega_a^2} \int_S \rho \cdot h \mathbf{\Phi}_\mu \mathbf{\Phi}_{\mu'} dS \cong -\int_S \frac{\widetilde{p} \mathbf{n} \mathbf{\Phi}_{\mu'}}{\widetilde{\omega}_a^2} dS \tag{3.19}$$

The modes $\mathbf{\Phi_\mu}$ are normal modes and obey the orthogonality relationship

$$\int_S \rho \cdot h \mathbf{\Phi}_\mu \mathbf{\Phi}_{\mu'} dS = m_\mu \delta_{\mu\mu'} \tag{3.20}$$

where the modal mass m_μ of the mode $\mathbf{\Phi_\mu}$ is defined as

$$\mathrm{m}_\mu = \int_S \rho \mathbf{\Phi}_\mu \mathbf{\Phi}_\mu \mathrm{dS} \ , \tag{3.21}$$

and where $\delta_{\mu\mu'}$ denotes the Kronecker symbol. Using orthogonality relationship (3.20) and the series expansion,

$$\frac{1}{\widetilde{\omega}_a^{\ 2}} \cong \frac{1 + 2\varepsilon \cos(t\theta)}{\omega_a^{\ 2}}, \tag{3.22}$$

relation (3.19) takes the form

$$m_{\mu'}\cdot\left(\omega^2-\omega_{\mu'}^2\right)\widetilde{A}_{\mu'}\cong-\int_S(1+2\varepsilon\cos(t\theta))\widetilde{p}(M)\mathbf{n}.\mathbf{\Phi}_{\mu'}(M)dS \tag{3.23}$$

The shell mechanical damping can be taken into account by introducing an structural damping term (involving $\eta_{\mu'}$ parameter) for each structural mode μ' into the equation (3.23).

$$m_{\mu'}\cdot\left(\omega^2-\omega_{\mu'}^2\left(1-j\eta_{\mu'}\right)\right)\widetilde{A}_{\mu'}\cong-\int_S(1+2\varepsilon\cos(t\theta))\widetilde{p}(M)\,\mathbf{n}\,\mathbf{\Phi}_{\mu'}(M)\,dS \tag{3.24}$$

Equation (3.24) shows that coupling between the plane acoustic wave and non-axisymmetric structural modes is permitted by the defects since in this case the right hand term of the equation is not equal to zero. This equation is equivalent to that presented by S. N. Yousri and F. J. Fahy in [YF77], but with the notations used in this work.

3.2.2.3. Determination of the inner acoustic field

In order to compute the forced response of the shell, the acoustic pressure $\widetilde{p}\left(\widetilde{M}\right)$ acting on the shell has to be replaced in the motion equation (3.24) by its expression according to the displacement field of the shell. Such expression is obtained using the integral representation [Bru98]. Considering that the surfaces S and $\widetilde{S}$ are the same, we can write the inner acoustic pressure as

$$\widetilde{p}(\widetilde{M})\cong p(M)=\int_{S\,,S,S_l}\left[G(M,M_0)\partial_n P(M)-p(M)\partial_n G(M,M_0)\right]dS_0 \tag{3.25}$$

The Green's function

$$G(M,M_0)=\frac{j}{2}\sum_\alpha\frac{\Psi_\alpha(M,\theta)\Psi_\alpha^*(M_0,\theta)}{k_{mn}}\cdot e^{jk_{mn}|z-z_0|} \tag{3.26}$$

is the Green's function of the infinite cylinder satisfying Neumann boundary conditions on the S surface of the wall. The acoustic modes $\Psi(r,\theta)$ are those of a non distorted cross section and are given by [MI86], [GT98a] and [PGR04]

$$\Psi_\alpha(r,\theta)=J_m\left(k_{Wmn}r\right)\cdot\sin\left(m\theta+s\pi/2\right)/\Lambda_\alpha\,, \tag{3.27}$$

where the normalization factor Λ_α is

$$\Lambda_\alpha^2=\frac{\pi a^2}{\varepsilon_m}\left(1-\gamma_{mn}^2\right)J_m^2\left(k_{Wmn}a\right),\ \text{with}\ \gamma_{mn}^2=\begin{cases}0 & m=0,\\ m^2/\left(k_{Wmn}a\right)^2 & m>0.\end{cases} \tag{3.28, 3.29}$$

The longitudinal eigenvalues k_{mn} are given by $k_{mn}^2=k^2-k_{Wmn}^2$ ($\mathrm{Re}(k_{mn})\geq 0$, $\mathrm{Im}(k_{mn})\geq 0$), the radial eigenvalue k_{Wmn} by $J_m'\left(k_{Wmn}a\right)=0$ $\left(k_{Wmn}\geq 0, n\geq 0\right)$ and ε_m is

the Neumann factor (ε_m = 1 if m=0, ε_m = 2 if m>0). The triplet $\alpha=(m,n,s)$ is used to group the 3 indices m,n,s which are circumferential, radial and symmetry modal indices respectively. Note that in expression (3.25), it has been supposed that $\widetilde{\Psi}(r,\theta)=\Psi(r,\theta)$. This is justified by the fact that the ovalisation parameter is supposed to be very small. The modes $\Psi_\alpha(r,\theta)$ play the role of a functional basis on which the acoustical field is expanded.
Using relations (3.8), (3.9), (3.10), the general expression of the field can be expressed as the superposition of travelling waves propagating in opposite directions with amplitudes depending on z:

$$\widetilde{p}(r,\theta,z)=\sum_{\alpha=(m,n,s)}\left[\left\{\widetilde{B}_\alpha^+ + \widetilde{D}_\alpha^+(z)\right\}e^{jk_{mn}z} + \left\{\widetilde{B}_\alpha^- + \widetilde{D}_\alpha^-(z)\right\}e^{jk_{mn}(l-z)}\right]\Psi_\alpha(r,\theta). \tag{3.30}$$

In relation (3.30), we keep the notation ~ since this expression takes into account the vibration of the distorted shell via the amplitude terms $\widetilde{D}_\alpha^+(z)$, $\widetilde{D}_\alpha^-(z)$, $\widetilde{B}_\alpha^+$, $\widetilde{B}_\alpha^-$. They are defined by

$$\widetilde{D}_\alpha^+(z)=\frac{-\rho}{2k_{mn}}\int_0^{2\pi}\int_0^z \dot{\tilde{w}}(z,\theta)\,e^{-jk_{mn}z_0}\Psi_\alpha(a,\theta)\,r\,d\theta \tag{3.31}$$

$$\widetilde{D}_\alpha^-(z)=\frac{-\rho}{2k_{mn}}\int_0^{2\pi}\int_z^l \dot{\tilde{w}}(z,\theta)\,e^{-jk_{mn}(z_0-l)}\Psi_\alpha(a,\theta)\,r\,d\theta \tag{3.32}$$

and

$$\widetilde{B}_\alpha^+ = \frac{1}{1+e^{2jk_{mn}l}}\left[\langle\overline{v}_{So}\,|\,\Psi_\alpha(r,\theta)\rangle_{S_0} + \widetilde{D}_\alpha^-(0)e^{jk_{mn}l} - \widetilde{D}_\alpha^+(l)e^{2jk_{mn}l}\right] \tag{3.33}$$

$$\widetilde{B}_\alpha^- = \frac{1}{1+e^{2jk_{mn}l}}\left[-\langle\overline{v}_{So}\,|\,\Psi_\alpha(r,\theta)\rangle_{S_0} - \widetilde{D}_\alpha^-(0)e^{2jk_{mn}l} - \widetilde{D}_\alpha^+(l)e^{jk_{mn}l}\right] \tag{3.34}$$

The inner product $\langle .|. \rangle$ used in (3.33), (3.34) is defined by the relationship $\langle f\,|\,g\rangle=\int_S f\,g^*\,dS$.

3.2.2.4. Light fluid approximation

Light fluid approximation is considered for the determination of the acoustic pressure $\widetilde{p}$, which is involved in the shell motion equation (3.24). The physical meaning of this approximation is schematically explained in figure 3.2. The block diagram describes the shell/inner fluid interaction when considering the approximation of light fluid in 5 steps. Several relations, using matricial relations introduced later are indicated on this figure.

1.- The tube is excited on the cross section $\widetilde{S}_0$ at the entrance by an imposed velocity $\overline{v}_{S_0}(\widetilde{M})$.

2.- An acoustic pressure field denoted p_a is generated in the tube by the excitation. At this stage, wall vibration effect on the inner pressure field is not considered and the pressure p_a is called 'blocked pressure'. This blocked pressure p_a is noted without ~ because it does not depend on the wall distortion.

3.- The distorted shell displacement field $\widetilde{X}$ is induced by the inner acoustic field p_a. Even if p_a is calculated without accounting for the shell distortion, $\widetilde{X}$ is noted with ~ because the displacement field depends on the distortion of the shell. Part of the acoustic energy of the air column is transformed into vibrating energy of the shell.

4.- Wall vibration generates, in turn, an additional acoustic radiated field $\widetilde{p}_r$ in the resonator.

5.- The resulting inner acoustic field of a vibrating shell is the sum of two contributions: The acoustic field due to the acoustic excitation of the tube at the entrance (p_a) and the radiated one generated by the wall vibration effect ($\widetilde{p}_r$).

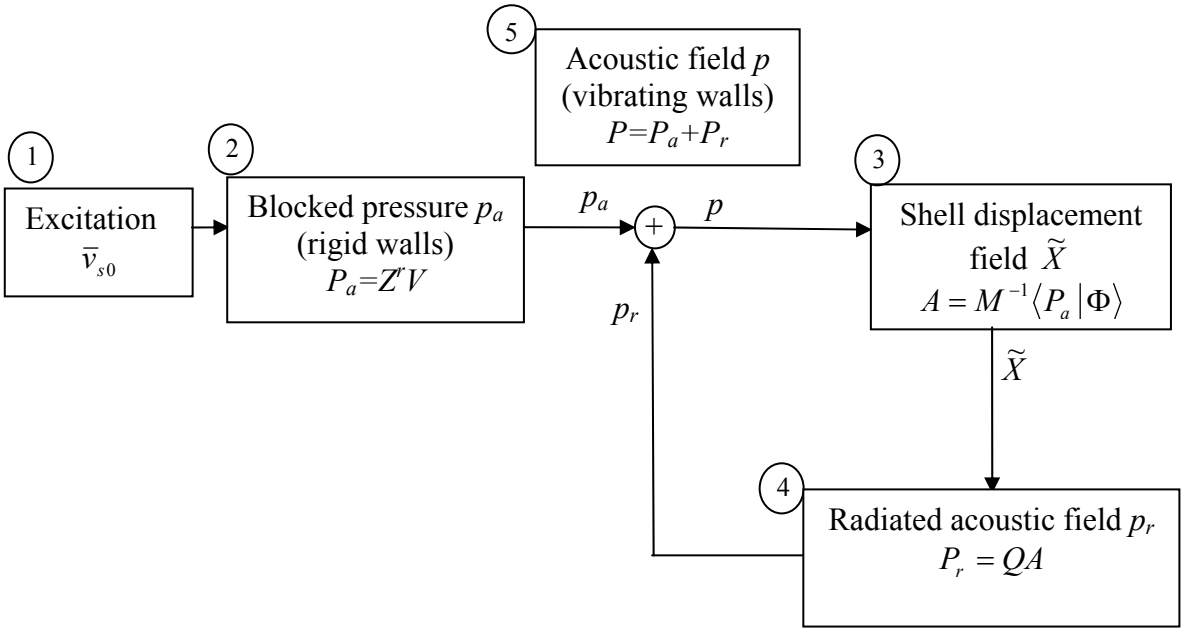

Figure 3.2: Block diagram describing the shell/inner fluid interaction. Acoustic pressure p_a refers to the blocked pressure or pressure calculated without wall vibration. Acoustic pressure p_r refers to the inner pressure radiated by the shell.

Such an approach can be used in order to compute the solution of the coupled problem using successive approximations of the fields: the pressure $p_a + \widetilde{p}_r$ being obtained, it can be used in turn to compute the shell response. The acoustic field radiated from the shell can then be computed and constitute an approximation of the acoustic field of higher order. Such computation can be repeated and the complete procedure can be organised in an iterative manner in order to converge to the solution of the coupled problem. A formulation of this iterative method is given in [Gau97].

In the light fluid approximation, the only responsible of the wall vibration is supposed to be the acoustic field generated by the excitation field, and not the radiated field engendered by the walls. It corresponds to the first step of the iterative method

mentionned above. Such approximation is equivalent to ignore the effect of the internal radiation impedance of the shell.

Assuming the light fluid approximation, the inner acoustic pressure which is present in the right hand term of the motion equation (3.24) is supposed to be p_a and *is* computed by ignoring the wall vibration. This is equivalent to set coefficients $\widetilde{\mathrm{D}}_{\alpha}^{+}(\mathrm{z})$, $\widetilde{\mathrm{D}}_{\alpha}^{-}(\mathrm{z})$ to zero in relation (3.30):

$$p_a(r,\theta,z) = \sum_{\alpha=(m,n,s)} \left[B_\alpha^+ e^{jk_{mn}z} + B_\alpha^- e^{jk_{mn}(l-z)} \right] \Psi_\alpha(r,\theta) \tag{3.35}$$

The amplitudes B_α^+, B_α^- are expressed as the projection of velocity distribution constituting the excitation field on the acoustical modes $\Psi_{\alpha}(\mathrm{r},\theta)$:

$$B_\alpha^+ = \frac{1}{1+e^{2jk_{mn}l}} \left\langle \bar{v}_{So} \middle| \Psi_\alpha(r,\theta) \right\rangle_{S_0} \tag{3.36}$$

$$B_\alpha^- = \frac{-1}{1+e^{2jk_{mn}l}} \left\langle \bar{v}_{So} \middle| \Psi_\alpha(r,\theta) \right\rangle_{S_0} \tag{3.37}$$

2-2-4 Modal coupling induced by shell distortion

Once the acoustic pressure is obtained as a multimodal expansion, the coupling between the acoustic modes and the structural modes can be evaluated. For this goal the expression of the internal pressure (3.35) is replaced in the right hand term of the shell motion equation (3.24). It is found that the coupling term $\int_S \tilde{p}\mathbf{n}\mathbf{\Phi}_{\mu'}(1+2\varepsilon\cos(t\theta))dS$ is the sum of two contributions I_n and I_d

$$\int_S \tilde{p}\mathbf{n}\mathbf{\Phi}_{\mu'}(1+2\varepsilon\cos(t\theta))dS = \int_S p_a\mathbf{n}\mathbf{\Phi}_{\mu'}(1+2\varepsilon\cos(t\theta))dS = I_n + I_d \tag{3.38}$$

where

$$\begin{aligned} I_n &= \int_S p_a \mathbf{n}\mathbf{\Phi}_{\mu'} dS \\ &= \sum_\alpha \frac{j\rho\omega}{k_{mn}} \frac{1}{a} \sqrt{\frac{\varepsilon_m}{\pi}} \frac{1}{\sqrt{1-\gamma_{mn}^2}} \frac{q\pi}{l} \frac{\tan(k_{mn}\cdot l)}{k_{mn}^2 - (q'\pi/l)^2} \left\langle v_{S0} \middle| \Psi_\alpha \right\rangle \cdot i_\alpha \end{aligned} \tag{3.39}$$

and

$$\begin{aligned} I_d &= 2\varepsilon \int_S p_a \mathbf{n}\mathbf{\Phi}_{\mu'} \cos(t\theta) dS \\ &= \varepsilon \sum_\alpha \frac{j\rho\omega}{k_{mn}} \frac{1}{a} \sqrt{\frac{\varepsilon_m}{\pi}} \frac{1}{\sqrt{1-\gamma_{mn}^2}} \frac{q\pi}{l} \frac{\tan(k_{mn}\cdot l)}{k_{mn}^2 - (q'\pi/l)^2} \left\langle v_{S0} \middle| \Psi_\alpha \right\rangle \cdot I_\alpha \end{aligned} \tag{3.40}$$

In these relations (3.39) and (3.40), the implicit notation $\mu' = (m', q', s')$ and $\alpha = (m, n, s)$ is assumed. The first contribution I_n is independent of the distortion parameter ε and refers to the fluid/shell coupling of a non-distorted shell. The term i_α which is present in the sum (3.39) is given by

$$i_\alpha = \int_0^{2\pi} \sin(m\theta + s\pi/2)\sin(m'\theta + s'\pi/2)d\theta = \frac{2\pi}{\varepsilon_m}(1 - \delta_{m0}\delta_{s0})\delta_{mm'}\delta_{ss'} \qquad (3.41)$$

As shows the expression (3.41), modal coupling between different family modes is forbidden by the term $\delta_{mm'}\delta_{ss'}$. This implies in particular that the plane mode (m=0) is uncoupled to structural modes of order $m' \neq 0$.

The second contribution I_d describes the specific soupling induced by the shell's defects and vanishes in the case of the non-distorted shell. The term I_α which is present in the expression of I_d is given by:

$$I_\alpha = \int_0^{2\pi} \sin(m\theta + s\pi/2)\sin(m'\theta + s'\pi/2)\cos(t\theta)\,d\theta\,, \qquad (3.42)$$

It depends on the modal numbers *m, m', s, s'* and on the parameter *t* related to the type of circumferential defect of the shell. Since the expression of I_α is quite long to express in the general case, we give its value in the special case t=2. It can be shown in this case that integral (3.42) is non-null only if

$$m + m' = 2 \qquad (3.43)$$

and if condition (3.43) is satisfied, we have

$$I_\alpha = \frac{\pi \cdot (-1)^{\delta_{mm'}}}{1 + \delta_{mm'}}(1 - \delta_{m0}\delta_{s0})(1 - \delta_{m'0}\delta_{s'0})\delta_{ss'}\,. \qquad (3.44)$$

Indices *m* and *m'* being natural numbers, only three couples of values provide non-null values of I: (*m=0,m'=2*), (*m=2,m'=0*) and (*m=1,m'=1*). Expression (3.44) provides useful information concerning the modal couplings. I_α is null if symmetry indeces s and s' are different, or if (*s=0 and m=0*) or if (*s'=0 and m'=0*). The distortion of the shell introduces the presence of an additional coupling between acoustical and structural modes of different circumferential indices: The plane acoustic mode is coupled to the ovaling modes of the shell (*m=0, m'=2*). As well, breathing modes are coupled to the second order acoustic modes (*m=2, m'=0*). Finally, bending modes are coupled to the first order acoustic modes (*m=1,m'=1*).

The major conclusion of this paragraph is the expression of the coupling term (3.38), which is involved in the shell motion equation (3.24). Integral i_α and I_α given by (3.41) and (3.44) provide conditions on the modal indices to permit modal coupling. It is

shown that coupling between acoustic modes and structural modes having circumferential indices are permitted by the shell's distortion.

3.2.3. Determination of the input impedance matrix

Once the modal coupling is evaluated, the expression of the input acoustic impedance can be obtained. For this aim, a matrix notation will be used (see appendix 3.A) in order to represent the multimodal formulation. In this notation, equation (3.24) can be written as

$$\mathbf{M}\cdot\mathbf{A}=\mathbf{E}\cdot\mathbf{V}\,, \tag{3.45}$$

Where **M** is a diagonal matrix whose elements consist of the expression $m_{\mu'}\left(-\omega^2+\omega_{\mu'}^2\cdot\left(1-j\eta_{\mu'}\right)\right)$ calculated for each modal index of the structural modal basis. In equation (3.45), the amplitude vector **V** for the acoustic velocity is given since the velocity is prescribed on the input surface S_0. Vector **A** represents the amplitude of the wall vibrations and matrix **E** (see appendix 3.A) the shell/fluid coupling. This coupling can be separated into two contributions (non-distorted coupling and distorted coupling):

$$\mathbf{E}=\mathbf{E}_n+\varepsilon\cdot\mathbf{E}_d \tag{3.46}$$

Both, vector **A** and matrix **E** can be deduced from equation (3.24). For a particular pattern of wall vibration amplitude generated by the acoustic field p_a, inner acoustic pressure radiated p_r by the shell is known in the form of a multimodal acoustic expansion given by equation (3.30). Projecting the inner pressure on a particular mode $\Psi_{\alpha'}$ of the acoustic basis on the surface S_0 we obtain

$$\left\langle\tilde{p}\left(\tilde{M}\right)\middle|\Psi_\alpha\right\rangle_{S0}=B_\alpha^++\tilde{D}_\alpha^+(0)+\left[B_\alpha^-+\tilde{D}_\alpha^-(0)\right]e^{jk_{mn}l}\,. \tag{3.47}$$

Note that, again, the light fluid approximation has been used when writing B_α^+ (and B_α^+) instead of $\tilde{B}_\alpha^+$ (and $\tilde{B}_\alpha^-$).

Using the matrix notation given in appendix 3.A the expression of the projections of the inner pressure on the transverse acoustic modes (3.47) can be expressed on the form:

$$\mathbf{P}=\mathbf{Z}^r\mathbf{V}+\mathbf{Q}\cdot\mathbf{A}\,, \tag{3.48}$$

where matrix **Q** can be deduced from equations (3.31), (3.32), (3.33), (3.34) and (3.47) and expressed in the matrix form as (see appendix 3.A for matricial notations)

$$\mathbf{Q}=\mathbf{Q}_n+\varepsilon\cdot\mathbf{Q}_d\,. \tag{3.49}$$

The impedance matrix $\mathbf{Z}^r$ in (3.48) is the impedance matrix of a rigid cylindrical duct. Indeed, for a rigid wall, we have **A**=0 and therefore in this case, we simply have

$\mathbf{P} = \mathbf{Z}^r \mathbf{V}$. Equations (3.45) and (3.48) provide an expression of the acoustic input impedance of the distorted shell: 3.

$$\mathbf{Z} = \mathbf{Z}^r + \left(\mathbf{Q}_n + \varepsilon \cdot \mathbf{Q}_d\right) \cdot \mathbf{M}^{-1} \cdot \left(\mathbf{E}_n + \varepsilon \cdot \mathbf{E}_d\right), \tag{3.50}$$

Expanding this equation (3.50) and ignoring terms in second order of ε we obtain an expression of the acoustic input impedance of a slightly distorted vibrating shell:

$$\mathbf{Z} \cong \mathbf{Z}^r + \mathbf{Q}_n \mathbf{M}^{-1} \mathbf{E}_n + \varepsilon \left(\mathbf{Q}_d \mathbf{M}^{-1} \mathbf{E}_n + \mathbf{Q}_n \mathbf{M}^{-1} \mathbf{E}_d\right). \tag{3.51}$$

3.3. Wall distortion influence on the acoustic input impedance

3.3.1. Truncations of the functional basis

The functional basis used to expand the shell displacement field is constituted by the modes of the shell whose cross section is perfectly circular. It is known that the eigenfrequencies of such a shell are not ordered as the modal indices are. In particular, the fundamental frequency (that is the lowest eigenfrequency) does not correspond generally to the first breathing mode but to a mode associated to a higher circumferential index. A discussion related to the value of the fundamental frequency of a shell is given in [Kor64]. This point is illustrated on figure 3.3: Dispersion curves and eigenfrequencies modes of a shell made of steel are presented depending on the values of the modal indices q and m.

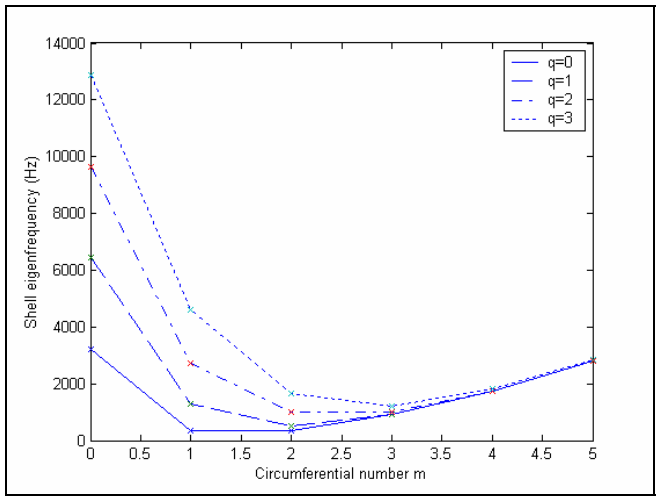

Figure 3.3: Shell eigenfrequencies of a steel shell for different circumferential modal index m and axial modal index q (E=210GPa, σ=0.28 ,ρ=7800kg/m3, a=14.25mm, L=0.5m, h=0.5mm). Eigenfrequencies of bending modes (m=1) and ovaling modes (m=2) are lower in frequency than breathing modes (m=0).

Acoustic and shell modal indeces are represented by α=(m,n,s) and μ'=(m',q',s') respectively. The simplest modal truncation rendering the effect of the distortion of the shell will be considered. Thus, the circumferential indeces *m* and *m'* vary from 0 to 2 in order to take into account the coupling between different shell family modes. The symmetry indeces *s* and *s'* vary from 0 to 1 to consider the

asymmetry of the shell. Indeces *q'* and *n* have the first value of the truncation (q'=1 and n=0). With this choice of modal indices, the set of modes include six acoustic modes and six shell modes represented on figure 3.4 and figure 3.5: values of α are (0,0,0), (0,0,1), (1,0,0), (1,0,1), (2,0,0), (2,0,1) and values of μ' are (0,1,0), (0,1,1), (1,1,0), (1,1,1), (2,1,0), (2,1,1).

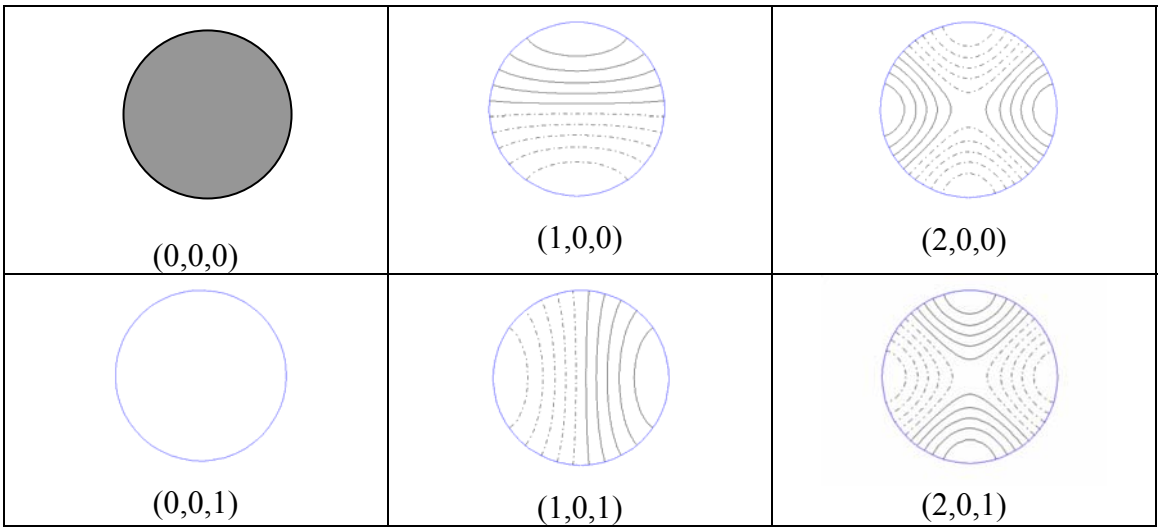

Figure 3.4: Representation of the first transverse acoustic modes used for numerical investigation presented in paragraph 3.3. Each mode is referred by the set of modal indices, $\alpha = (m, n, s)$ where m is the circumferential index (m=0,1,2), n the radial index (n=0), and s the index of symmetry (s = 0,1).

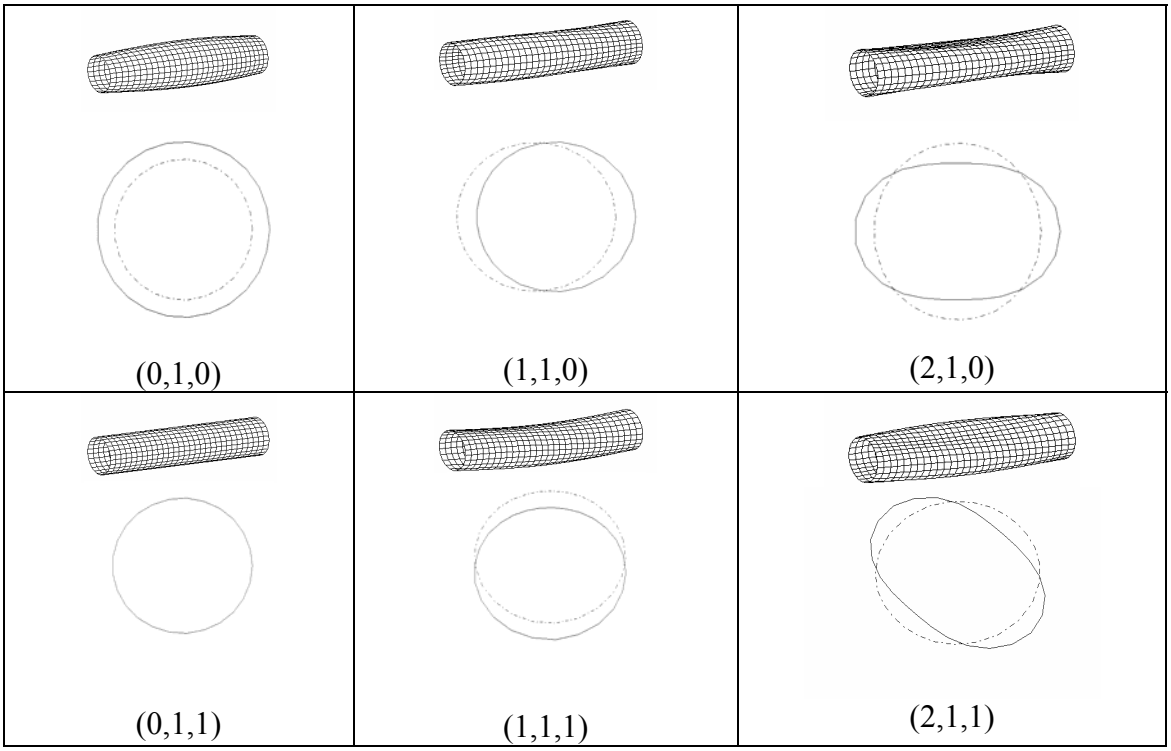

Figure 3.5: Representation of the first structural modes used for numerical investigation presented in paragraph 3.3 Each mode is referred by the set of modal indices, $\mu = (m,q,s)$ where m denotes the circumferential index (m=0,1,2), q denotes the axial index (q=1), s is the index of symmetry (s=0,1).

3.3.2. Interaction between plane acoustic mode and first asymmetric shell modes: expression of the correction factor for the input impedance

The influence of the angular distortion of the shell on the acoustic behaviour of the tube is now considered. Matrices **Q**, **M** and **E** are represented for this particular truncation in appendix B. The factor correction of the plane mode can be calculated as:

$$Z_{(0,0,1)(0,0,1)} = Z^{r}_{(0,0,1)(0,0,1)}\left(1 + C_{(0,0,1)(0,0,1)}\right) \tag{3.52}$$

where

$$C_{(0,0,1)(0,0,1)} = \left(Q_{(0,0,1)(0,1,1)} \cdot M^{-1}_{(0,1,1)(0,1,1)} \cdot E_{(0,1,1)(0,0,1)} + Q_{(0,0,1)(2,1,1)} \cdot M^{-1}_{(2,1,1)(2,1,1)} \cdot E_{(2,1,1)(0,0,1)}\right) Z^{-1}_{(0,0,1)(0,0,1)} \tag{3.53}$$

The first term of the sum is the fluid/structure coupling due to the cylindrical shape of the shell as it was obtained in [PGR04]. The second term is linked to the distortion of the shell. The factor correction can be expressed as:

$$C_{(0,0,1)(0,0,1)} = C_n + C_d \tag{3.54}$$

where

$$C_n(\omega)=\frac{4\pi\rho\cdot c}{m_{(0,1,1)}}\left(\frac{\pi}{l}\right)^2\frac{\omega\cdot\tan(\omega l/c)}{\left[(\omega/c)^2-(\pi/l)^2\right]^2\left[\omega^2-\omega_{(0,1,1)}^2\cdot(1-j\eta_{(0,1,1)})\right]} \tag{3.55}$$

and

$$C_d(\omega)=\varepsilon\frac{\pi\rho\cdot c}{m_{(2,1,1)}}\left(\frac{\pi}{l}\right)^2\frac{\omega\cdot\tan(\omega l/c)}{\left[(\omega/c)^2-(\pi/l)^2\right]^2\left[\omega^2-\omega_{(2,1,1)}^2\cdot(1-j\eta_{(2,1,1)})\right]} \tag{3.56}$$

Thus, the correction factor of the input acoustic impedance of the plane mode can be interpreted as the sum of two contributions: the first one represents the fluid/shell coupling corresponding to a shell with a perfectly cylindrical cross-section (C_n). As presented in [PGR04], this term tends to a maximum when a mechanical resonance is reached. This mechanical resonance is defined by the eigenfrequency of the first breathing mode ($\omega_{(0,1,1)}$), its modal mass ($m_{(0,1,1)}$) and structural damping ($\eta_{(0,1,1)}$). The second contribution (C_d) is an additional term related to the coupling of the first ovaling mode (2,1,1) and the plane acoustic mode. This term is proportional to the distortion of the shell (ε) and tends to a maximum when a mechanical resonance for the ovaling mode is reached: this mechanical resonance is defined by the eigenfrequency of the first ovaling mode ($\omega_{(2,1,1)}$), its modal mass ($m_{(2,1,1)}$) and structural damping ($\eta_{(2,1,1)}$).

It can be seen from equation (3.50) that the input acoustic impedance of the plane mode can be drastically perturbed by the wall vibration if the correction factor $C_{(0,0,1)(0,0,1)}$ is significant compared to unity. As presented in [PGR04], three conditions lead to great values of both correction factors C_n and C_d in equations (3.53) and (3.54) and three phenomena underlay this singular behaviour: mechanical resonances, a spatial coincidence effect and acoustic resonances. If two of these phenomena take place simultaneously, the perturbation effect becomes significant and the acoustic resonances and antiresonances of the tube can be significantly altered.

3.3.3. Numerical results

The correction factor of the input acoustic impedance is analysed in this paragraph in order to establish and identify the contribution of the distortion of the shell to the acoustic response of the tube. The geometrical features of the shell which are used for the numerical applications are: length l=0.5m, radius a=14.25mm and thickness h=0.35mm and the distortion parameter is fixed at ε=0.05. Figure 6 represents the two contributions of the correction factor against frequency of a shell made of steel ($E=210\cdot10^9 N/m^2$, σ=0.28, $\rho_S=7800kg/m^3$): the non-distorted (C_n) and the distorted (C_d) correction factor. It can be seen that, at low frequencies, the coupling due to the distortion of the shell is more important than the one resultant from the non-distorted contribution. The elliptical distortion of the cross-section of the shell favours the coupling between the plane mode and the first ovaling shell mode. The eigenfrequency of the first breathing shell mode (f_{Rb1}= 3243Hz) can be identified as a peak of the non-

distorted correction factor. The eigenfrequency of the first ovaling shell mode (f_{Ro1}= 1159Hz) can be observed as a maximum of the distorted correction factor.

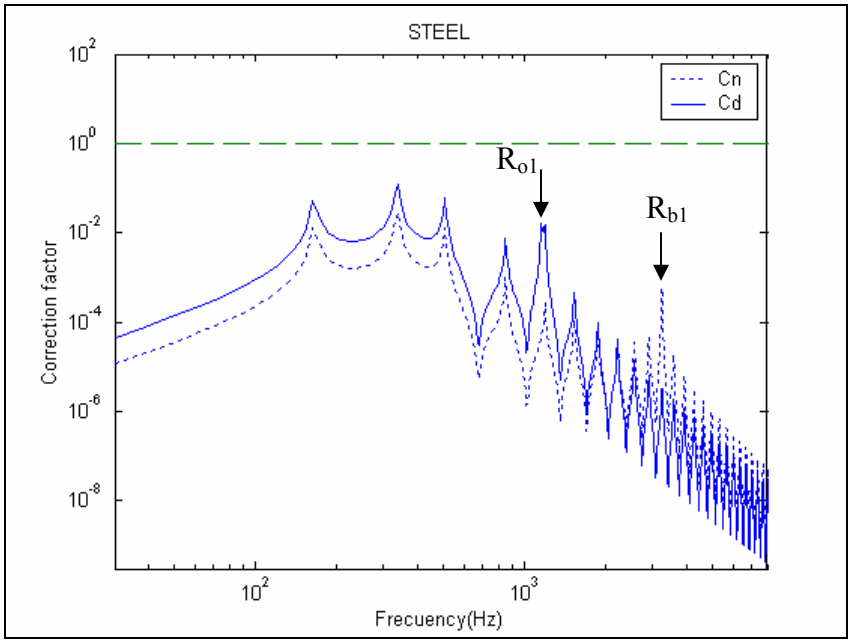

Figure 3.6: Distorted (C_d) and non-distorted (C_n) correction factor of the acoustic input impedance induced by wall vibration against frequency. The thickness of the shell is h=0.35mm and the material the shell is made of is steel: its Young's modulus is $E=210\cdot10^{9}N/m^{2}$, its Poisson's ratio is σ=0.28 and its density $\rho_S=7800kg/m^{3}$. C_n is altered by the eigenfrequency of the first breathing shell mode (f_{Rb1}= 3243Hz) which is bigger than peak in C_d corresponding to the eigenfrequency of the first ovaling shell mode (f_{Ro1}= 1159Hz).

It can be seen in figure (3.6) that f_{Ro1} is smaller than f_{Rb1}. This means that the distortion of the shell favours the coupling of lower frequency modes (ovaling modes) with the air column providing more important effects on the acoustic behaviour of the tube. For some materials, the eigenfrequency of the first ovaling mode can be lower enough to strongly alter the acoustic input impedance of the tube. It is the case of lead, silver, gold and tin.

In figure 3.7, the eigenfrequency of the first ovaling shell mode is represented against the thickness of the different shells made of these materials. It can be seen that, in these cases, the mechanical resonance can be produced at frequencies near the acoustic resonance of the tube.

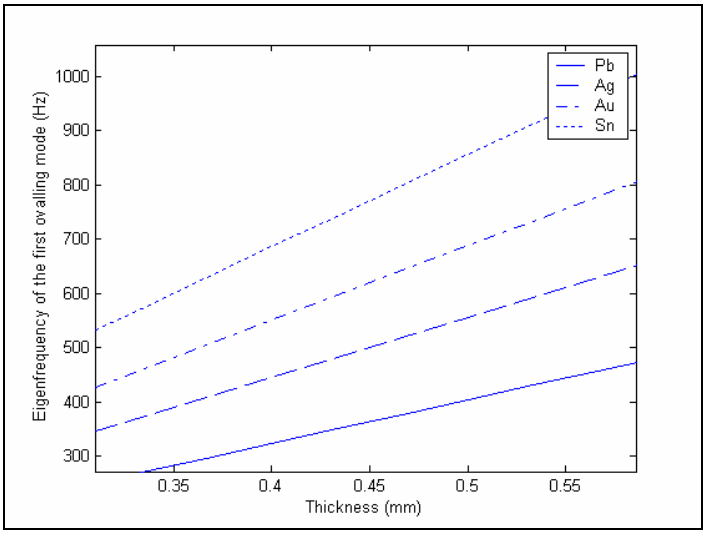

Figure 3.7: Eigenfrequency of the first ovaling shell mode against the thickness of the shell for different shells made of four different materials (Lead(Pb), Silver(Ag), Gold(Au) and Tin(Sn)). The geometry of the shell is fixed at: length l=0.5m and radius a=14.25mm

For fixed values of the length and the radius of the shell, the correction factor or the acoustic input impedance is analysed for two shells made of silver ($E=30\cdot10^9 N/m^2$, $\sigma=0.37$, $\rho_S=10490 kg/m^3$) and gold ($E=79\cdot10^9 N/m^2$, $\sigma=0.44$, $\rho_S=19300 kg/m^3$). In both cases, the thickness of the shell can be fitted in order to superpose the first mechanical resonances of the shell with the second acoustic resonance at 515.1Hz. In the case of the gold shell (h=0.376), the shell is thinner than the silver shell (h=0.466mm).

In figures 3.8a) and 3.8b) the correction factor and the acoustic input impedance of silver shell are represented. Important changes in the two first acoustic resonances that appear as peaks in the acoustic impedance plot of the acoustic impedance due to wall vibrations of the distorted shell can be seen in both cases when comparing with the non-vibrating shell reference. Thus, the acoustic behaviour of the shell is notably affected by the vibroacoustic coupling engendered by the distortion of the shell.

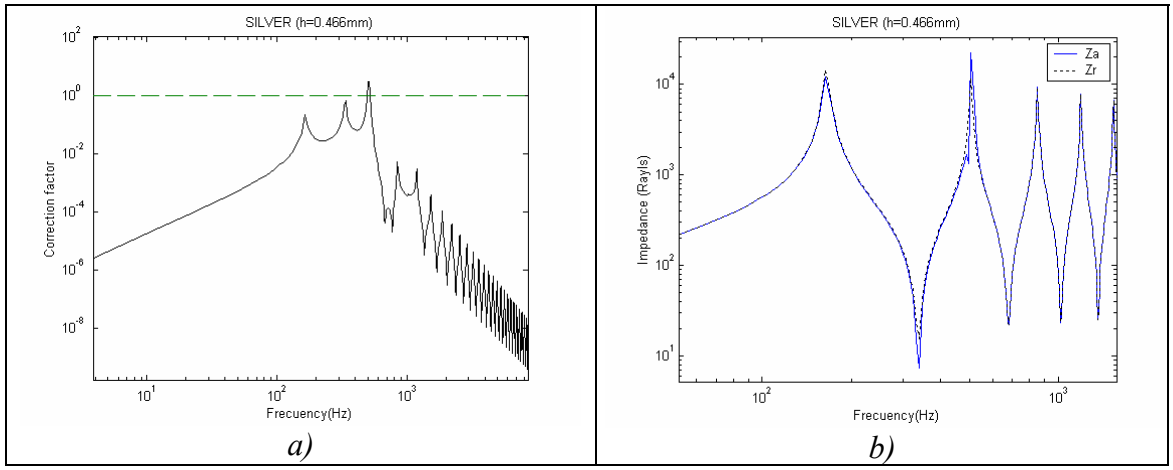

Figure 3.8: a) Correction factor and b) input acoustic impedance (Z^a) of a wall vibrating cylinder made of silver ($E=30\cdot10^9 N/m^2$, its Poisson's ratio is $\sigma=0.37$ and its density $\rho_S=10490 kg/m^3$). The reference of the acoustic input impedance of a rigid shell is represented (Z^r) in b). The geometry of the shell is: length l=0.5m, radius a=14.25mm and thickness h=0.466mm and the distortion parameter is fixed at $\varepsilon=0.05$. The eigenfrequency of the first ovaling mode (f_{b1}) is placed at the third acoustic resonance (f_3)

Provided that the distortion of the shell is the main responsible of the significance of the fluid/shell coupling, an in-depth evaluation of this relationship is of interest. Figure 3.9 shows the non-distorted correction factor corresponding to different shells with different distortion factors (ε=0.05, ε=0.25 and the latter ε=0 corresponding to a non-distorted shell). It can be seen that the bigger the distortion, the bigger the correction factor of the acoustic input impedance, and, thus, bigger the wall vibration effect. For this shell, a distortion factor bigger than ε=0.25, provides a correction factor significant (bigger than unity). However, it must be pointed out that these distortion factors are out of the range of validity of the vibroacoustic model hypothesis (limitations given by equations (3.13) (3.14) and (3.22)).

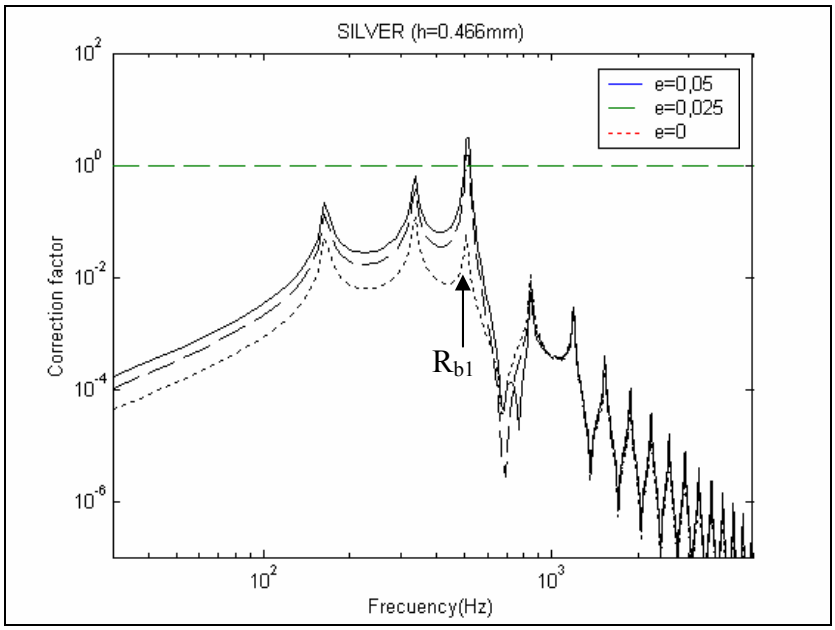

Figure 3.9: Correction factor of four different distorted shells made of steel ($E=210\cdot10^9 N/m^2$, $\rho_S=7800\ kg/m^3$ and $\sigma=0.28$). The distortion factor of each shell is $\varepsilon=0.05$, $\varepsilon=0.025$ and $\varepsilon=0$ (the latter is non-distorted). The eigenfrequency of the first ovaling mode (f_{b1}) is placed at the third acoustic resonances (f_3)

Although the distortion factor of the shell is very small, the wall vibration effect can be very important when the structural losses of the modes of the shell (η) are small enough. In figure 10, the correction factor of three different distorted shells made of silver ($E=30\cdot10^9 N/m^2$, $\rho_S=10490\ kg/m^3$ and $\sigma=0.37$) with different structural losses ($\eta=0.1$, $\eta=0.01$ and $\eta=0.001$) have been represented. The distortion parameter is always $\varepsilon=0.01$, that is, the distortion represents a 1% of the radius: 0.14mm of distortion compared to 14.25mm. It can be seen that E, σ, ρ_S and h have been chosen so that the eigenfrequency of the first ovaling mode coincides with the third acoustic resonance of the tube. It can be seen in figure 10 that the curve corresponding to a shell having a material with structural losses of $\eta=0.001$, greatly surpasses unity. In this case, wall vibration effect is significant.

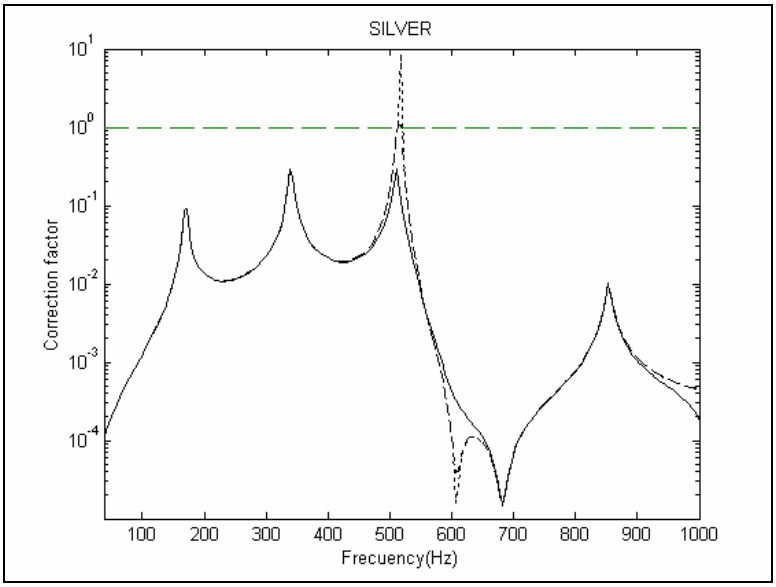

Figure 3.10: Correction factor of a three different distorted shells (ε=0.01) made of silver ($E=30\cdot10^9 N/m^2$, $\rho_S=10490\ kg/m^3$ and σ=0.37) with different structural losses (η=0.1, η=0.01 and η=0.001) . The wall vibration effect is important when the structural losses are small enough even if the distortion factor of the shell is very small. The eigenfrequency of the first ovaling mode (f_{b1}) is placed at the third acoustic resonances (f_3)

3.4. Conclusion

A vibroacoustic model of a simply supported distorted cylindrical shell has been developed and the influence of the distortion of the shell on the inner fluid/shell coupling has been quantified. It is shown that distortion of the shell induce coupling between modes whose circumferential indices are different and coupling coefficients between these modes are predicted by the model. The influence of the wall vibration on the acoustic behaviour of a distorted tube can be understood as a correction of the acoustic matrix impedance which is called “correction factor”. The correction factor of the input acoustic impedance matrix of the distorted vibrating resonator was obtained as a sum of two contributions: The first (C_n) describes the interaction between the breathing modes and the plane acoustic mode and the second (C_d) describes the interaction between the ovaling modes and the plane acoustic mode. When considering slightly distorted shells, this second factor can be more important than the first. In fact, for some materials, the shell mechanical response is such a way that the eigenfrequency of the ovaling modes is small enough to alter the acoustic input impedance of the tube. A numerical application permits to show the interaction between the plane acoustic mode and the first ovaling mode when the distortion of the shell is small. Previous experimental results obtained with slightly distorted organ pipes can be interpreted with the model proposed. The validity of the results is limited by the hypothesis of the model: the distortion of the shell must be very small. This model approaches a well-known problem in the field of wind instruments: the wall vibration effect. Simulations on the time domain of distorted tubes could provide additional information about the fluid/shell coupling by means of the oscillation regime vibrating distorted pipes.

Appendix 3.A: Matrix notations

The matrix formulation of the problem is useful to describe the multimodal approach. Thus, vectors

$$\mathbf{A}_m = \begin{bmatrix} A_{(m,1,s)} \\ \vdots \\ A_{(m,Q,s)} \end{bmatrix}, \quad \mathbf{P}_m = \begin{bmatrix} P_{(m,0,s)} = \langle p \,|\, \Psi_{(m,0,s)} \rangle \\ \vdots \\ P_{(m,N,s)} = \langle p \,|\, \Psi_{(m,N,s)} \rangle \end{bmatrix}, \quad \mathbf{V}_m = \begin{bmatrix} V_{(m,0,s)} = \langle V_{S_0} \,|\, \Psi_{(m,0,s)} \rangle \\ \vdots \\ V_{(m,N,s)} = \langle V_{S_0} \,|\, \Psi_{(m,N,s)} \rangle \end{bmatrix} \tag{A1,A2,A3}$$

describe the unknown modal amplitudes for a given circumferential index m. For each m, the mechanical basis is truncated to Q modes and the acoustic basis is reduced to N modes. Grouping these amplitudes vectors as

$$\mathbf{A} = \begin{bmatrix} \mathbf{A}_1 \\ \vdots \\ \mathbf{A}_m \\ \vdots \\ \mathbf{A}_M \end{bmatrix}, \quad \mathbf{P} = \begin{bmatrix} \mathbf{P}_1 \\ \vdots \\ \mathbf{P}_m \\ \vdots \\ \mathbf{P}_M \end{bmatrix}, \quad \mathbf{V} = \begin{bmatrix} \mathbf{V}_1 \\ \vdots \\ \mathbf{V}_m \\ \vdots \\ \mathbf{V}_M \end{bmatrix}, \tag{A4,A5,A6}$$

we obtain modal amplitude vectors for the shell displacement **A**, the acoustic pressure **P** and the velocity **V**.

The rigid impedance matrix $\mathbf{Z}^{\mathbf{r}}$ is a diagonal matrix that corresponds to the input acoustic impedance of the cylinder with rigid walls, and therefore, it does not take into account the wall vibration effect:

$$\mathbf{Z}^r = \begin{bmatrix} Z^r_{(0,0,0),(0,0,0)} & 0 & 0 \\ 0 & \ddots & 0 \\ 0 & 0 & Z^r_{(m,n,s),(m',n',s')} \end{bmatrix} \tag{A8}$$

The Boldtype of $\mathbf{Z}^r$ represents the matricial character of the rigid impedance and each element written in italics represents a scalar. Matrix **M** describes the mechanical behaviour of the shell:

$$\mathbf{M} = \begin{bmatrix} M_{(0,1,0),(0,1,1)} & 0 & 0 \\ 0 & \ddots & 0 \\ 0 & 0 & M_{(m,q,s),(m',q',s')} \end{bmatrix}. \tag{A10}$$

Matrices **Q** and **E** contain the vibroacoustic coupling terms:

$$\mathbf{E} = \begin{bmatrix} E_{(0,1,0),(0,0,0)} & \cdots & E_{(0,1,0),(m,n,s)} \\ \vdots & \ddots & \vdots \\ E_{(m',q',s'),(0,0,0)} & \cdots & E_{(m',q',s'),(m,n,s)} \end{bmatrix}, \tag{A11}$$

and

$$\mathbf{Q} = \begin{bmatrix} Q_{(0,0,0),(0,1,0)} & \cdots & Q_{(0,0,0),(m',q',s')} \\ \vdots & \ddots & \vdots \\ Q_{(m,n,s),(0,1,0)} & \cdots & Q_{(m,n,s),(m',q,s')} \end{bmatrix}. \tag{A12}$$

The product of $\mathbf{Q}\cdot\mathbf{M}^{-1}\cdot\mathbf{E}$ provides the factor correction which is not a diagonal matrix because **Q** and **E** are not diagonal. Off-diagonal terms of matrix C represent coupling between shell modes and acoustic modes.

Appendix 3.B: Matrix notations for the truncation considered

In order to evaluate the wall vibration effect on the acoustic behaviour of the shell, the simplest modal truncation rendering the effect of the distortion of the shell has been considered. Thus, m and m' vary from 0 to 2, s and s' vary from 0 to 1 and indeces q and n have the first value of the truncation (q=1 and n=0). This implies that the coupling between six acoustic modes and six shell modes is considered. For this truncation, matrices $\mathbf{Q}_{\alpha\mu'} = \mathbf{Q}_{(m,n,s)(m',q',s')}$, $\mathbf{M}_{\mu\mu'} = \mathbf{M}_{(m,q,s)(m'q',s')}$ and $\mathbf{E}_{\mu'\alpha} = \mathbf{E}_{(m',q',s')(m,n,s)}$ can be represented as (6x6) matrices:

$$\mathbf{Q}_{\alpha\mu'} = \begin{pmatrix} 0 & 0 & 0 & 0 & 0 & 0 \\ 0 & Q_{(0,0,1)(0,1,1)} & 0 & 0 & 0 & Q_{(0,0,1)(2,1,1)} \\ 0 & 0 & Q_{(1,0,0)(1,1,0)} & 0 & 0 & 0 \\ 0 & 0 & 0 & Q_{(1,0,1)(1,1,1)} & 0 & 0 \\ 0 & 0 & 0 & 0 & Q_{(2,0,0)(2,1,0)} & 0 \\ 0 & Q_{(2,0,1)(0,1,1)} & 0 & 0 & 0 & Q_{(2,0,1)(2,1,1)} \end{pmatrix} \tag{B1}$$

and

$$\mathbf{M}_{\mu\mu'} = \begin{pmatrix} M_{(0,1,0)(0,1,0)} & 0 & 0 & 0 & 0 & 0 \\ 0 & M_{(0,1,1)(0,1,1)} & 0 & 0 & 0 & 0 \\ 0 & 0 & M_{(1,1,0)(1,1,0)} & 0 & 0 & 0 \\ 0 & 0 & 0 & M_{(1,1,1)(1,1,1)} & 0 & 0 \\ 0 & 0 & 0 & 0 & M_{(2,1,0)(2,1,0)} & 0 \\ 0 & 0 & 0 & 0 & 0 & M_{(2,1,1)(2,1,1)} \end{pmatrix} \tag{B2}$$

and

$$\mathbf{E}_{\mu'\alpha} = \begin{pmatrix} 0 & 0 & 0 & 0 & 0 & 0 \\ 0 & E_{(0,1,1)(0,0,1)} & 0 & 0 & 0 & E_{(0,1,1)(2,0,1)} \\ 0 & 0 & E_{(1,1,0)(1,0,0)} & 0 & 0 & 0 \\ 0 & 0 & 0 & E_{(1,1,1)(1,0,1)} & 0 & 0 \\ 0 & 0 & 0 & 0 & E_{(2,1,0)(2,0,0)} & 0 \\ 0 & E_{(2,1,1)(0,0,1)} & 0 & 0 & 0 & E_{(2,1,1)(2,0,1)} \end{pmatrix}.$$

(B3)

The impedance correction ($Z = Z^r + Z^c$) for this truncation can be evaluated by the product of matrices (B1), (B2) and (B3):

$$\mathbf{Z^c}_{\alpha\alpha'''} = \mathbf{Q}_{\alpha\mu'} \cdot \mathbf{M}^{-1}_{\mu'\mu''} \cdot \mathbf{E}_{\mu''\alpha'''}$$

$$\mathbf{Z^c}_{(m,n,s)(m''',n''',s''')} = \mathbf{Q}_{(m,n,s)(m',q',s')} \cdot \mathbf{M}^{-1}_{(m',q',s')(m'',q'',s'')} \cdot \mathbf{E}_{(m'',q'',s'')(m''',n''',s''')}$$

$$\mathbf{Z^c}_{\alpha\alpha'} = \begin{pmatrix} 0 & 0 & 0 & 0 & 0 & 0 \\ 0 & Z^c_{(0,0,1)(0,0,1)} & 0 & 0 & 0 & Z^c_{(0,0,1)(2,0,1)} \\ 0 & 0 & Z^c_{(1,0,0)(1,0,0)} & 0 & 0 & 0 \\ 0 & 0 & 0 & Z^c_{(1,0,1)(1,0,1)} & 0 & 0 \\ 0 & 0 & 0 & 0 & Z^c_{(2,0,0)(2,0,0)} & 0 \\ 0 & Z^c_{(2,0,1)(0,0,1)} & 0 & 0 & 0 & Z^c_{(2,0,1)(2,0,1)} \end{pmatrix} \tag{B4}$$

where

$$\begin{aligned}
Z^c_{(0,0,1)(0,01)} &= Q_{(0,0,1)(0,1,1)} M^{-1}_{(0,1,1)(0,1,1)} \cdot E_{(0,1,1)(0,0,1)} + Q_{(0,0,1)(2,1,1)} M^{-1}_{(2,1,1)(2,1,1)} \cdot E_{(2,1,1)(0,0,1)} \\
Z^c_{(0,0,1)(2,0,1)} &= Q_{(0,0,1)(0,1,1)} M^{-1}_{(0,1,1)(0,1,1)} \cdot E_{(0,1,1)(2,0,1)} + Q_{(0,0,1)(2,1,1)} M^{-1}_{(2,1,1)(2,1,1)} \cdot E_{(2,1,1)(2,0,1)} \\
Z^c_{(1,0,0)(1,0,0)} &= Q_{(1,0,0)(1,1,0)} M^{-1}_{(1,1,0)(1,1,0)} \cdot E_{(1,1,0)(1,0,0)} \\
Z^c_{(1,0,1)(1,0,1)} &= Q_{(1,0,1)(1,1,1)} M^{-1}_{(1,1,1)(1,1,1)} \cdot E_{(1,1,1)(1,0,1)} \\
Z^c_{(2,0,0)(2,0,0)} &= Q_{(2,0,0)(2,1,0)} M^{-1}_{(2,1,0)(2,1,0)} \cdot E_{(2,1,0)(2,0,0)} \\
Z^c_{(2,0,1)(0,0,1)} &= Q_{(2,1,1)(0,1,1)} M^{-1}_{(0,1,1)(0,1,1)} \cdot E_{(0,1,1)(0,0,1)} + Q_{(2,0,1)(2,1,1)} M^{-1}_{(2,1,1)(2,1,1)} \cdot E_{(2,1,1)(0,0,1)} \\
Z^c_{(2,0,1)(2,0,1)} &= Q_{(2,0,1)(0,1,1)} M^{-1}_{(0,1,1)(0,1,1)} \cdot E_{(0,1,1)(2,0,1)} + Q_{(2,0,1)(2,1,1)} M^{-1}_{(2,1,1)(2,1,1)} \cdot E_{(2,1,1)(2,0,1)}
\end{aligned} \tag{B5}$$

Capítulo 4

Simulation in the time domain of simple-reed instruments with vibrating walls

Este capítulo reproduce un artículo enviado para su publicación[2] *y un complemento en francés y en español al final del capítulo. En este artículo, se propone un modelo físico de instrumento de viento de lengüeta simple a fin de evaluar la influencia del material de construcción en su respuesta acústica. La introducción del artículo recoge las diferentes aportaciones en la literatura científica relacionados con el problema de la influencia del material de construcción y el fenómeno de la vibración de las paredes en el comportamiento acústico de un instrumento de viento.*

Un modelo simple de instrumento, de tipo clarinete, permite simular las oscilaciones periódicas que corresponden al régimen principal de oscilación del instrumento. La técnica propuesta por Schumacher [Sch91] se utiliza para estudiar las auto-oscilaciones de un instrumento de viento de lengüeta simple. Esta técnica integra las ecuaciones que gobiernan el comportamiento acústico del instrumento y su acoplamiento con el músico.

La respuesta acústica del resonador en este modelo toma en consideración los efectos de vibración de paredes dados por el modelo vibroacústico propuesto en el capítulo 2 (artículo [PGR04]). La impedancia acústica de entrada de un instrumento vibrante rige el comportamiento acústico del cuerpo del instrumento. Las conclusiones del capítulo 2 nos muestran que cuando se consideran los materiales de construcción habituales no se observa ningún efecto de vibración de las paredes. Sin embargo, las estructuras construidas con materiales que tienen valores suficientemente pequeños del módulo de Young (E) y densidad (ρ), presentan efectos de vibración de las paredes que pueden ser importantes. Estos valores corresponden a materiales irrealistas.

Las consecuencias de las vibraciones de pared sobre el instrumento vibrante pueden ser evaluadas teniendo en cuenta la impedancia acústica de entrada en las simulaciones numéricas en el dominio temporal.

Las simulaciones muestran que el acoplamiento vibroacústico puede actuar sobre el comportamiento acústico del instrumento. Se analizan las señales simuladas para los

[2] *Enviada para su publicación a la revista* Journal of Sound and Vibration *en abril de 2004*

instrumentos de paredes vibrantes en relación a la referencia de un instrumento rígido (paredes no vibrantes). Se observan cambios del tiempo de ataque, cambios de timbre y cambios de régimen de oscilación (notas multifónicas).

Al final del capítulo, se presenta un complemento en el que se exponen simulaciones con instrumentos deformados. Como se ha visto en el capítulo 3, la deformación de la estructura provoca el acoplamiento del modo acústico plano con el primer modo oval que tiene lugar a más baja frecuencia que el primer modo de respiración. Este acoplamiento puede alterar significativamente la impedancia acústica del instrumento a la "frecuencia de ejecución" del instrumento ('playing frequency') y así, alterar significativamente su régimen de oscilación. Las simulaciones presentadas muestran que, en efecto, la distorsión del cuerpo del instrumento favorece la aparición del fenómeno de vibración de paredes a en condiciones realistas en el ámbito de las aplicaciones musicales.

Ce chapitre reproduit un article rédigé en anglais soumis à la revue Journal of Sound and Vibration et un complément en français et en espagnol en fin du chapitre. Dans cet article, un modèle physique d'instrument à vent à anche simple est proposé dans le but d'évaluer l'influence du matériau de construction dans sa réponse acoustique. L'introduction de l'article résume les différentes approches scientifiques dans la littérature au problème de l'influence du matériau de construction et l'importance de la vibration de paroi dans le comportement acoustique d'un instrument à vent en situation de jeu.

Un modèle simple d'instrument type clarinette permet de simuler les oscillations périodiques qui correspondent au régime principal d'oscillation de l'instrument. La technique proposée par Schumacher [Sch81] est utilisée pour étudier les auto-oscillations d'un instrument à vent à anche simple. Cette technique intègre les équations gouvernant le comportement acoustique de l'instrument et son couplage avec le musicien.

La réponse acoustique du résonateur dans ce modèle prend en compte les effets de vibration de parois donnés par le modèle vibroacoustique proposé dans le chapitre 2 (article [PGR04]). L'impédance acoustique d'entrée d'un instrument vibrant régit donc le comportement acoustique du corps de l'instrument. Les conclusions du chapitre 2 nous montrent que quand on considère des matériaux de construction habituelle aucun effet significatif de vibrations de paroi n'est observé. Pourtant, des coques construites avec des matériaux ayant des valeurs suffisamment faibles du module de Young (E) et de masse volumique (ρ), présentent des effets de vibration de paroi qui peuvent être importants. Ces valeurs correspondent à des matériaux irréalistes. Les conséquences des vibrations de paroi sur l'instrument vibrant en situation de jeu, peuvent être évaluées en prenant en compte l'impédance acoustique d'entrée dans les simulations numériques dans le domaine temporel.

Les simulations montrent que le couplage coque/fluide interne peut agir sur le comportement acoustique de l'instrument. Les signaux simulés pour les instruments à parois vibrantes sont analysés par rapport à la référence d'un instrument rigide (parois non vibrantes). Des changements du temps d'attaque, des changements de timbre et des changements de régime d'oscillation (notes multiphoniques) sont observés.

En fin de chapitre, un complément est présenté dans lequel des simulations avec des instruments distordus est présenté. Comme vu dans le chapitre 3, la distorsion de la coque induit le couplage du mode acoustique plan avec le premier mode ovalisant qui a lieu à fréquence plus basse que le premier mode de respiration. Ce couplage peut altérer notablement l'impédance acoustique de l'instrument à la fréquence de jeu de l'instrument et donc, altérer fortement son régime d'oscillation. Les simulations présentées montrent que, la distorsion de la coque peut donner lieu à un effet important des vibrations de parois, et cela pour des valeurs des paramètres E et ρ réalistes quand on vise des applications musicales.

4.1. Introduction

The vibration effect of the instrument walls on its sound quality is a widely debated issue, although no clear results have yet been obtained. Manufacturers of wind instruments often state that the construction materials play an essential role in the acoustic quality of the instrument. Some experiences indicate that the material used can have an effect on the sound quality of the instrument. Frequently, wind musicians perceive the vibration on the instrument walls through the tact. A popular element to estimate the quality of a metal wind instrument consists of beating the horn and listening to the sound emitted by it. In the debates held by musicians, instrument-makers and scientists, the possible role of the nature of the material that the instrument is made of, is a common subject. Some musicians and instrument-makers can sometimes consider that the sound is a property of the structure, and not of the air column. The terms used to describe the timbre of an instrument are not well defined. This fact seems to reinforce the importance of the effect of the materials for listeners. The perception of distinguishable differences between instruments made of different materials is based on the differences in which the varying properties of these materials have an effect on the manufacturing process of the instruments. All these reasons render it difficult to evaluate the contribution made by the wall vibrations to the radiated field that is finally detected by the audience.

From the scientific point of view, the evaluation and quantification of the role played by the material of the instrument on its acoustic response is not straightforward. Due to the important influence of the instrument's excitation on its sound, it is very difficult to obtain meaningful results through experiments that compare several pipes built with different materials. The difficulties in outlining the role of the material in conditions of real interpretation, as well as the existence of several related, and often ignored variables, help explain the numerous existing debates on this subject. However, many scientific studies have aimed to, and still aim to address all the phenomena related to the influence of the construction material and the importance of wall vibration on the acoustic behaviour of a wind instrument.

In 1909, Miller [Mil09] carried out a review of the studies and research developed up to that time. Miller believed that the material used in its construction, can influence the quality of an instrument. He pointed out that the flute is the instrument more prone to this phenomenon, since its pipe is very thin: between 0.2 and 0.3 mm. Boner and Newman [BN40] carried out a study of the effect of the materials on the steady-state acoustic spectrum of organ flue pipes. They compared the level of different components of the spectrum and noticed slight differences in the superior harmonics. They conclude that the wall vibration effect must be very small compared to the sound generated by an air column. Knauss and Yeager [KY41] stimulated the walls of a cornet played mechanically at different frequencies. They concluded, from the measurements obtained, that the sound radiation is negligible, and deduced that the vibration of the air column masks any contribution made by the walls. Parker [Par47] carried out a comparative study of the musical sound spectra produced by wood and metal clarinets stimulated through artificial blowing. He concluded that there were no notable differences between instruments. Backus [Bac64], through experiments, estimated the

level of sound radiated outwards by a clarinet. For this, he filled an artificially stimulated resonator with an absorbing material so that the sound radiated by its edges was absorbed. This permits the measurement of the contribution to the acoustic field emitted by the instrument, due to the acoustic radiation of the vibrating structure. The sound radiated is 48dB below the sound normally produced by the instrument. Coltman [Col71] shows, through a series of blind reconnaissance tests, that flutists are unable to distinguish between instruments with the same geometry, but constructed with different materials. Neither the nature of the materials, nor the width of the wall, lead to the perception of audible differences either by the musician or by the audience. Backus and Hundley [BH66] present a local model of the wall impedance that allows us to take into account the approximate axisymmetrical vibration of the pipe, and predicts a reduction in the acoustic resonance frequencies as a result of this phenomenon. Gibiat et al. [GBP97] reported 6 dB variations in the harmonic spectrum of a simplified wind instrument, when the pipe was grasped or clamped. Malte Kob [Kob00] carried out an experiment with baroque organ flue pipes with and without damping of the walls. The results indicate that when the pipe is blown, some structural modes are stimulated and, in turn, significantly change some components in the transient spectra, although the effect is very small. A spectacular phenomenon linked to vibration effects have been observed and studied by Nederveen and Dalmolt [ND04] using distorted organ tubes. They propose a phenomenological model to explain the changes in frequency and level observed in experiments with thin-walled organ flue pipes. In [Gau97], a vibroacoustic model of a simplified instrument has been proposed in order to quantify the wall vibrations effect of its body on tone. This simplified instrument consists in a simply supported cylindrical elastic shell filled and surrounded with fluid. Such a model enables the calculation in the frequency domain of the forced response of the system taking into account 3 kinds of couplings: the shell/internal fluid coupling, the shell/lateral external fluid coupling and the inter-modal coupling induced by acoustic radiation at the end of the tube.

The aim of this paper is to estimate the consequences of wall vibrations on the oscillations of clarinet-like instruments, taking into account the impedance in time-domain simulations. A physical model of a simplified simple-reed instrument is proposed for evaluating the influence of the material it is made of on its acoustic behaviour. For this objective, a vibroacoustic model is used to determine the possible effect of wall vibration on the response of the air column. In this model, the body of the instrument is assimilated to a simply supported, thin-walled cylindrical shell and only the coupling between the resonator of the instrument and the air column is taken into account. External coupling and inter-modal coupling have been ignored. A simplified model of clarinet-like instruments permits a simulation of the self-sustained oscillations. The input acoustic impedance of the instrument, calculated by means of the vibroacoustic model, constitutes the numerical entrance of the time-domain simulations. Simulations corresponding to different configurations are compared with an instrument with non-vibrating walls in order to evaluate the influence of wall vibration effect on the oscillation regime of the instrument and its timbre.

This paper consists of five sections. Following the introduction, the complete model of the instrument is presented in Section 4.2. It is supposed to be a system composed of an excitation mechanism and resonator. The wall vibration effect is introduced by means of a vibroacoustic model that provides a correction of the input acoustic impedance of the instrument. In Section 4.3, the numerical simulation approach is adopted. Section 4.4 is

devoted to analysing the effects of the wall vibration on the acoustic response of the instrument, from the analysis of numerical simulations in the time domain and the special playing conditions. Finally, the conclusions of the study are presented in section 4.5.

4.2. Model of the simplified instrument

This part of the paper is dedicated to the description of the model of the instrument. The model adopted is based on the coupling of two subsystems: the resonator and the excitation mechanism. There are numerous works dedicated to the study of these parts (see for example [HKW95]). The excitation mechanism of wind instruments, through the action of blowing, permits the introduction of a volume of air on the resonator, which, in turn, generates sound. In this paper, the instruments excited by a simple-reed, such as the clarinet, will be analysed. The other part of the instrument is the resonator. It is the body of the instrument. From a physical viewpoint, it can be described as a linear system characterised by its input acoustic impedance.

4.2.1. A basic model of the excitation mechanism

The movement of the reed is controlled by the pressure difference between the oral cavity of the instrumentalist (p_{oc}) and the pressure on the inner channel of the reed (p_m): $\Delta p = p_{oc} - p_m$. Up to the main resonance frequency of the clarinet's reed (between 2 and 3 kHz), the acoustic behaviour of the reed is dominated by the elasticity. In other words, the mass effect can be ignored, and it can, therefore, be considered as a memoryless system, with an infinite resonance frequency. Therefore, although the reed presents a more complex behaviour pattern, a simple, but realistic, model can be used to characterise it by means of a simple harmonic oscillator characterised by a rigidity constant k (see for example the recent paper by Dalmont et al [DGO03]).

The strength exerted on the reed is $S \cdot \Delta p$, where S is the effective surface of the reed exposed at Δp. If y_o is the movement of the reed with regard to its equilibrium position, Hooke's law can be described as follows:

$$y = y_0 - \frac{S \cdot \Delta p}{k} \tag{4.1}$$

The movement of the reed controls the volume of the air entering the channel, which can be determined by means of the Bernouilli Equation. The oral cavity can be seen as a large volume of air at a constant pressure p_{co}. When requiring the preservation of energy, the Bernouilli equation gives the value of the jet entering the channel, according to its size:

$$u = w \cdot y \left(\frac{2|\Delta p|}{\rho} \right)^{1/2} \operatorname{sgn}(\Delta p) \tag{4.2}$$

where w and y are, respectively, the width and height of the channel, and ρ is the air density. The assumption that the reed has no mass, leads to the conclusion that the relationship between the pressure and the speed at equation (4.2) is independent of time.

If the pressure difference is larger than a limit value p_m, the reed is supposed to close the opening and the flow entering into the mouthpiece is equal to zero. The limit value p_m for which the reed closes the opening is given by $p_m=ky_0/S_r$. It is the minimum value of the mouth pressure for which the static solution corresponding to the reed blocked against the lay is stable. Finally, the volume flow u can be written as a non-linear function of the acoustic pressure

$$u = \omega \cdot y_0 \left(1 - \frac{\Delta p}{p_m}\right) \left(\frac{2|\Delta p|}{\rho}\right)^{1/2} \operatorname{sgn}(\Delta p). \tag{4.3}$$

This model corresponds reasonably to reality except that in practice the reed channel seems to be never completely closed.

4.2.2. The resonator

This section aims to describe the acoustic behaviour of the resonator. As such, a linear model is used to illustrate its behaviour. The resonator can be characterised in the frequency domain ($e^{-j\omega t}$) y means of its input acoustic impedance $Z(\omega)$

$$P(\omega) = Z(\omega) \cdot U(\omega) \tag{4.4}$$

where $P(\omega)$ and $U(\omega)$ are the Fourier transform of the pressure p(t) and the volume flow u(t). As a result of this linear model, if the acoustic input impedance of the resonator is known, the acoustic behaviour of the instrument can be characterized.

When considering a open-ended cylindrical resonator with non-vibrating walls, the acoustic input impedance is well known and given by

$$Z^r = -jZ_0 \tan(kl) \text{ with } Z_0 = \frac{\rho \cdot c}{S} \tag{4.5}$$

where l is the length of the cylinder, ρ and c are the density and the velocity of sound in the air, respectively, S is the transverse section and k is the wavenumber. The maxima of the module of the input acoustic impedance correspond to the acoustic resonances of the tube. They can be established as the odd multiples of the fundamental frequency

$$f_n = (2n-1) \cdot f_1 = (2n-1)\frac{c}{4l}, \tag{4.6}$$

where $n \in \mathrm{N}$, f_1 is the fundamental frequency, c is the sound velocity of the air, and l is the length of the resonator. If losses in the instrument are taken into account, the acoustic resonances are slightly out of harmony.

4.2.2.1. The vibroacoustic model

The expression (4.5) refers to a pipe whose walls do not vibrate. That is, a cylinder of infinitely rigid walls. In order to describe the wall vibration effect, the acoustic input

impedance of a vibrating resonator must be considered. When a single-reed instrument is blown, the air inside the resonator is stimulated.
This inner acoustic pressure stimulates the shell, producing the vibration of its walls. This fluid/shell coupling can change the acoustic behaviour of the instrument. There is another minor source stimulating the walls: At the mouthpiece of a blown instrument, there is a force applied at the reed. This force transmits the vibration from the mouthpiece to the walls of the resonator. This second source of vibration has not been considered in the vibroacoustic model. Thus, the resonator is supposed to be the main source responsible for introducing energy into the walls through coupling with the air column and its walls.

At this point the vibroacoustic model developed in [GT98a] is introduced. In particular, results obtained in [PGR04] are used. In this work, a vibroacoustic multimodal model, describing the inner fluid/shell coupling of a vibrating wall cylinder excited acoustically at the entrance, is developed. The coupling between the structure and the external fluid is neglected, since its influence on the impedance is weaker. It is assumed that the resonator, which constitutes the body of the instrument, is a thin-walled homogeneous and isotropic cylinder, of length *l,* mean radius *a,* and width *h* as shown in figure 4.1. In addition, the material of the shell is supposed to be characterized by the Young's modulus E, a Poisson modulus *v* and density ρ_s. The resonator is supposed to be simply supported at both ends. The analytical formulation permits the evaluation of the effect of wall vibrations on the acoustic behaviour of an instrument in these circumstances.

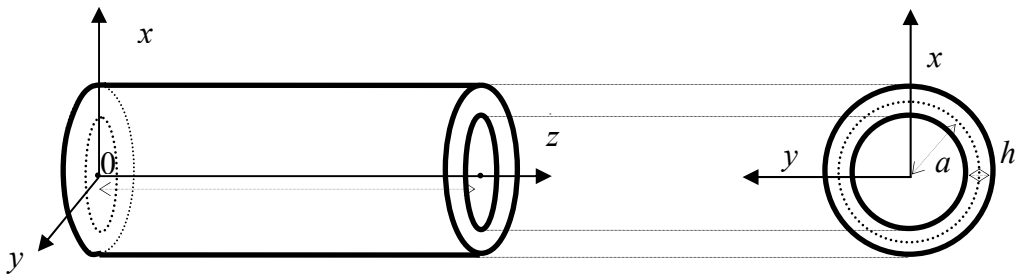

Figure 4.1: Representation of the cylindrical resonator and its geometric parameters

The coupling between the vibration modes of the cylindrical structure and the acoustic modes of the air column introduces an alteration in the acoustic input impedance of the cylinder. This variation is calculated using the integro-modal method taking into account shell vibration. The model only considers the internal radiation effects. The acoustic impedance of a wall-vibrating cylinder (Z) on the plane mode is obtained by taking into account a correction factor for the impedance (C) of a rigid cylinder with the same mechanical and elastic features, and the same boundary conditions (Z^r):

$$Z(\omega) = Z^r(\omega)\left[1 + C(\omega)\right] \tag{4.7}$$

The correction factor C depends on the cylinder features, the medium, and the excitation:

$$C(\omega)=\frac{4\pi\rho\cdot c}{m_\mu}\left(\frac{\pi}{l}\right)^2\frac{\omega\tan(\omega l/c)}{\left[(\omega/c)^2-(\pi/l)^2\right]^2\left[\omega^2-\omega_\mu^2\cdot(1-j\eta_\mu)\right]} \tag{4.8}$$

where ω_μ is the eigenpulsation of the shell motion equation associated to the first shell breathing mode μ=(m,q)=(1,0) , m_μ is its modal mass and η_μ is the shell structural damping. It can be seen that special conditions like the mechanical resonance condition ($\left[(\omega/c)^2-(\pi/l)^2\right]=0$) and spatial coincidence effect ($\left[\omega^2-\omega_\mu^2\cdot(1-j\eta_\mu)\right]=0$) lead to maximum values of the correction factor of the input impedance.

4.2.2.2. Wall vibration effects: Vibroacoustic coupling

The vibroacoustic model presented for the resonator accounts for the wall vibration effect, through the consideration of correction factor *C* of the input acoustic impedance of a rigid wall cylinder. For the simulations, only the acoustic plane mode and the first breathing mode of the structure (which is the first axisymmetric structural mode) have been considered. The eigenfrequency of other modes are too high to be significant in this application.

The correction factor for a typical resonator corresponding to a clarinet with the features represented in table 4.1, is negligible. The module of the correction factor is smaller than 0.1% in the frequency range of interest. However, when looking at much less dense and more elastic resonators, important effects can be observed.

Radius (a)	**14.25mm**
Length (l)	**0.5m**
Width (h)	**0.5mm**
Density (ρ_s)	**7800kg/m^3**
Young's Modulus (E)	**210 N/m^2**

Table 4.1: Geometric and elastic parameters of the resonator

Three physical phenomena can be associated with these effects: the mechanical resonance, the coincidence condition, and the acoustic resonance. These effects are discussed and illustrated with selected numerical applications in [PGR04]. We just recall here some useful conclusions. The formation of stationary waves in the air column stimulates the vibration of the walls and excites some shell modes on the structure at specific frequencies. In turn, the wall vibration has an influence on the inner pressure in the instrument. When considering the usual materials of woodwind construction, the wall vibration effect is negligible. However, for a fixed value of the geometrical parameters of the cylinder, it is shown that for low enough values of Young's modulus (E) and density (ρ), the wall vibration effect can be much important. Consequently, the acoustic input impedance can be strongly affected. Under these circumstances, the mechanical resonance is superposed by one of the other two effects, in such that the influence of the wall vibration effect on the acoustic input acoustic impedance of the resonator is no longer negligible. The effect of this fluid/shell

coupling is an alteration in the antiresonances of the input acoustic impedance of the tube.

Next, numerical simulations in the time domain will show that this effect has an influence on the oscillation regime of the instrument.

4.3. Numerical simulation

4.3.1. Simulation model

Simulations of the time domain have been used by several authors in several application fields, such as the implementation of real-time synthesizers, or the study of the dynamic behaviour of an oscillating system. They are used in this work in order to obtain the periodic oscillations that correspond to the oscillation regimes of the instrument. These methods evaluate the features of the inner or external pressure, minimising the errors. There are two methods depending on the analysis of the resonator: frequential methods and methods in the time domain. In the frequential methods, the resonator is considered as a filter and is represented by its acoustic input impedance. In the time domain, the reflection function governs the behaviour of the resonator. The main interesting feature of the simulations in the time domain, with regard to the methods in the frequency domain, is that they also permit the simulation of transients, as well as stationary regimes. This technique only permits the calculation of the pressure at the entrance of the instrument. Considering the resonator as a junction of small elements, the pressure at any point in the resonator can be calculated [Duc90]. The resolution of an equation by methods in the time domain, using the reflection function, constitutes a non-linear differential system [Kee92]. This continuous system is discretised with classical methods of numerical analysis or signal processing, like Runge-Kutta [BA89], Euler [Sch81], or bilinear transformation [Kee92].

The technique proposed by Schumacher [Schu81] is used in this paper to study the self-oscillation state of a simple reed instrument, since it is one of the most common techniques employed to study the features of these instruments. This technique has been chosen due to its simplicity in realistically describing the basic behaviour of the instrument, without creating a complicated numerical algorithm. It consists of the assumption that the resonator acts as a linear filter. Through the simulations in the time domain, the behaviour of instruments made of different materials can be analysed and predicted. The acoustic input impedance of the resonator calculated by the vibroacoustic model explained in section 4.2, constitutes the input of the simulations in the time domain. The behaviour of the resonator is completely determined by the input impedance or, equivalently, by the reflection coefficient,

$$R(\omega) = \frac{Z(\omega) - Z_0}{Z(\omega) + Z_0} \tag{4.9}$$

where Z_0 is the characteristic impedance of the inner fluid. In the time domain, the resonator can be described by means of the impulse response h(t), which is the inverse Fourier transform of the impedance:

$$p(t) = h(t) * u(t) = \int_{-\infty}^{\infty} h(t-s)u(s)ds \tag{4.10}$$

The integration of function *h(t)* uses up much calculation time, due to its time extension. The use of the reflection function *r(t)* is more efficient than the use of the impulse response. The reflection function is simply the inverse Fourier transform of the reflection coefficient as defined in equation (9). After some calculations, the convolution equation (10) can be written as:

$$p(t) = Z_0 v(t) + r(t) * \left(p(t) + Z_0 v(t)\right) \tag{4.11}$$

The implementation of this method enables us to obtain a numerical solution in the time domain for the inner pressure of the instrument when oscillating. B. Gazengel et al. [GGA95] analyse the difficulties related to the problem of carrying out simulations of the input acoustic impedance in the time domain. The numerical error can be minimised if the value of the imaginary part of the input impedance is required to be null on the sampling frequency.

The time domain simulation constitutes a very useful study tool, since it permits the study of the transient and stationary regimes of an instrument, and the varying of the control parameters. Moreover, it offers a signal that can be heard. Once the input acoustic impedance of the instrument is known, the sound that a specific instrument makes under specific prime conditions can be synthesised. In this paper simulations in the time domain are used as an analysis tool to quantify the magnitude of the vibration effect on the instrument walls.

The physical model described above is concerned with the inner acoustic field. As such, it does not take the external acoustic field, created by the instrument, into account. The study of the acoustic behaviour of the instrument involves analysing the internal acoustic pressure. An evaluation of the external acoustic field generated by the instrument, can be obtained by convolving the simulated signal with a digital high pass filter (an infinite impulse response filter). This filter takes into consideration the sound radiation emitted by the instrument see [BK88].

4.3.2. The parameters for the simulated signal analysis

The compound model of the instrument developed in this work provides the simulated sound emitted by a “virtual” instrument, made of any kind of material. The behaviour of the resonator is characterised by the input acoustic impedance of the instrument, and the excitation mechanism implemented in the numerical simulation. The performance of the musician and the qualities of the mouthpiece can be specified through the control parameters of the simulation. The analysis of the simulated signals permits the evaluation of the importance of the wall vibration effect on the acoustic response of the instrument through reference to the non-vibrating (rigid) instrument.

In order to discern the role of the wall vibration effect, two parameters are used to quantify the perceptual effects of simulated signals on the timbre: the attack time and the spectral centroid. The spectral envelope of the sound emitted by an instrument, is the

main determinant responsible in its timbre for the self-sustained sound in a permanent regime. Several parameters have been defined relating to the relative magnitude of the maximums of the spectrum. The spectral centroid (SC) permits the evaluation of the spectrum of the signal with a single value. This is defined as the normalized Fourier amplitude-weighted frequency average of the radiated pressure:

$$SC = \frac{\sum_{k=1}^{N_\nu} k\alpha_k}{\sum_{k=1}^{N_\nu} \alpha_k} \tag{4.12}$$

where α_k is the amplitude of the k^{th} harmonic and N_ν is the number of harmonics considered to compute the spectral centroid. In single-tone research and in a quasi-musical context, a multitude of authors (see for example [MWD95]) have found that the long-time-average spectral centroid maps suitably with the primary dimension of multidimensional perceptual spaces.

Apart from the spectral distribution, it is well known that an important parameter in the definition of the perceptual features which define the timbre of an instrument, is the attack time [KMW94]. Two sounds with the same spectrum, but different transient attacks, present important differences in timbre. Attack time is related to the duration of the transient of the signal. A practical non-dimensional parameter to evaluate the duration of the transitory regime is defined by

$$\tau = \frac{t_{attack}}{T} \tag{4.13}$$

where t_{attack} is the transitory attack time and T is the period of the signal. Attack time is evaluated as the rise time measured from the time the amplitude envelope reaches a threshold of 10% of the maximum amplitude, to the time it takes to attain this maximum amplitude. In this paper, the attack time and the spectral centroid of the simulated signals are calculated in order to appraise the relative contributions of the attack and steady state on the timbre of the instrument.

4.3.3. A reference case: an instrument with rigid walls

An analysis of the instrument with non-vibrating walls is the starting point for evaluating the significance of the wall vibration effect. This particular case is very important, since it constitutes the reference point by which to evaluate the magnitude of the wall vibration effect. Next, the parameters defined in section 4.3.2 will be used to analyse the simulated signal corresponding to the rigid instrument. Since the instrument walls do not vibrate, the acoustic input impedance of the vibroacoustic model used is described by equation (4.5). The instrument simulated is 0.5m long, and 6mm in radius. The control parameters for the simulation in the time domain are given in table 4.2. Viscothermal dissipation at the boundaries has been considered in the simulations.

Some parameters used in the simulations have been chosen to coincide with the distinctive parameters of a typical clarinet: 14.25 mm. in radius, 0.5 mm. in width and

0.5 m. in length. Table 4.2 shows the control parameters of the simulations that have been established for superficial stiffness, reed width, and the opening of the mouthpiece at rest, as well as the feeding pressure. These values correspond to the typical values of a clarinet's mouthpiece and resonator, and the normal practice of an interpreter.

Feeding Pressure (P_a)	**2300 Pa**
Superficial stiffness of the reed (k)	**7.5 10^6Pa/m**
Width of the reed (w)	**10 mm**
Opening of the reed at rest (y_0)	**0.8 mm**

Table 4.2: Control parameters of the simulations in the time domain

Figure 4.2 shows the simulated pressure signal. After a very brief transitory period of 25ms, the instrument reaches a stationary regime of 2000Pa in width. This value lies below the feeding pressure (2300Pa). The fundamental frequency for this clarinet is f_1=170Hz, and, as such, the period of the signal T=5.9ms. The non-dimensional attack time for the rigid-walled instrument is τ=4.2. The sample frequency is 25000Hz.

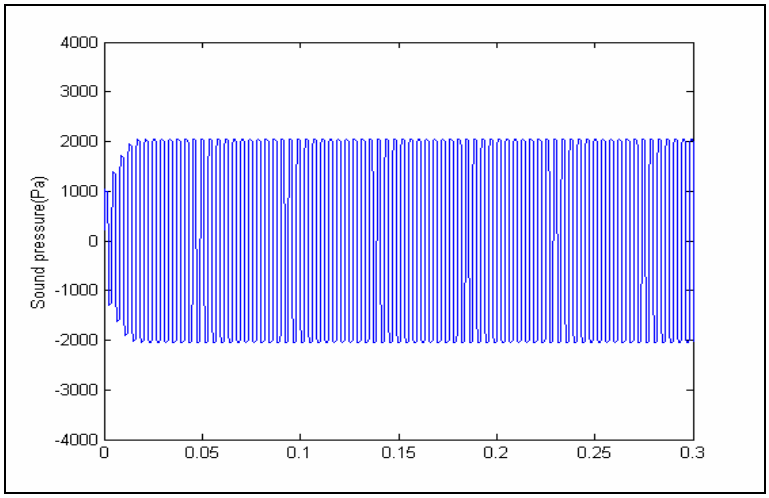

Figure 4.2: Transient of an instrument with rigid walls

The sonogram of the simulated signal is represented in figure 4.3. The sonogram is a representation on the grey scale of the sound power level in which the y-axis represents the frequency, and the x-axis the time. Since the transient is very brief, the signal represents a spectral distribution which is, virtually, independent of time. The spectral content of the signal is representative of a cylindrical pipe open at one of its extremes: the distribution of odd/varying harmonics can be seen in the sonogram.

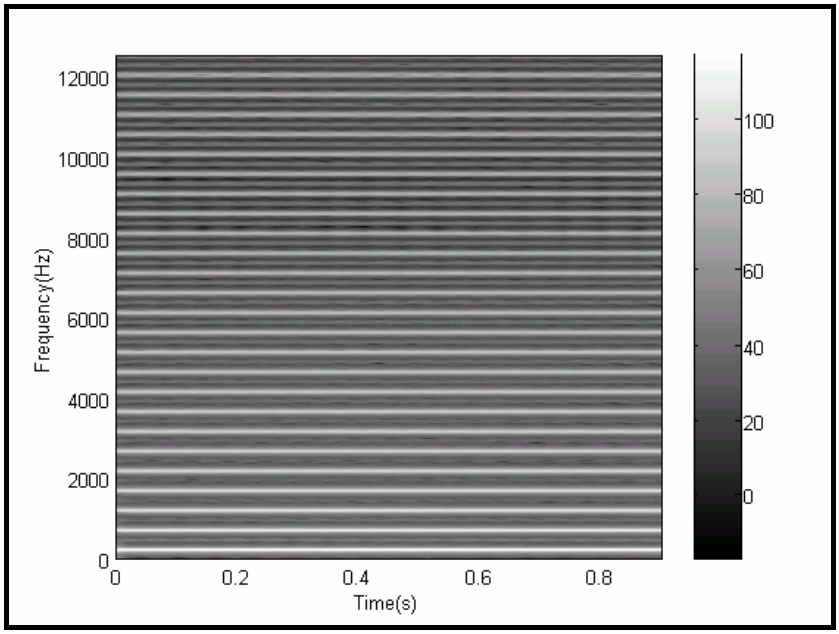

Figure 4.3: Sonogram of the simulated signal corresponding to an instrument whose resonator is a rigid-walled cylinder

The spectral centroid is calculated by conducting spectral analyses for the steady state of the signal. The simulated signal is divided into overlapping sections, each of which is windowed by a symmetric Hanning window of 512 points, then zero padded to 8192 points. In table 4.3, the spectral centroid has been calculated considering the different values of the feeding pressure.

Blowing pressure (Pa)	SC
1700	1.11
2000	1.48
2150	1.66
2300	1.87

Table 4.3: The spectral centroid calculated from the simulated signals corresponding to a cylinder with non-vibrating walls excited by different blowing pressures.

It can be seen that the spectral centroid increases as the feed pressure grows, moving away from the oscillation threshold. The first 20 harmonics have been considered in the calculation of the spectral centroid. The blowing pressure for playing conditions in a clarinet is about 2300 Pa. In these conditions, the spectral centroid of the simulated signals corresponding to a rigid-wall instrument is SC=1.87.

4.3.4. Main wall vibration effects on the acoustic response of the instrument

When the vibration of the instrument walls is considered, part of the mechanical vibration energy can be exchanged with the vibration acoustic energy of the particles of the air column of the resonator, which constitutes the body of the instrument. For sufficiently low values of Young's modulus (E) and density (ρ) of the material of the

resonator, the vibroacoustic model described in section 2, predicts important changes in its acoustic impedance [PGR04]. In these conditions, the wall vibration effect can be of great importance. The numerical simulation of an instrument of such characteristics can pinpoint a change in its oscillation regime. Next, the signals simulated by instruments built with these materials are analysed in order to evaluate the importance of the wall vibration phenomenon. Due to the vibration of the instrument walls, some significant changes are outlined from the point of view of the perception of the signal simulated by the instrument. Among these, three must be pointed out: the increase of the attack time, the change in timbre and the Wolf note.

4.3.4.1. Increase of the transient attack

It has been ascertained that the attack time of a complex tone is a substantial factor in the discrimination of musical sounds, and, as such, is linked to the timbre. The starting transient is the most important phase for the subjective recognition of musical transients. Figure 4.4 shows the transients of the simulations in the time domain corresponding to the instruments made of steel, aluminium, wood and polymer. The thickness of the instrument walls (h=0.5mm) is supposed to be the same for all the simulations. It should be pointed out that this value is not a realistic value for brass instruments and even less for woodwind instruments. Therefore, the results must be carefully interpreted.

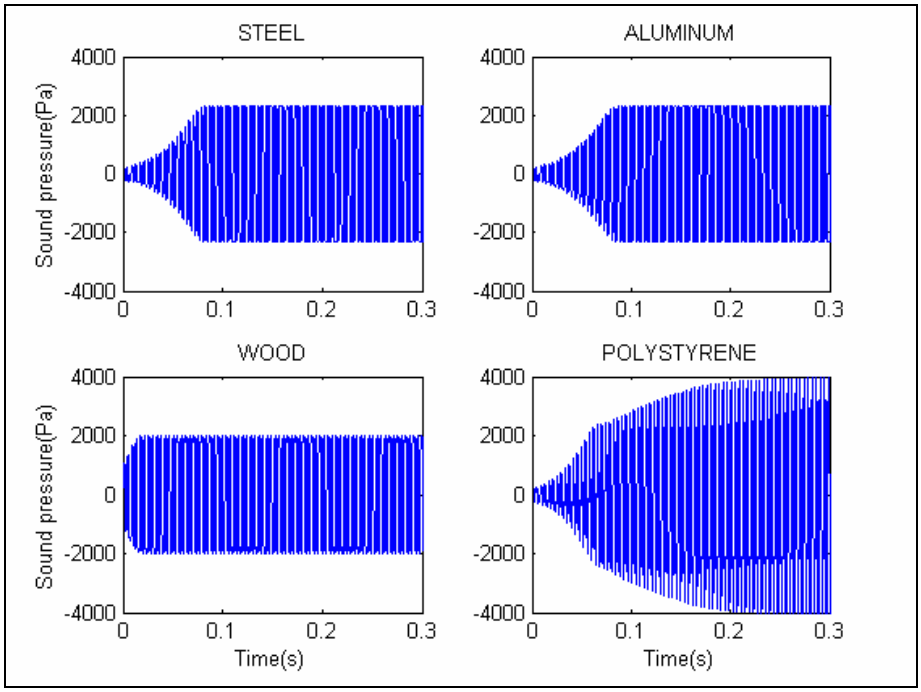

Figure 4.4: Transients corresponding to the simulated signals of instruments made of different materials: steel, aluminium, wood, and polymer

Young's modulus and the density of each material and the corresponding eigenfrequency of the first breathing mode of the shell are shown in table 4.4.

	Density ρ_S (kg/m^3)	Young's Modulus E (10^9 N/m^2)	First shell eigenfrequency (Hz)
Steel	**7800**	**210**	**3181**
Aluminium	**2710**	**70**	**3116**
Wood	**525**	**13**	**3051**
Polymer	**1050**	**3**	**1036**

Table 4.4: The Young's modulus, the density, and the corresponding eigenfrequency of the first breathing mode of the shell for materials used to simulate different instruments.

It can be seen that, out of the four transitions, the one that corresponds to the wood instrument shows fewer differences with regard to the instrument of non-vibrating walls. The two instruments made of metal have a very similar response. The most notable difference in comparison with the rigid-walled instrument is that the duration of the transient regime is higher (around 80 ms). Finally, the anomalous behaviour of the polymer instrument must be pointed out. In this case, the transient is abnormally big and presents two distinctive behaviours: from 0 to 60 ms, the response is similar to that of a metallic instrument, and from 60 ms to the stationary regime (≈ 300 ms), the increase of the amplitude is softer. This behaviour, which affects the oscillation regime of the instrument, can be explained in terms of the fluid/structure coupling. As a consequence of the energetic efficiency of the vibration provided by the polymer walls, the signal generated by the instrument presents an abnormally high amplitude (4000Pa compared with the 2000Pa of the rigid instrument).

4.3.4.2. Change of spectral centroid

When Young's modulus and the density of the material of the instrument are sufficiently low, the vibroacoustic coupling between the walls and the air column can affect its timbre. Steady state spectra analysis of the simulated signals of wall-vibrating instruments can reveal the influence of the wall vibration effect on the timbre. In the first example, the spectra of the steady state inner pressure simulated by the polymer and rigid resonators of two instruments are shown in figure 4.5.

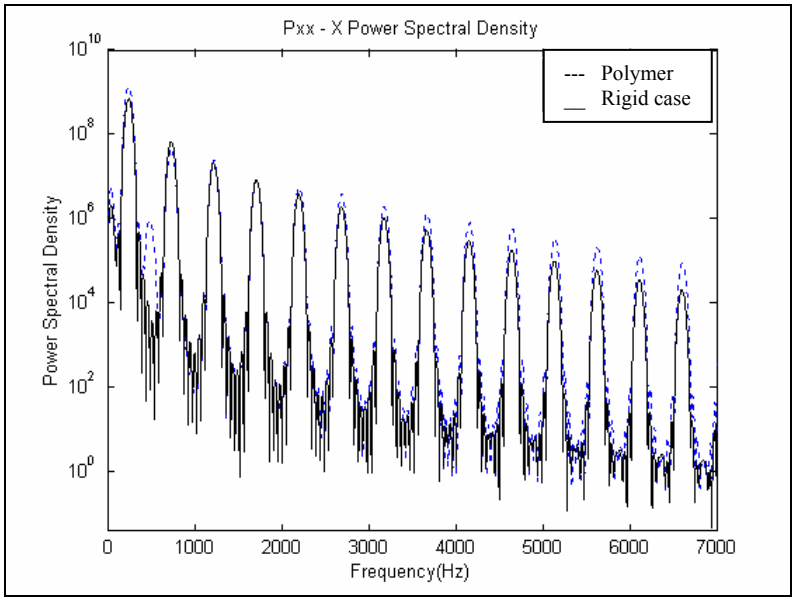

Figure 4.5: Steady-state spectrum of simulated signals corresponding to both instruments made of polymer and wood shells.

It can be observed that the spectrum of the polymer instrument is richer in higher harmonics than the one calculated using the instrument with non-vibrating walls (rigid). Of course, these results must be carefully interpreted, as the limitations of the proposed model should be taken into account. In order to objectively quantify the change in timbre of the instrument, the spectral centroid of the simulated signals corresponding to the instruments made of different materials, is calculated in this section. Tables 4.5 and 4.6 show the spectral centroid obtained from simulations of instruments made of different kinds of wood and polymer, respectively. Young's modulus, the density of the material, and the eigenfrequency of the first breathing mode are shown, together with the corresponding spectral centroid calculated for each simulated signal.

Wood	E (N/m^2)	ρ (kg/m^3)	First shell eigenfrequency	SC
	10	300	1869	1.92
	3	1000	561	1.81
	1	800	362	3.00
	0.1	200	229	5.00

Table 4.5: The spectral centroid calculated from simulated signals corresponding to instruments made from different types of wood. The Young's modulus, the density and the eigenfrequency of the first shell mode of each kind of wood are represented.

Polymer	E (N/m^2)	ρ (kg/m^3)	First shell eigenfrequency	SC
	9	1500	1502	1.87
	1	1000	613	1.01
	1	2000	434	1.03
	0.5	1000	434	1.03

Table 4.6: The spectral centroid calculated from simulated signals corresponding to instruments made from different types of wood. Young's modulus, the density and the first shell eigenfrequency of each kind of wood, are represented.

As Young's modulus and the density of the material of the instrument become smaller and smaller, the wall vibration effect grows in importance. The acoustic resonances of the air columns are altered and the spectral centroid changes in comparison with the value of the non-vibrating resonator (SC=1.87). The sound effect produced by the walls during this process is that of a filter of sound generated by the instrument in a steady state, which involves a change in its timbre. A possible interpretation of this is that when the fluid/shell coupling is produced, the energy needed for the walls to vibrate is obtained from the air vibrating inside the resonator.

4.3.4.3. The Wolf note

For some mechanical parameters of the resonator, the time domain simulations show an unpleasant sound without any apparent reason. A similar phenomenon, which is termed the Wolf note, often appears in the stringed instruments with least bows (in particular, the cello). This parasite note is produced when the instrument stimulates two nearby, resonant frequencies. The tuning and the sonority of the note are strongly altered. In the case of string instruments, the Wolf note is the audible product of the coupled oscillation of the string and the body of the instrument [Fir78], [PCG91]. When produced, the string oscillates at a frequency which is very close to the resonance of a part of the instrument. As a consequence of this, the musician loses control of the instrument. Wind instrument musicians are also aware of the Wolf note and could refer to it as "multiphonic sound", although it is not so common.

The vibroacoustic model of the instrument developed in this work permits an investigation of the conditions that favour the appearance of this phenomenon. If the fluid/structure coupling underlies the phenomenon of the Wolf note, numerical simulations in the time domain with clarinet-like instruments with vibrating walls could be used to illustrate the generation of quasi-periodic regimes.

For a given geometry of a clarinet-like instrument with vibrating walls, different resonator materials and control parameters have been simulated in order to generate a Wolf note. It has been found that an instrument that is 0.5m long, 6mm in radius, and which is made of a material of Young's modulus $E=5.4\cdot10^6$ and volumetric density $7800kg/m^3$, emits a Wolf note when it is simulated with the control parameters shown in table 4.2. The simulated signal can be observed in figure 4.6.

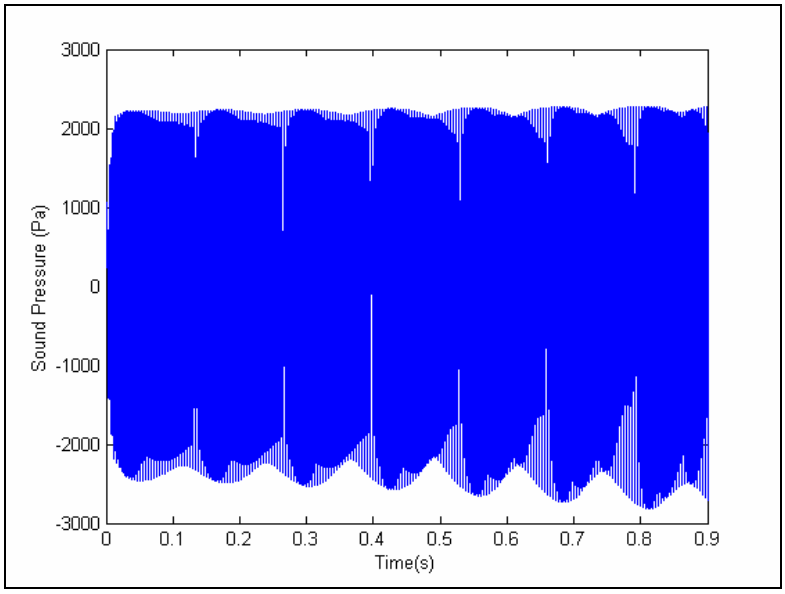

Figure 4.6: Simulation in the time domain obtained for an instrument emitting a Wolf note

The amplitude variation is characteristic of this phenomenon. The beating effect on the amplitude modulation is asymmetric (this is more important for the minimums than the maximums of the signal). It has a constant frequency of about 8Hz and increases with time.

Indeed, the parameters for which the Wolf note has been simulated are completely unrealistic with regard to a real wind instrument. However, the aim of this paper has been to show that the Wolf note phenomenon can be associated with the wall vibration effect. In [ND04], through experimentation, Nederveen and Dalmont discovered oscillations similar to the Wolf note kind in a slightly elliptical organ pipe and proceeded to suggest that asymmetries can cause the coupling of wall and air vibrations.

Hurgen suggests in [HL02], that asymmetric “elliptical” modes of a cylindrical tube could provide a mechanism by which the wall vibrations can affect the tone produced by the instrument. Thus, a possible way to explain the presence of the Wolf note phenomenon in a real instrument, involves the development of a vibroacoustic model of a vibrating, distorted shell.

4.4. Conclusion

The influence of the material on the acoustic response of wind instruments is investigated. The shell/fluid coupling is supposed to be the main source responsible for introducing energy into the walls. A vibroacoustic model of the resonator accounts for the wall vibration effect and provides an expression of the acoustic input impedance of a vibrating resonator. In general, vibroacoustic coupling between the wall vibration and the air column does not lead to audible effects, except for some special values of material and geometry characteristics; in theses cases the wall vibration effect becomes very important. Numerical simulations of wind instruments are used to show the influence of the fluid/structure coupling on the oscillation regime of a simplified clarinet-like instrument with vibrating walls. Three main effects due to wall vibrations are observed on the simulations caused by the wall vibration effect: An increase of the transient attack, a change of the spectral centroid and the “Wolf note” phenomenon.

4.5. Complemento: Simulación temporal de un instrumento de viento de lengüeta simple con el cuerpo ligeramente deformado.

Hemos visto que para una estructura perfectamente cilíndrica, solamente si el módulo de Young y la densidad del material que constituye el cuerpo del instrumento son suficientemente pequeños, se producen fenómenos de acoplamiento fluido/estructura importantes entre las paredes del instrumento y la columna de aire. En ese caso, la frecuencia del primer modo de respiración es suficientemente débil, lo que provoca un acoplamiento fluido/estructura importante.
En estas condiciones, el acoplamiento entre el primer modo de respiración de la estructura y el modo acústico plano implica un cambio importante de la impedancia acústica de entrada del tubo. Sin embargo, este fenómeno corresponde a instrumentos construidos con materiales cuyas características físicas no son reales. Dicho de otro modo, el fenómeno de vibración de paredes no es significativo en el caso de estos instrumentos de perfil perfectamente cilíndrico.

Entonces, ¿cómo se pueden explicar los fenómenos de vibraciones de paredes referenciados en [ND04]? En el capítulo 3, el modelo vibroacústico propuesto muestra que pueden ocurrir acoplamientos adicionales cuando se consideran estructuras ligeramente distorsionadas. En efecto, la distorsión induce un acoplamiento entre el primer modo oval y el modo acústico plano. Puesto que la frecuencia de este modo de estructura es, en general, bastante pequeña, el acoplamiento interviene sobre las primeras frecuencias acústicas del tubo para estructuras construidas con materiales realistas. La particularidad de este acoplamiento se debe a que los primeros modos de estructuras no son los modos asociados a los índices circunferenciales menores. En particular, el primer modo de estructura puede ser un modo oval (asociado a un orden circunferencial m=2). En estas circunstancias, el defecto de ovalización de la estructura produce un acoplamiento que puede ocasionar un cambio en el régimen de oscilación del instrumento y puede, por tanto, explicar efectos importantes de vibración de pared sobre el comportamiento acústico del instrumento.

El objetivo de este complemento es utilizar simulaciones temporales para mostrar el efecto potencial de la vibración de las paredes sobre el régimen de oscilación de un instrumento del tipo clarinete que presenta defectos de ovalización. Con este objetivo, se ha utilizado el modelo de simulación de un instrumento de viento de lengüeta simple, analizado en el capítulo 4, con la impedancia acústica de un tubo cilíndrico vibrante deformado dado por el modelo vibroacústico del capítulo 3. Se analizan señales temporales simuladas que corresponden al régimen de oscilación de instrumentos con defectos en esta sección para destacar fenómenos de vibración de paredes importantes. El parámetro de señal utilizado para este estudio es el Centro de Gravedad Espectral CGE (Spectral Centroid en inglés), que es la media de las frecuencias harmónicas de la distribución espectral de la señal ponderada por la amplitud de cada resonancia.

4.5.1. Acoplamiento vibroacústico en estructuras deformadas

Como se presenta en el capítulo 3, el fenómeno de vibración de paredes viene determinado por la frecuencia propia del primer modo oval de la estructura y, por tanto, el material puede influir sobre el sonido que produce. La tabla 1 reagrupa los valores de la frecuencia propia del primer modo de respiración (f_{b1}) y del primer modo oval (f_{o1}), para ocho estructuras de longitud l=0.5m, de radio a=14.25mm y de espesor h=0.5mm construidas con diferentes metales caracterizados por el módulo de Young (E), el módulo de Poisson σ y la masa por unidad de volumen (ρ).

Material	**E (GPa)**	**ρ (kg/m^3)**	**σ**	**f_{b1}(Hz)**	**f_{o1}(Hz)**
Plomo	16	11340	0.44	742	378
Platino	61	21450	0.38	1015	557
Plata	30	10490	0.37	1022	557
Oro	79	19300	0.44	1192	688
Estaño	50	7310	0.36	1586	857
Cobre	130	8920	0.34	2386	1254
Acero	210	7800	0.28	3244	1652
Aluminio	70	2710	0.35	3094	1658

Tabla 4.7: Propiedades físicas (módulo de Young, coeficiente de Poisson y densidad) de diferentes metales y frecuencias propias correspondientes a los primeros modos de respiración (f_{b1}) y oval (f_{o1}) para estructuras de longitud l=0.5m, de h=0.5 de espesor y de radio a=14.25mm.

La primera frecuencia de resonancia del modo oval es menor que la frecuencia de resonancia del modo de respiración para todas las estructuras (ver tabla 4.7), lo que confirma la idea ya enunciada, es decir, que el primer modo de estructura no es el que tiene los índices modales más débiles. En particular, para ciertos metales, como el plomo, el platino, la plata y el oro, la resonancia mecánica del modo oval (f_{o1}) es del mismo orden de magnitud que las primeras frecuencias acústicas del tubo. Esto significa que pueden ocurrir acoplamientos fluido/estructura importantes en estas circunstancias.

El material con el que la estructura está hecha no es el único factor determinante de las propiedades resonantes mecánicas de la estructura. La geometría también lo es. En consecuencia, para una longitud 1=0.5 y un radio de la estructura a=14.25mm, se puede buscar el espesor para que la frecuencia propia del premier modo oval coincida con una de las primeras resonancias acústicas, alterando así el comportamiento acústico del instrumento. La figura 1 ilustra la impedancia de entrada acústica de una estructura de plomo con un espesor tal que permita que se produzcan fenómenos importantes de vibración de paredes. Con estas dos condiciones, la primera frecuencia del modo oval es f_{o1}=347.8Hz.

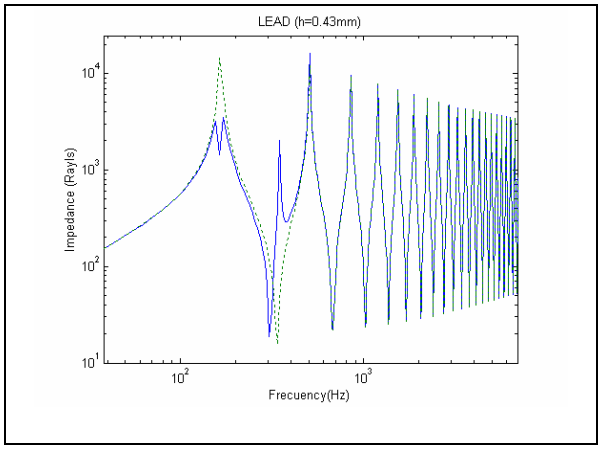

Figura 4.7: Impedancia acústica de entrada de un cilindro con paredes vibrantes (Za) construido en plomo (E=16·109N/m, σ=0.44 y ρS=11340 kg/m3). La referencia de un tubo rígido está representada en línea discontinua (Zr). Las características geométricas son: longitud l=0.5, radio a=14.25mm y espesor h=0.43mm

4.5.2. Simulación temporal

Una vez hemos visto que la distorsión de la estructura favorece el acoplamiento fluido/estructura para estructuras de determinados espesores, analizaremos el régimen de oscilación de instrumentos construidos con estas estructuras mediante simulaciones temporales. La figura 4.8 muestra la señal temporal que corresponde al instrumento construido con una estructura de plomo presentado anteriormente.

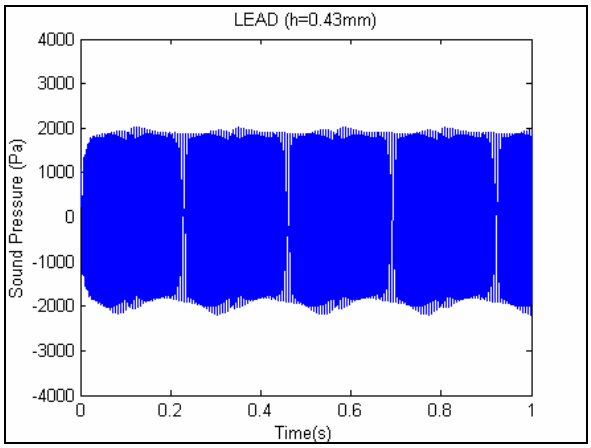

Figura 4.8: Señal temporal simulado correspondiente a un instrumento fabricado en plomo (E=16GPa, σ=0.44 y ρ=11340kg/m3). El cuerpo del instrumento es una estructura deformada (ε=0.1) de espesor h=0.43mm, de longitud l=0.5m y de radio a=14.25mm. El régimen de oscilación del instrumento corresponde a una nota multifónica (Nota del Lobo)

La señal presenta el batido típico de las notas multifónicas, explicadas en el capítulo 3. En esta sección se consideraron sonidos multifónicos para estructuras perfectamente cilíndricas construidas con materiales que no eran realistas (módulo de Young y densidad muy pequeños). La obtención de una nota multifónica mediante la simulación en el dominio temporal muestra que pueden ocurrir cambios importantes en el régimen de oscilación del instrumento cuando se consideran estructuras ligeramente distorsionadas construidas en plomo. Sin embargo, cabe destacar que este fenómeno

solamente ha sido obtenido para un instrumento construido en plomo con una distorsión de, como mínimo, $\varepsilon>0.095$ y para valores muy específicos de la geometría de la estructura. En este estudio se ha fijado la relación de esbeltez (coeficiente entre el radio y la longitud) en un valor particular y se han considerado diferentes valores de espesor de la estructura. Se han llevado a cabo simulaciones con otros materiales, sin embargo, sólo se han observado cambios importantes en el régimen de oscilación con el plomo. En la tabla 4.8 se presenta un estudio de la evolución del Centro Espectral de Gravedad en función de la deformación de la estructura.

ε	CGS
0	2.1
0.08	2.1
0.085	2.2
0.09	2.3
0.095	2.6
0.1	3.8

Tabla 4.8: Centro Espectral de Gravedad (CGS) calculado a partir de la señal temporal simulada correspondiente a instrumentos con h=0.5mm de espesor construidos en plomo (E=16GPa, ρ=11340kg/m^3, σ=0.44), en función del parámetro de deformación ε. Las primeras frecuencias de respiración y de ovalización de la estructura son f_{b1}=700Hz y f_{o1}=404Hz respectivamente. La frecuencia fundamental es f_1=170.5Hz para todas las simulaciones.

El valor del CGE para una estructura con ε=0.08 es el mismo que para una estructura perfectamente cilíndrica (CGS=2.1). Esto significa que el acoplamiento no es significativo para las estructuras no deformadas. En este caso, la perturbación de la impedancia de entrada es demasiado pequeña como para alterar el régimen de oscilación del instrumento. Sin embargo, la deformación de la estructura provoca un acoplamiento fluido/estructura importante, que se muestra por el cambio del CGE de las señales simuladas para las estructuras más deformadas. El régimen de oscilación del instrumento, en este caso, se encuentra muy alterado por el acoplamiento adicional del primer modo oval con el modo acústico plano. La distribución espectral en régimen transitorio de la nota multifónica simulada correspondiente al instrumento deformado en ε=0.1 es muy diferente que la de un instrumento con las paredes no vibrantes puesto que el CGE vale 3.8.

4.5.3. Variación del espesor de la estructura

Después del análisis de los resultados y la búsqueda de fenómenos de vibraciones de paredes en el régimen de oscilación del instrumento, el espesor de la estructura parece ser un parámetro muy importante en relación con el acoplamiento vibroacústico. Para mostrar la sensibilidad del fenómeno a este parámetro, se se han estudiado las señales simuladas por diferentes instrumentos de plomo con diferentes espesores. La tabla 3 muestra los resultados obtenidos por el CGE de las señales simuladas para todas las estructuras. La relación de esbeltez de las estructuras es la misma.

h	f_{b1}	f_{o1}	f_1(Hz)	CGE
0.40	700.00	324	170.5	1.7
0.41	700.01	332	161.3	1.4
0.42	700.01	340	493	3.1
0.43	700.01	348	170.5	3.8
0.44	700.02	356	170.5	2.2
0.45	700.02	364	170.5	2.0

Tabla 4.9: Centro Espectral de Gravedad (CGS) calculado a partir de la señal temporal simulada correspondiente a instrumentos construidos en plomo (E=16GPa, ρ=11340kg/m^3, σ=0.44) con una estructura distorsionada (ε=0.1) y diferentes espesores.

Podemos ver en la tabla 3 que la frecuencia propia del primer modo oval de la estructura depende en gran medida del espesor de la estructura. Esto explica que el CGE varíe notablemente con el espesor de la estructura. Estos resultados confirman que el acoplamiento vibroacústico tiene un efecto sobre el régimen de oscilación del instrumento para valores muy particulares de su espesor. Solamente en este caso, el fenómeno de vibración de las paredes es significativo. Cabe destacar que el régimen de oscilación de la estructura con un espesor de 0.43mm se produce en la doceava (tercer armónico). En este caso, como la frecuencia propia del primer modo oval es muy próxima al segundo parcial, favorece este régimen de oscilación. Por otro lado, la frecuencia fundamental de la estructura con un espesor de 0.42mm desciende ligeramente de 170.5 Hz a 161.3Hz. Para otros valores de espesor de la estructura, la frecuencia fundamental de los instrumentos es la que corresponde a un instrumento rígido (con paredes que no vibran) puesto que el acoplamiento vibroacústico no es suficientemente importante.

4.5.4. Conclusión

Se ha analizado el régimen de oscilación de diferentes instrumentos con la estructura deformada mediante simulaciones en el dominio temporal. Se han estudiado diferentes materiales y geometrías. Se observan notas multifónicas únicamente para un instrumento construido en plomo y una geometría muy particular. Para este tipo de material, puesto que la frecuencia del primer modo oval es muy pequeña, se pueden ajustar los parámetros que definen la geometría del cuerpo del instrumento de tal manera que esta frecuencia coincida con la segunda resonancia acústica del tubo. Esto provoca una perturbación importante de la impedancia de entrada, y, por tanto, un comportamiento autooscilante particular. En este caso, la deformación de la estructura causa un acoplamiento vibroacústico que se traduce en un cambio de régimen de oscilación. También se han observado variaciones importantes del Centro Espectral de Gravedad, asociadas al fenómeno de vibración de las paredes. La validez de los resultados obtenidos está condicionada por la principal limitación del modelo: la deformación del tubo sonoro ha de ser suficientemente pequeña.

4.5 Complément: Simulation temporelle d'un instrument à vent anche simple dont le corps est légèrement distordu.

Nous avons vu que pour une coque parfaitement cylindrique, seulement si le module de Young et la densité du matériau constituant le corps de l'instrument sont suffisamment petits, des phénomènes de couplage fluide/structure importants se produisent entre les parois de l'instrument et la colonne d'air. Dans ce cas, la fréquence du premier mode de respiration est suffisamment faible, ce qui induit un couplage fluide/structure important. Le mode plan est en effet le premier mode qui couplé avec l'onde plane.
Dans ces conditions, le couplage entre le premier mode de respiration de la structure et le mode acoustique plan se traduit par un changement important de l'impédance acoustique d'entrée du tuyau. Néanmoins, ce phénomène correspond à des instruments construits avec des matériaux dont les caractéristiques physiques sont irréalistes. Autrement dit, le phénomène de vibration de parois n'est pas significatif dans le cas des instruments a perce parfaitement cylindrique.

Alors, comment peut-on expliquer les phénomènes de vibrations de parois référencés dans [ND04] ? Dans le chapitre 3 le modèle vibroacoustique proposé montre que des couplages additionnels peuvent avoir lieu quand on considère des coques légèrement distordues. En effet, la distorsion de la coque induit un couplage entre le premier mode ovalisant et le mode acoustique plan. La fréquence de ce mode de coque étant en général assez faible, le couplage intervient sur les premières fréquences acoustiques du tuyau pour des coques construites avec des matériaux réalistes. La particularité de ce couplage vient du fait que les premiers modes de coques ne sont pas les modes associés à des indices circonférentiels les plus faibles. En particulier, le premier mode de coque peut être un mode ovalisant (associé à un ordre circonférentiel m=2). Dans ces circonstances, le défaut d'ovalisation de la coque induit un couplage qui peut agir fortement sur le régime d'oscillation de l'instrument et qui peut donc expliquer des effets importants de vibration de paroi sur le comportement acoustique de l'instrument.

L'objectif de ce chapitre 4b est d'utiliser des simulations temporelles pour montrer l'effet potentiel de vibrations de paroi sur le régime d'oscillation d'un instrument type clarinette présentant des défauts d'ovalisation. Dans ce but, le modèle de simulation d'un instrument à vent a anche simple exposée dans le chapitre 4a a été utilisé avec l'impédance acoustique d'un tuyau cylindrique vibrant distordu donné par le modèle vibroacoustique du chapitre 3. Des signaux temporels simulés correspondant au régime d'oscillation d'instruments avec des défauts sont analysés dans cette partie pour mettre en évidence des phénomènes de vibration de parois importants. Le paramètre de signal utilisé pour cette étude est le Centre Spectral de Gravité (Spectral Centroid) qui est la moyenne des fréquences harmoniques de la distribution spectrale du signal pondérée par l'amplitude de chaque résonance.

4.5.1 Couplage vibroacoustique pour des coques distordues

Comme présenté dans le chapitre 3, le phénomène de vibration de parois est déterminé par la fréquence propre du premier mode d'ovalisation de la coque et de ce fait le matériau peut avoir une influence sur le son produit. La table 4.7 regroupe les valeurs de la première fréquence propre du premier mode de respiration (f_{b1}) et le premier mode ovalisant (f_{o1}), ceci pour huit coques de l=0.5m de longueur, de a=14.25mm de rayon et

de h=0.5mm d'épaisseur construites avec différents métaux caractérisés par le module de Young (E), le module de Poisson σ et sa masse volumique (ρ).

Matériel	E (GPa)	ρ (kg/m^3)	σ	f_{b1}(Hz)	f_{o1}(Hz)
Plomb	16	11340	0.44	742	378
Platine	61	21450	0.38	1015	557
Argent	30	10490	0.37	1022	557
Or	79	19300	0.44	1192	688
Étain	50	7310	0.36	1586	857
Cuivre	130	8920	0.34	2386	1254
Acier	210	7800	0.28	3244	1652
Aluminium	70	2710	0.35	3094	1658

Table 4.7: Propriétés physiques (module de Young, coefficient de Poisson et masse volumique) de différents métaux et fréquences propres correspondantes pour les s premiers modes de respiration (f_{b1}) et ovalisant (f_{o1}) pour des coques de longueur l=0.5m, de h=0.5 d'épaisseur; et de rayon a=14.25mm.

La première fréquence de résonance du mode ovalisant est plus petite que la fréquence de résonance du mode de respiration pour toutes les coques (voir table 1), ce qui confirme l'idée déjà énoncée, à savoir que le premier mode de coque n'est pas celui qui a les indices modaux les plus faibles. En particulier, pour certains métaux comme le plomb, le platine, l'argent et l'or, la résonance mécanique du mode ovalisant (f_{o1}) est de l'ordre de grandeur des premières fréquences acoustiques du tuyau. Ceci veut dire que des couplages fluide/structure importants peuvent avoir lieu dans ces circonstances.

Le matériau constituant la structure n'est pas l'unique facteur déterminant les propriétés résonantes mécaniques de la coque, la géométrie aussi. En conséquence, pour une longueur l=0.5 et un rayon de la coque a=14.25mm, on peut chercher l'épaisseur de manière que la fréquence propre du premier mode ovalisant coïncide avec une des premières résonances acoustiques altérant, ainsi, le comportement acoustique de l'instrument. La figure 4.7 illustre l'impédance d'entrée acoustique d'une coque construite en plomb avec une épaisseur telle que des phénomènes importants de vibration de parois ont lieu. Dans ces deux conditions la première fréquence du mode ovalisant est f_{o1}=347.8Hz.

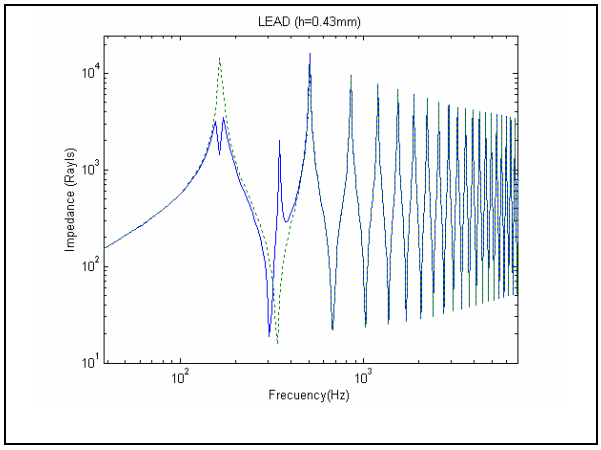

Figure 4.7: Impédance acoustique d'entrée d'un cylindre avec des parois vibrante (Z^a) construite en plomb ($E=16\cdot10^9 N/m^2$, $\sigma=0.44$ et $\rho_S=11340\ kg/m^3$). La référence d'un tuyau rigide est représentée en traits (Z^r). Les caractéristiques géométriques sont : longueur l=0.5, rayon a=14.25mm et épaisseur h=0.43mm

4.5.2. Simulation temporelle

Après avoir vu que la distorsion de la coque favorise le couplage fluide/structure pour des coques avec des épaisseurs particulières, nous analysons maintenant le régime d'oscillation d'instruments construits avec ces coques, au moyen de simulations temporelles. La figure 4.8 montre le signal temporel correspondant à un instrument construit avec la coque en plomb présentée précédemment.

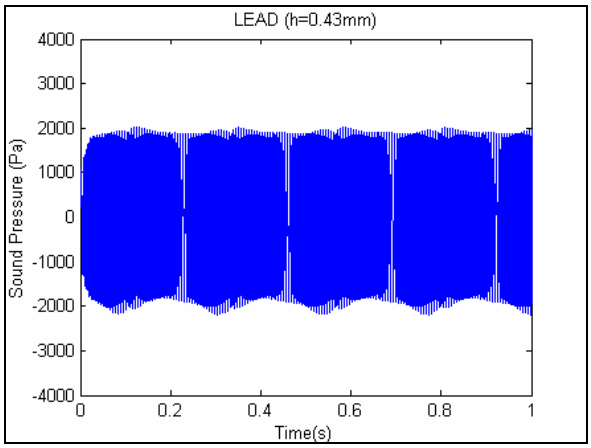

Figure 4.8: Signal temporel simulé correspondant à un instruments construit en plomb (E=16GPa, σ=0.44 et ρ=11340kg/m3). Le corps de l'instrument est une coque distordue (ε=0.1) de h=0.43mm d'épaisseur, l=0.5m de longueur et a=14.25mm de rayon. Le régime d'oscillation de l'instrument correspond a une note multiphonique (Note du loup)

Le signal présente le battement typique des notes multiphoniques exposées dans le chapitre 4. Dans ce chapitre, des sons multiphoniques ont été observés pour des coques parfaitement cylindrique construites avec des matériaux pas réalistes (module de Young et densité très petits). L'obtention par simulation dans le domaine temporel d'une note multiphonique montre que des changements importants du régime d'oscillation de l'instrument peuvent avoir lieu quand on considère des coques légèrement distordues construites en plomb. Néanmoins, il faut remarquer que ce phénomène n'a été observé que pour un instrument construit en plomb avec une distorsion d'au moins ε>0.095 et

pour des valeurs très spécifiques de la géométrie de la coque. Dans cette étude, l'élancement a été figé, et différents valeurs de l'épaisseur de la coque ont été considérées. Des simulations avec d'autres matériaux ont été faites, des changements importants du régime d'oscillation n'ont été observés qu'avec le matériau plomb. Dans la table 4.8, une étude de l'évolution du Centre Spectral de Gravité en fonction de la distorsion de la coque est présentée.

ε	CGS
0	2.1
0.08	2.1
0.085	2.2
0.09	2.3
0.095	2.6
0.1	3.8

Table 4.8: Centre Spectral de Gravité (CGS) calculé à partir du signal temporel simulé correspondant à instruments avec h=0.5mm d'épaisseur construit en plomb (E=16GPa, ρ=11340kg/m^3, σ=0.44), en fonction du paramètre de distorsion ε. Les premières fréquences de respiration et d'ovalisation de la coque sont f_{b1}=700Hz et f_{o1}=404Hz respectivement. La fréquence de jeu est f_1=170.5Hz pour toutes les simulations.

La valeur du CGS pour une coque avec ε=0.08 est le même que celui d'une coque parfaitement cylindrique (CGS=2.1). Ceci traduit le fait que le couplage n'est pas significatif pour des coques pas distordues. Le mode de respiration joue un rôle négligeable et la perturbation de l'impédance d'entrée est trop faible. Pourtant, la distorsion de la coque induit un fort couplage fluide/structure qui est montré par le changement du CGS des signaux simulés pour des coques plus distordues. Le régime d'oscillation de l'instrument est dans ces cas, biaisé par le couplage additionnel du premier mode ovalisant avec le mode acoustique plan. La distribution spectrale de la note multiphonique émise par l'instrument distordue par ε=0.1 est notablement perturbée, puisque le CGS vaut 3.8.

4.5.3. Variation de l'épaisseur de la coque

Suite à l'analyse des résultats et la recherche de phénomènes de vibrations de parois dans le régime d'oscillation de l'instrument, l'épaisseur de la coque semble être un paramètre très important vis-à-vis du couplage vibroacoustique. Pour montrer la sensibilité du phénomène à ce paramètre, une étude des signaux simulés par différents instruments en plomb avec différentes épaisseurs a été faite. La table 4.9 montre les résultats obtenus pour le CGS des signaux simulés pour toutes les coques. L'élancement des coques est toujours le même.

h	f_{b1}	f_{o1}	f_1(Hz)	CGS
0.40	700.00	324	170.5	1.7
0.41	700.01	332	161.3	1.4
0.42	700.01	340	493	3.1
0.43	700.01	348	170.5	3.8
0.44	700.02	356	170.5	2.2
0.45	700.02	364	170.5	2.0

Table 4.9: Centre Spectral de Gravité (CGS) calculé à partir du signal temporel simulé correspondant à instruments construit en plomb (E=16GPa, ρ=11340kg/m^3, σ=0.44) avec une coque distordue (ε=0.1) et différentes épaisseurs.

On peut voir à la table 4.9 que la fréquence propre du premier mode d'ovalisation de la coque dépend fortement de l'épaisseur de la coque. Ceci explique que le CGS varie aussi notablement avec l'épaisseur de la coque. Ces résultats confirment que le couplage vibroacoustique a un effet sur le régime d'oscillation de l'instrument pour des valeurs très particulières de son épaisseur. Seulement dans ce cas, le phénomène de vibrations de parois s'avère important. C'est remarquable que le régime d'oscillation de la coque ayant une épaisseur de 0.43mm est à la douzième. Dans ce cas, la fréquence propre du premier mode ovalisant étant très proche du 2nd partiel, elle favorise ce régime d'oscillation. D'autre part, la fréquence fondamentale de la coque avec une épaisseur de 0.42 est légèrement descendue de 170.5 Hz à 161.3Hz . Pour d'autres valeurs de l'épaisseur de la coque, la fréquence de jeu des instruments est celle qui correspond à un instrument rigide (avec les parois qui ne vibrent pas) puisque le couplage vibroacoustique n'est pas assez important.

4.5.4. Conclusion

Le régime d'oscillation de différents instruments avec le corps distordu a été analysé au moyen de simulations dans le domaine temporel. Différents matériaux et géométries ont été étudiés. Des notes multiphoniques sont observées uniquement pour un instrument construit en plomb et une géométrie très particulière. Pour ce type de matériau, la fréquence du premier mode d'ovalisation étant très faible, il est possible d'ajuster la géométrie de telle sorte que cette fréquence coïncide avec la deuxième résonance acoustique du tuyau. Cela conduit alors à une perturbation importante de l'impédance d'entrée, donc à un comportement auto-oscillant différent du cas rigide. Dans ce cas, la distorsion de la coque induit donc, un couplage vibroacoustique qui se traduit par un changement de régime d'oscillation. Des variations importantes du Centre Spectral de Gravité ont été également observées associées au phénomène de vibration de paroi. La validité des résultats obtenus est conditionnée par la principale limitation du modèle liée à la petitesse du paramètre de distorsion du tuyau sonore.

Capítulo 5

Wave propagation in a fluid filled rubber tube: theoretical and experimental results.

El objeto de este artículo redactado en inglés, que se enviará para su publicación, es cuantificar experimentalmente el efecto de vibración de las paredes e interpretar los fenómenos vibroacústicos observados. Para ello, se midió la impedancia acústica de entrada de un tubo de caucho. El material se ha elegido de tal manera que los efectos de vibración sean significativos y, por lo tanto, se reflejen sobre el comportamiento acústico del tubo.

El análisis de medidas a partir del modelo multimodal expuesto en el Capítulo 2 tiene en cuenta una gran cantidad de modos (52 modos mecánicos por debajo de la frecuencia fundamental del tubo). Como el número de modos es tan elevado, no resulta adecuado aplicar este método en el caso de un tubo membranoso de caucho. Por este motivo, se propone un método de tipo "desarrollo por ondas", que presenta dos simplificaciones respecto del método desarrollado en el Capítulo 2. Por un lado, el operador de Donnell se ha sustituido por el operador de membrana en la ecuación de movimiento de la estructura (véase Anexo B, para la relación entre ambos). Por otra, el campo de presión no se obtiene como un desarrollo multimodal sino a partir de una ecuación de ondas planas no homogénea. Esta ecuación, contiene un término de impedancia de pared que permite dar cuenta del efecto de vibración de las paredes en el campo de presión interno. En este método, el campo acústico resulta ser la representación de la suma de tres ondas: la primera es la onda de Korteweg, que es una onda acústica plana que se propaga en el fluido; está fuertemente acoplada a las vibraciones de las paredes. Las otras dos ondas se propagan principalmente en la estructura y se corresponden con movimientos acoplados longitudinales y de flexión. Se puede diferenciar tres comportamientos en diferentes rangos de frecuencia de la onda de Korteweg en los que la propagación es subsónica, evanescente y supersónica. Se ha definido y obtenido una velocidad de onda equivalente para comparar los cálculos teóricos y los resultados experimentales a partir de la impedancia acústica de entrada.

L'objectif de ce chapitre rédigé en anglais en vue de le soumettre pour publication, est de mesurer des effets de vibration de parois et d'interpréter les phénomènes vibroacoustiques observés. Dans ce but, l'impédance acoustique d'entrée

d'un tuyau en caoutchouc a été mesurée. Le matériau a été choisi de manière à rendre les effets de vibration importants sur le comportement acoustique du tuyau.

L'analyse des mesures à partir du modèle multimodal exposée dans le chapitre 2 met en jeu un grand nombre de modes (52 modes mécaniques en dessous de la fréquence fondamentale du tuyau). Puisque le nombre de mode est trop important, la mise en oeuvre de cette méthode n'est pas très adaptée au cas du tuyau membranaire en caoutchouc. Pour cette raison, une méthode de type 'développement en ondes' est introduite. Cette méthode, présente deux simplifications par rapport à la méthode développée au chapitre 2. D'une part, l'opérateur de Donnell a été remplacé par l'opérateur de membrane à l'équation de mouvement de la coque (l'annexe B à la fin de ce document décrit la relation entre les deux). D'autre part, le champ de pression n'est plus obtenu comme un développement multimodal mais à partir d'une équation d'ondes planes inhomogène. Cette équation contient un terme d'impédance de parois qui rend compte des effets de vibration de parois dans le champ de pression interne. Dans cette méthode, le champ acoustique est représenté comme la somme de 3 ondes : la première est l'onde de Korteweg qui correspond à l'onde acoustique plane se propageant dans le fluide et est fortement couplée aux vibrations de parois. Les deux autres ondes se propagent principalement dans la structure et correspondent aux mouvements couplés longitudinaux et de flexion. Trois plages fréquentielles peuvent être bien différentiées pour l'onde de Korteweg dans lesquels la propagation est subsonique, évanescente et supersonique. Une vitesse d'onde équivalente est définie et obtenue afin de comparer les calculs théoriques et les résultats expérimentaux à partir de l'impédance acoustique d'entrée.

5.1. Introduction

The vibroacoustics of cylindrical ducts has been extensively studied and presented in the relevant literature since numerous applications in mechanical engineering involve fluid-filled pipes with yielding walls. In the present paper, attention is focused on the wave propagating mainly within the fluid column. A theoretical and experimental study of the acoustic plane wave perturbed by the wall vibrations of a rubber tube is presented. The stretched rubber tube is modelled as a membrane submitted to a static tension. Its longitudinal and flexural motions coupled with the acoustic oscillation described by the plane wave, lead to a system in which three waves can co-exist.

A complete fluid-filled tube model is based on the shell model (using 3D elasticity [Kum72], Donnell's thin shell theory [FF82], or Flugge-Timoshenko's theory [Trd95]) and on a multimodal expansion of the inner acoustic pressure. However, the results for wave propagation at low frequency in fluid-filled vibrating pipes have, over the years, been described in the literature in a simpler manner and can be applied to a cylindrical membrane. Such a simple model is based on the hypothesis that the reaction of the wall is local and can be modelled by a wall admittance. In this model, the plane wave approximation is retained in the air column and the forces applied to an elementary fluid volume consist of two cross sections very close to each other are related to the compressibility effect and to the wall effect. This is called the distensibility effect [Lig01]. In such a system, the wave speed of the acoustic plane wave depends on both compressibility and distensibility effects. Because of the wall motions, the acoustic plane wave becomes strongly dispersive and an effective wave speed for the medium can be defined. Subsonic, evanescent and supersonic frequency ranges can be distinguished. This model [Lam98] was first presented during the 19th century, and this kind of wave is called Korteweg's wave or Moens-Korteweg's wave and has been presented in several reference works [MPT79], [MI86], [Lig01]. Korteweg's model corresponds to a simplified model giving an approximation of the first of the 5 waves listed above. In the literature, several authors have independently developed such a model. In the following, we propose a review of several fields for which this model has been derived and applied.

An application of Korteweg's model is related to biomechanics, and concerns the propagation of waves in the airway and in blood vessels. In the publications mentioned below, Korteweg's name does not generally appear although the model is used. For medical application, a non-invasive technique called AAAR (airway area by acoustic reflection, [JF86], [FWG80]) has been developed to determine the geometry of the airway of a patient. An acoustic pulse is generated in the patient's mouth and the acoustic reflection coming from the airway can be measured. The model of wave propagation in the vibrating duct is required in order to determine the profile of the cross section from the echo measurement using an inverse method. Among the limitations of this technique [Son74], the airway wall vibrations play an important role. The local admittance assumption leads to the Korteweg's wave model being used to take these into account, employing a limited number of parameters. A model for the vocal tract is also requested for application to speech synthesis and analysis [FWG80], [Fre81].

Another application of Korteweg's wave is related to wave propagation in blood vessels. In this case, the distensibility of the tube is of far greater importance than the compressibility of the fluid, so that here the fluid can be regarded as incompressible

[Lig01]. Note that in an attempt to model wave propagation in blood vessels, a much more complete model which takes into account the influence of the viscosity of the liquid, the internal damping in the tube wall and the lateral constraint of the wall is given in [Cal89]. Two waves are found in the low frequency range, which correspond to a mainly longitudinal wave in the wall and a quasi-plane wave in the fluid (Korteweg's wave). These waves are found to be the low frequency limits of the solution of a complete dispersion equation.

Experimental validations of Korteweg's model, including measuring the variation of wave speed versus frequency, are not numerous in the literature. Phase velocity can be determined from the distance between crests where standing waves were observable. The comparison of the phase velocity, experimentally obtained and modelled using a local admittance hypothesis, can be achieved and provides a way of fitting phase velocities with the attenuation constant. When applied to physiology, such measurements are given in [RK78] for a rubber tube and an excised canine trachea and in [GB81] for a rubber tube. In such ducts with vibrating walls, if the local admittance hypothesis is not retained, a membrane equation has to be written. For an unstretched membrane tube, the acoustic field can be described using the superposition of two waves [KK90]: the Korteweg's wave and the longitudinal wave in the membrane. Both waves are present in the fluid and the structure, and as such, it can be said that the local admittance hypothesis cannot be applied. Such a discussion related to the validity of the local admittance hypothesis is given in [GT96]. In this study related to an acoustic wave guide with yielding walls, the measurement of the acoustic speed of sound is measured using the Kundt method and an important variation in the speed of sound according to frequency, is observed. A numerical simulation using the finite element method is employed to calculate the pressure and shell displacement fields. It is shown that the local impedance hypothesis is not always valid and that the two waves are present.

Since Korteweg's wave is strongly damped within a particular frequency range, it has been pointed out that this property can be used for structure-borne sound attenuation. Flexible tubes can be used to attenuate both fluid-borne and structure-borne waves. The introduction of flexible segments in a piping system is a convenient passive technique which can be used to reduce structure-borne sound. Since such flexible segments also affect the fluid-borne sound, these should be taken into consideration when calculating the insertion loss or the transfer matrix of a pipe assembly. The dispersion equation for the coupled system is found using a membrane theory and allows the calculation of the insertion loss in a flexible segment. For the same objective, a model has been developed for flexible segments modelled using a thin shell theory (Kennard's theory) and using expansion throughout the 'in vacuo' modes of the shell [Mar88].

In this paper, the influence of the wall vibration on the air column is studied. The aim is to compare different models and to confirm to what extent the Korteweg's model is adequate for describing the problem. The measurements of the input impedance are conducted. In order to facilitate the comparison with theoretical models, an equivalent wave speed is defined using the analogy with the rigid tube impedance.

The paper is structured as follows: following this introduction and short bibliographic review, a vibroacoustic model of a stretched membrane is developed in section 2. The dispersion equation is produced, and the solutions discussed, then a free waves expansion is used to compute the acoustic input impedance of the tube. In section 3, the measurements of the acoustic input impedance are presented and are used to determine equivalent wave speeds. Finally, some concluding remarks are given in section 4. The motion equations of the stretched membrane are given in an appendix.

5.2. Vibroacoustic models of a fluid filled rubber tube

5.2.1. Equations of the model

Let us consider a cylindrical pipe filled with a compressible fluid. The influence of the external fluid is ignored. The pipe has a length L, a mean radius a, a wall thickness h, and is assumed to be thin so that h/a<<1. The coordinate system is given in Figure 5.1; x and z are the axial and radial coordinates, u and w are the membrane displacements according to these directions.

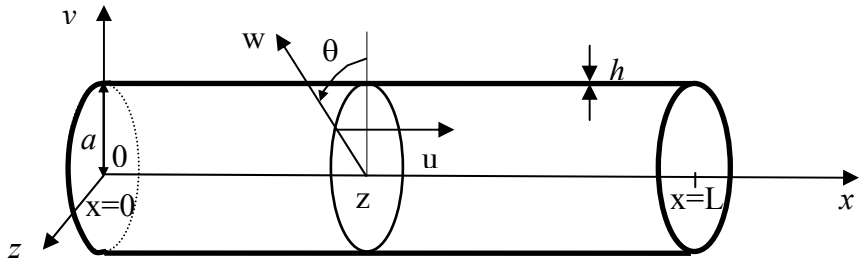

Figure 5.1: co-ordinates and displacement sign convention for the vibrating cylindrical membrane.

Assuming linear elasticity approximations, and taking into account a static tension T, the equations governing axisymmetrical vibrations of the membrane can be written as follows:

$$\begin{pmatrix} \dfrac{\partial^2}{\partial x^2} - \dfrac{1}{{c_L}^2}\dfrac{\partial^2}{\partial t^2} & \dfrac{\nu}{a}\dfrac{\partial}{\partial x} \\ -\dfrac{\nu}{a}\dfrac{\partial}{\partial x} & \dfrac{1-\nu^2}{E}\dfrac{T}{A}\dfrac{\partial^2}{\partial x^2} - \dfrac{1}{a^2} + \dfrac{1}{{c_L}^2}\dfrac{\partial^2}{\partial t^2} \end{pmatrix} \begin{pmatrix} u \\ w \end{pmatrix} = \begin{pmatrix} 0 \\ \dfrac{-p}{\rho {c_L}^2 h} \end{pmatrix}, \qquad (5.1)$$

where E, ρ and ν are the Young's modulus, the density, and the Poisson's ratio of the rubber material, respectively. c_L is the speed of the longitudinal waves inside the material and is given by $c_L = \sqrt{E/\rho\left(1-\nu^2\right)}$. The acoustic pressure in the tube denoted by p and $A = 2\pi ah$ is the cross-section area of the pipe. Since the material is supposed to be visco-elastic, the Young's modulus is supposed to be complex valued.

On the other hand, assuming linear acoustic approximations and the plane wave propagation, the acoustic pressure p satisfies the following inhomogeneous wave equation:

$$\frac{\partial^2 p}{\partial x^2} - \frac{1}{c^2}\frac{\partial^2 p}{\partial t^2} = \frac{2\rho_0}{a}\frac{\partial^2 w}{\partial t^2}, \qquad (5.2)$$

where c is the speed of sound in air, and ρ_0 the density of air. The term on the right hand side of equation (5.2) accounts for the wall vibration effect in the inner pressure field.

Equations (5.1) and (5.2) give a set of three linear second order differential coupled equations, as a function of the three variables u, w and p, depending on space co-ordinate x and time t. Further details of how these equations were obtained are given in appendix 5.A.

5.2.2. Dispersion curves

5.2.2.1. General case (ν≠0, T≠0)

When looking for travelling-wave solution with a harmonic excitation of angular frequency ω, the variables *u(x), w(x)* and *p(x)* are assumed to be of the form $u = u_0 e^{j\lambda x}$, $w = w_0 e^{j\lambda x}$ and $p = p_0 e^{j\lambda x}$ with λ the wavenumber to be determined (the temporal factor $e^{j\omega t}$ is omitted).

The harmonic variables may now be substituted into equations (5.1) and (5.2) in order to obtain the dispersion equation. First of all, the set of three equations is obtained:

$$\begin{pmatrix} -\lambda^2 + k^2 & 0 & \frac{2\rho_0}{a}\omega^2 \\ 0 & -\lambda^2 + {k_L}^2 & \frac{\nu}{a} j\lambda \\ \frac{1}{\rho {c_L}^2 h} & -\frac{\nu}{a} j\lambda & -\frac{1-\nu^2}{E}\frac{T}{A}\lambda^2 - \frac{1}{a^2} + {k_L}^2 \end{pmatrix} \begin{pmatrix} p_0 \\ u_0 \\ w_0 \end{pmatrix} = \begin{pmatrix} 0 \\ 0 \\ 0 \end{pmatrix}, \qquad (5.3)$$

where $k=\omega/c$ and $k_L=\omega/c_L$ are the wavenumbers associated with the uncoupled acoustic and longitudinal waves, respectively.

The equations (5.3) have non-trivial solutions if the determinant of the matrix is equal to zero. Then the following dispersion equation is obtained:

$$\left[-\frac{1-\nu^2}{E}\frac{T}{A}\lambda^2 - \frac{1}{a^2} + {k_L}^2\right]\left[{k_L}^2 - \lambda^2\right]\left[k^2 - \lambda^2\right] - \frac{\nu^2\lambda^2}{a^2}\left[k^2 - \lambda^2\right] - \frac{2}{ah}\frac{\rho_0}{\rho}{k_L}^2\left[{k_L}^2 - \lambda^2\right] = 0. \qquad (5.4)$$

Dispersion equation *(5.4)* is a polynomial equation of the sixth order, which can produce six wave number roots $\pm\lambda_1, \pm\lambda_2, \pm\lambda_3$, corresponding to three axisymmetric waves propagating along the x-axis of the membrane tube. Note that the term $\frac{2\rho_0}{ah\rho}$ present in equation (5.4) is the fluid loading term. The smaller the thickness and radius of the cylinder, the bigger the coupling phenomena. The equation (5.4) is solved by using the values of the parameters given in Table 5.1.

Geometry	Characteristics of the material (rubber type)
Inner radius: 0.015m Thickness: 0.0018m Length: 0.553m	Density: 0.921 Young's modulus: E=E'+jE'' E'=2.10^{6}Pa and E''= 0.25 E' Poisson's ratio : 0.5

Table 5.1: Characteristics of the studied membrane

Two cases are studied: the conservative case (where dissipation is not considered) and the non-conservative case where acoustic and mechanical dissipations are taken into account. In the first case, the two celerities c and c_L are real numbers. In the second case, dissipation phenomena imply that the celerities (and the wave numbers) become complex. In a harmonic regime and at low frequency, the acoustic dissipation is mainly due to the thermoviscous phenomena localised at the wall boundaries. The dissipation and the dispersive effect is then taken into account using the following complex wave number:

$$k = \frac{\omega}{c} + \alpha \cdot (1 - j) = \frac{\omega}{c_m}, \qquad (5.5)$$

where $\alpha \approx 3 \cdot 10^{-5} \sqrt{f} / a$ (at 20°C), f being the frequency and a the radius of the tube, c_m being a complex wave speed. Otherwise, the mechanical dissipation is taken into account using a complex Young's modulus E_c, and then, the wave speed c_L becomes complex too.

For a wave associated to a given wavenumber λ, the complex wave speeds $c_m = \omega / \lambda$ are given in Figure 5.2 for two cases: the conservative case (a), the dissipative case (b). Notice that the real part Re(c_m), always positive, and the imaginary part Im(c_m), always negative, of the complex speed velocity c_m, are displayed in the same graph. In the conservative case (Figure 5.2a), three curves corresponding to the three waves are displayed. In this case c_m is purely real or purely imaginary: the purely imaginary case corresponds to the evanescent wave case, the purely real case corresponds to the propagating wave case. At high frequencies, one of the wave speed curves tends toward the speed of sound in air (typically 340 m/s). A frequency range (between 450 and 700 Hz) can still be distinctly observed where the wave is evanescent. Subsequently, three frequency ranges can highlighted: the low frequency one (up to 450 Hz approximately), the medium one (from 450 to 700 Hz) and the high frequency one.

The wave number solutions are complex for the dissipative case (Figure 5.2b). Here, the three curves corresponding to the three waves are displayed as follows: the real part of c_m, which is always positive, is displayed in the positive half-plane, and the imaginary part of c_m, which is always negative, is displayed in the negative half-plane.

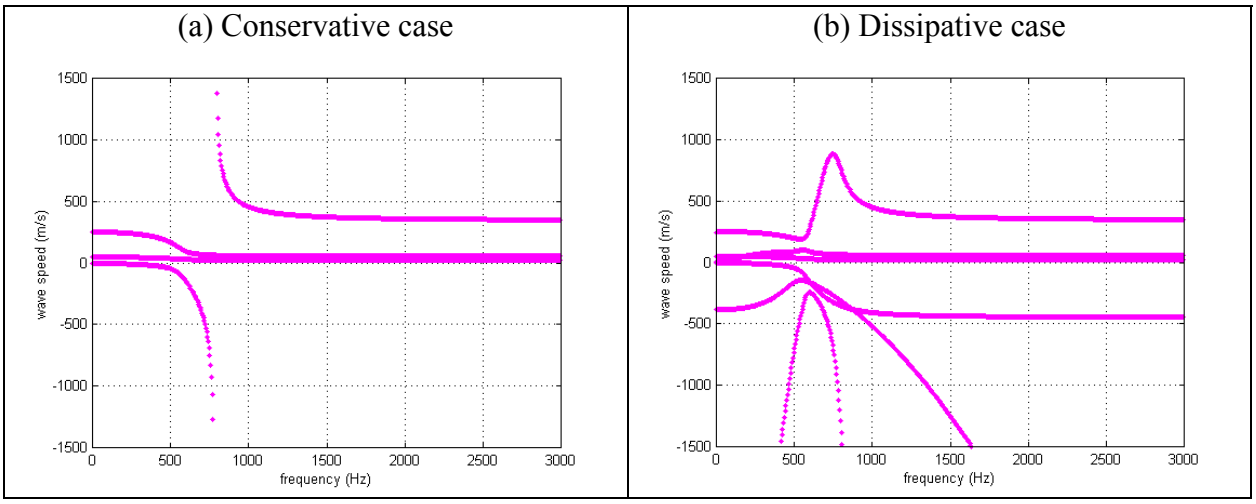

Figure 5.2: Dispersion curves (ν≠0 and T≠0), conservative case (a) and dissipative case (b). Real part and imaginary part of the complex wave speed c_m in m/s as a function of frequency in Hz.

The solution of the dispersion equation (5.4) can be interpreted by considering two simplified cases: the case where both the static preload and the Poisson's ratio are assumed to be zero, and the case where the static preload is set to zero.

5.2.2.2. Korteweg's hypothesis (ν=0, T=0)

Considering the case where T=0 and ν=0, the dispersion equation takes a simple form and the wavenumbers are:

$$\lambda = \pm k_L \text{ and } \lambda = \pm \frac{\omega}{c_K}, \tag{5.6}$$

where

$$c_K{}^2 = \frac{c^2}{\left[1 + 2\rho_0 / \left[ah\rho\left(1/a^2 - k_L{}^2\right)\right]\right]}. \tag{5.7}$$

Two waves are propagating in the medium: a purely longitudinal wave in the membrane (wave number k_L) and the Korteweg's wave (wave number ω / c_K), whose wave speed is denoted by c_K. The numerical simulation is given in Figure 5.3 using the parameters of Table 5.1. The longitudinal wave involves membrane displacement in the axial direction only and is strictly uncoupled from bending displacement w and acoustic pressure p. Korteweg's wave involves coupled oscillations between acoustic pressure p and bending membrane displacement w. In this case, no axial displacement is involved. This wave is strongly dispersive. Three frequency ranges can be distinguished from expression (5.7). The upper and lower limits of each ranges can be calculated exactly, ignoring any kind of damping.

In the range [0, f_a] where $f_a = c_L/(2\pi a)$ is the ring frequency of the membrane, the wave speed c_K is real and the propagating wave is subsonic ($c_K < c$, c being the speed of sound without any couplings). In this range, the wave speed c_K varies from

$c_K{}^2 = \dfrac{c^2}{\left[1+2\rho_0/ah\rho/a^2\right]}$ for f=0Hz (Korteweg-Lamb correction) to $c_K = 0$ for $f = f_a$.

In the range $[f_a, f_a\sqrt{1+2a\rho_0/(h\rho)}]$, wave speed c_K is a complex imaginary number ($c_K \leq 0$) and the corresponding wave is purely evanescent. This range corresponds to a stop band. In the range $[f_a\sqrt{1+2a\rho_0/(h\rho)}, \infty]$, the wave speed is, once again, real and the propagating wave is supersonic ($c_K > c$). For high frequencies, the Korteweg's wave speed c_K tends towards c. Such a simple definition of ranges is possible because the damping phenomena are ignored (Figure 5.3a). If these are taken into account, in the subsonic and supersonic ranges the complex wave speed c_K has an imaginary part leading to wave attenuation. In the stop band, the real part of the wave speed c_K is not strictly equal to zero and a propagation phenomenon exists (Figure 5.3b).

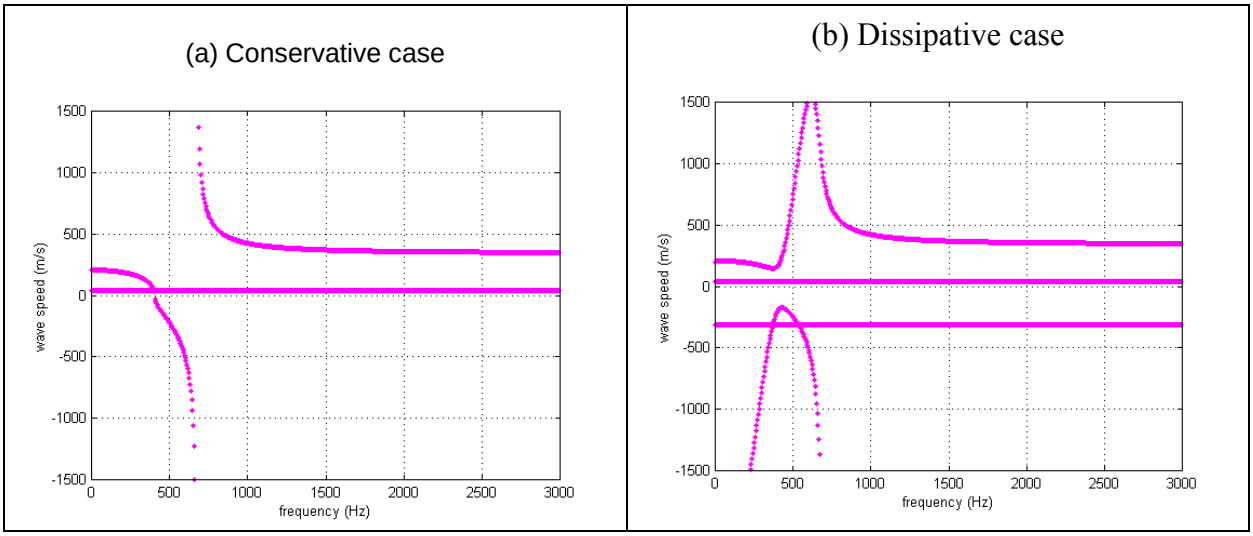

Figure 5.3: Dispersion curves (Korteweg's hypothesis, ν=0 and T=0), conservative case (a) and dissipative case (b). Real part and imaginary part of the complex wave speed c_m in m/s as a function of frequency in Hz.

5.2.2.3. Unstretched case (ν≠0, T=0)

Setting the static preload T to 0 in the dispersion equation (5.4) leads to

$$\lambda = \pm k_1, \lambda = \pm k_2, \qquad (5.8)$$

where

$$k_1{}^2 = (-b+\sqrt{\Delta})/2 \text{ and } k_2{}^2 = (-b-\sqrt{\Delta})/2, \qquad (5.9)$$

with

$$\beta = \left[(1/a^2 - k_L{}^2)(k^2 + k_L{}^2) + \nu^2 k^2/a^2 + 2\rho_0 k_L{}^2/(ah\rho)\right] / \left[k_L{}^2 - (1+\nu^2)/a^2\right],$$
$$\text{and } \Delta = \beta^2 - 4k_L{}^2 k^2 \left[1/a^2 - k_L{}^2\right] / \left[(1-\nu^2)/a^2 - k_L{}^2\right],$$

Two waves are propagating in the medium. At high frequencies it can be verified that the wave numbers k_1 and k_2 tend towards k and k_L. The corresponding waves tend towards the plane wave in fluid and towards the longitudinal waves in the membrane, each wave being uncoupled from the other. The wave associated to k_1 is close to

Korteweg's wave, and slightly disturbed by the coupling between longitudinal and flexural motion induced by the Poisson's ratio. The wave associated to k_2 is close to the longitudinal wave in the membrane. Note that the two dispersion curves do not cross, as mentioned in [FF82]. Near the possible cross points, the shape of the curves have corners and the two curves 'exchange' their branches (Figure 5.4).

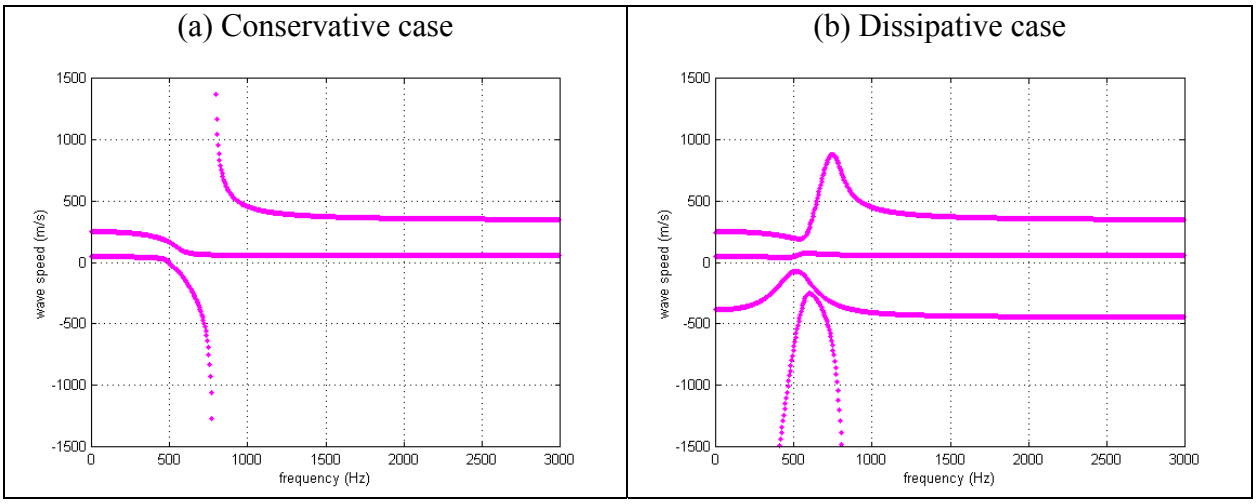

Figure 5.4: Dispersion curves (unstretched case, v≠0 and T=0), conservative case (a) and dissipative case (b). Real part and imaginary part of the complex wave speed c_m in m/s as a function of frequency in Hz.

5.2.3. Acoustic input impedances

Here, the wavenumbers established in the former chapter are used to calculate the acoustic input impedance for the fluid-filled membrane tube. For this calculation, the membrane is supposed to be clamped at both ends. Subsequently, the boundary conditions at both x=0 and x=L of the tube are : u(0) = u(L) = w(0) = w(L) = 0. Moreover, the acoustic boundary conditions are p(L) = 0 (at the open end of the pipe) and v(0) = v_o (the known harmonic excitation at the input). The input impedance Z is the ratio between the acoustic pressure and the acoustic velocity at x=0. The acoustic pressure throughout the length of the tube, can be written as the superposition of the six previously described waves, as follows:

$$p = A_1 e^{j\lambda_1 x} + B_1 e^{-j\lambda_1 x} + A_2 e^{j\lambda_2 x} + B_2 e^{-j\lambda_2 x} + A_3 e^{j\lambda_3 x} + B_3 e^{-j\lambda_3 x} . \qquad (5.10)$$

The Euler equation gives a relationship between the acoustic pressure and the acoustic velocity:

$$j\omega\rho_0 v = -\frac{\partial p}{\partial x} . \qquad (5.11)$$

The acoustic velocity can be written using the equations (5.10) and (5.11) as follows:

$$v = -\left[\lambda_1\left(A_1 e^{j\lambda_1 x} - B_1 e^{-j\lambda_1 x}\right) + \lambda_2\left(A_2 e^{j\lambda_2 x} - B_2 e^{-j\lambda_2 x}\right) + \lambda_3\left(A_3 e^{j\lambda_3 x} - B_3 e^{-j\lambda_3 x}\right)\right] \Big/ \omega\rho_0 . \qquad (5.12)$$

It yields the following expression of the acoustic input impedance:

$$Z = \frac{p(x=0)}{v(x=0)} = \frac{A_1 + B_1 + A_2 + B_2 + A_3 + B_3}{\lambda_1\left(A_1 - B_1\right) + \lambda_2\left(A_2 - B_2\right) + \lambda_3\left(A_3 - B_3\right)}\omega\rho_0 \,. \tag{5.13}$$

The six unknowns are the amplitudes A_1, A_2, A_3, B_1, B_2 and B_3. Using equations (5.10) and (5.12) the six boundary conditions yield to six linear equations of six unknowns written in a matrix form as follows:

$$\begin{bmatrix} f_1(\lambda_1) & f_1(-\lambda_1) & f_1(\lambda_2) & f_1(-\lambda_2) & f_1(\lambda_3) & f_1(-\lambda_3) \\ f_2(\lambda_1) & f_2(-\lambda_1) & f_2(\lambda_2) & f_2(-\lambda_2) & f_2(\lambda_3) & f_2(-\lambda_3) \\ f_3(\lambda_1) & f_3(-\lambda_1) & f_3(\lambda_2) & f_3(-\lambda_2) & f_3(\lambda_3) & f_3(-\lambda_3) \\ f_4(\lambda_1) & f_4(-\lambda_1) & f_4(\lambda_2) & f_4(-\lambda_2) & f_4(\lambda_3) & f_4(-\lambda_3) \\ f_5(\lambda_1) & f_5(-\lambda_1) & f_5(\lambda_2) & f_5(-\lambda_2) & f_5(\lambda_3) & f_5(-\lambda_3) \\ f_6(\lambda_1) & f_6(-\lambda_1) & f_6(\lambda_2) & f_6(-\lambda_2) & f_6(\lambda_3) & f_6(-\lambda_3) \end{bmatrix} \begin{bmatrix} A_1 \\ B_1 \\ A_2 \\ B_2 \\ A_3 \\ B_3 \end{bmatrix} = \begin{bmatrix} v_\circ \\ 0 \\ 0 \\ 0 \\ 0 \\ 0 \end{bmatrix} \tag{5.14}$$

where

$$\left.\begin{aligned} f_1(\lambda_i) &= -\lambda_i / (\omega\rho_0) \\ f_2(\lambda_i) &= e^{j\lambda_i L} \\ f_3(\lambda_i) &= \frac{\lambda_i^2 - k^2}{2\rho_0\omega^2/a} \\ f_4(\lambda_i) &= \frac{\lambda_1^2 - k^2}{2\rho_0\omega^2/a} e^{j\lambda_i L} \\ f_5(\lambda_i) &= \frac{jv\lambda_i}{2\rho_0\omega^2} \frac{k^2 - \lambda_i^2}{k_L^2 - \lambda_i^2} \\ f_6(\lambda_i) &= \frac{jv\lambda_i}{2\rho_0\omega^2} \frac{k^2 - \lambda_i^2}{k_L^2 - \lambda_i^2} e^{j\lambda_i L} \end{aligned}\right\} / i = \{1,2,3\} \,.$$

By solving equation (5.14), the six unknowns can be determined. Then, the acoustic input impedance of a membrane waveguide (5.13), including the tension, can be calculated.

Specific input impedances (dimensionless impedances $Z_{adim} = \frac{Z}{\rho_0 c / S}$) are plotted in Figure 5.5 by using the numerical values given in Table 5.1 for 2 tension values. Two simulated cases – with and without tension – are presented together, showing the slight influence of the tension on the calculated impedance.

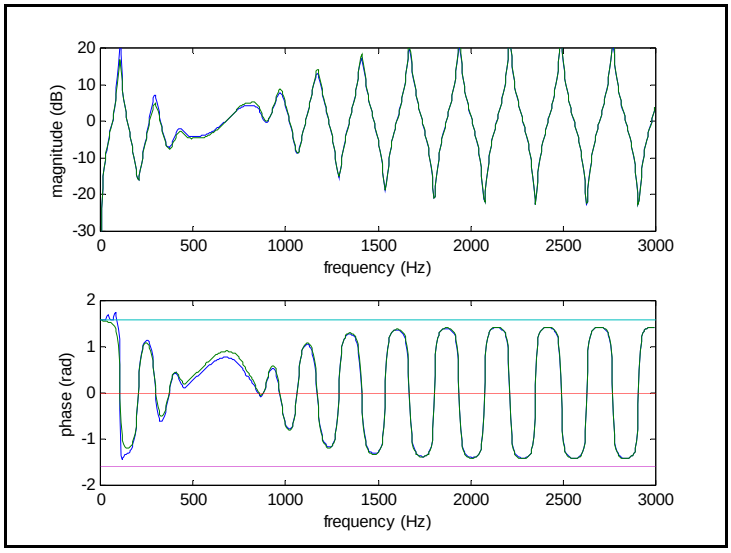

Figure 5.5: Magnitude and phase of the specific acoustic input impedance with and without tension (T=50 N) as a function of frequency in Hz.

At a high frequency, the calculated input impedance is similar to that of a rigid tube. This indicates that the wave whose speed tends towards c_o at high frequency (Figure 5.2) is predominant. At a low frequency, several resonances can be observed and seem to correspond to a wave speed lower than c_o. At the medium frequency range, around 500 Hz, no resonance emerges. This can be interpreted by the fact that only evanescent waves propagate (Figure 5.2). Within this range, the fluid/membrane coupling is very important.

5.2.4. Equivalent wave speeds

The separation of the three waves is not possible rendering a direct comparison between the theoretical dispersion curves and the experimental results impossible. In order to compare theoretical calculations with experimental results, an equivalent wave speed c_{eq} is defined. This equivalent wave speed may allow a partial comparison, defining a kind of general speed of sound, integrating all the wave effects. This is calculated from the input impedance. The equivalent speed c_{eq} is defined through an analogy with the input impedance of a lossless rigid open tube (2.11) which is given by:

$$Z_o = j\frac{\rho c}{S}\tan(kL), \qquad (5.15)$$

Subsequently, for any impedance c_{eq} is defined as :

$$c_{eq} = \frac{\omega L}{(k\ L)_{eq}}. \qquad (5.16)$$

with

$$(k\ L)_{eq} = \arctan\left(Z_o \big/ j(\rho c / S)\right) + n\pi\ . \qquad (5.17)$$

where n is an integer. Indeed, an ambiguity exists since the arctangent function gives a result between $-\pi/2$ and $\pi/2$ for its real part (Figure 5.6). To obtain the correct velocity, for the rigid pipe, the integer n needs to be incremented after each phase jump (this is usually called "unwrapping"). In the present case, a difficulty appears due to the fact that the wave number does not increase monotically. Indeed, there is a frequency range for which the waves are evanescent. So the two frequency bands in which the waves are non evanescent have to be considered separately. The first band is from zero to the first cut-off frequency. The second band is from the second cut-off frequency to infinity. For the first band the initial value of n is zero. For the second band the initial value n_0 at the beginning of the band is obtained when taking into account the fact that the equivalent speed tends towards the speed of sound when the frequency tends toward infinity (Figure 5.6).

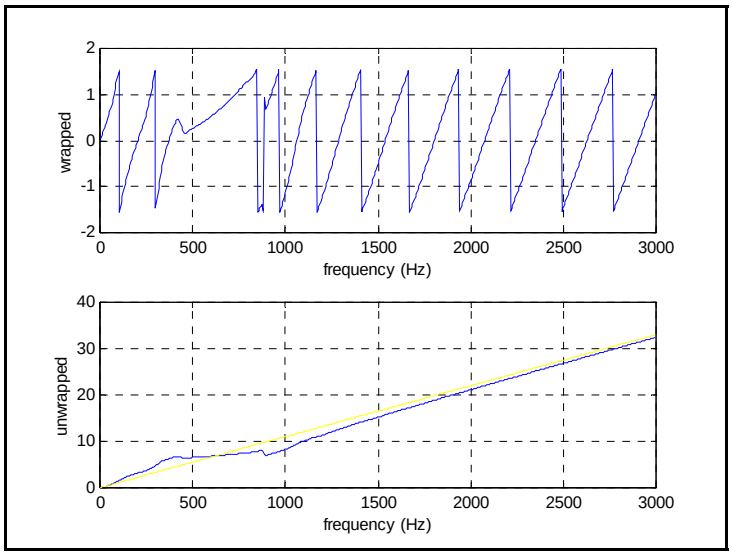

Figure 5.6: Not unwrapped (high) and unwrapped (low) variable $(kL)_{eq}$. Theoretical input impedance of the rigid tube (yellow line)

The equivalent speed velocity c_{eq} is then directly calculated from the correctly unwrapped function by using equation (5.16). The results are displayed in Figure 5.7; the wave speeds coming from the dispersion curves (Figure 5.2b) are repeated in Figure 5.7. Some conclusions can be drawn from these results. At the high frequency range, c_{eq} is accurately superimposed on the one speed wave curve which tends towards c_o=350m/s at a very high frequency. This indicates that for the high frequency range, one of the three waves is predominant. At the low frequency range, c_{eq} is not superimposed onto either of the speed wave curves. This suggests that at the low frequency range, the three waves may make a significant contribution to the impedance. In the medium range, no clear conclusions can be reached, which is not surprising given that the evanescent behaviour is predominant in that range.

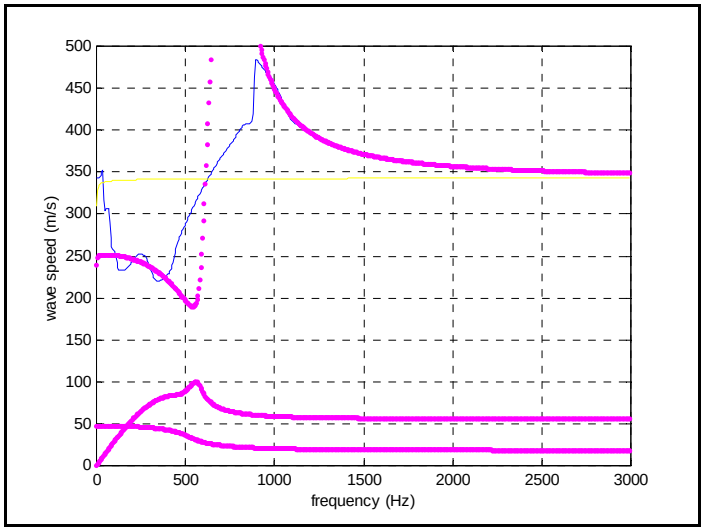

Figure 5.7: Wave speeds in an unstretched membrane (magenta dotted curves) compared with equivalent wave speeds (blue curve). Theoretical input impedance of the rigid tube (yellow line).

5.3. Measurements and discussion

5.3.1. Experimental set-up and procedure

The input impedance is measured using the impedance sensor described in [CC96]. This sensor uses a half-inch electrostatic microphone cartridge as a volume velocity source and an electret microphone as a pressure sensor. The microphone cartridge and the electret microphone are fixed onto a stiff metal plane which constitutes the reference plane for the measurements. The use of a microphone cartridge as a source is attractive because its frequency response is flat and its mechanical impedance is relatively high. However, the limitation of this source is that, for the amplitude of a given input signal, the volume velocity is proportional to the frequency and tends towards zero with frequency. The measurements are carried out in an anechoic chamber with a dual-phase lock-in amplifier including a sine source used for both excitation and demodulation. It is calibrated using the procedures for input and transfer impedance measurements described in [DB92]. The rubber tube is fixed to the impedance sensor with a specially designed set-up which allows the variation of the tension in the tube (Figure 5.8). For verification, before measuring the rubber tube, the input impedance of a rigid aluminium tube of approximately the same dimensions is measured and compared with a theoretical model. Considering the uncertainties in the model (especially in the radiation impedance), the measurement is considered to be in accordance with the model.

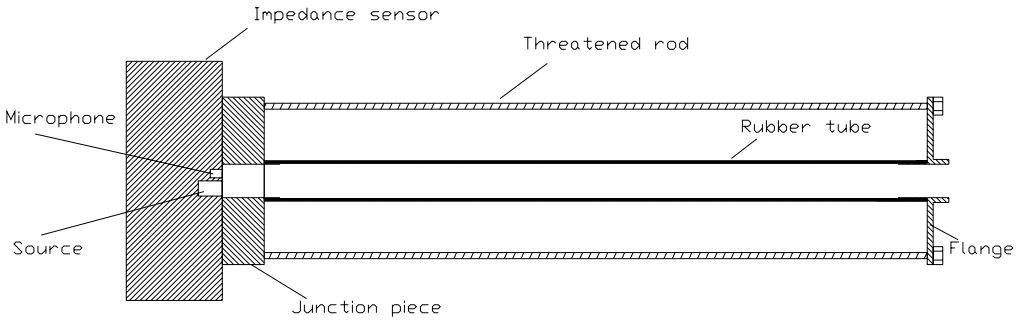

Figure 5.8: Experimental set-up

5.3.2. Measured input impedances estimated equivalent wave speeds

Measurements have been conducted on the rubber tube whose characteristics are given in Table 5.1. The measured input impedance of the rubber tube without static preload is displayed in Figure 5.9. Three frequency ranges can be observed in the curve. For the higher frequency range, above 1000Hz, regularly spaced impedance peaks can be seen with the input impedance tending towards that of a rigid tube. Two resonances can be seen in the lower frequency range, up to 600Hz. The frequency difference between these two resonances indicates that the corresponding speed wave is lower than c_o, the acoustic wave speed in air. In the medium frequency range, between 600 and 1000 Hz, only one resonance of a low Q-factor is present. This confirms the theoretical results (Figure 5.5): in this range, the fluid-membrane coupling is very important, and the evanescent wave behaviour is predominant. The experimental input impedance curve is very similar to the theoretical one. The frequency ranges are slightly different which may be explained by the fact that the actual Young's modulus value is slightly different from the one used in the calculation. It can also be noticed that the amplitude of the resonance peaks are lower in the experiment. This may be explained by the fact that neither the radiation impedance, nor the membrane radiation have been taken into account.

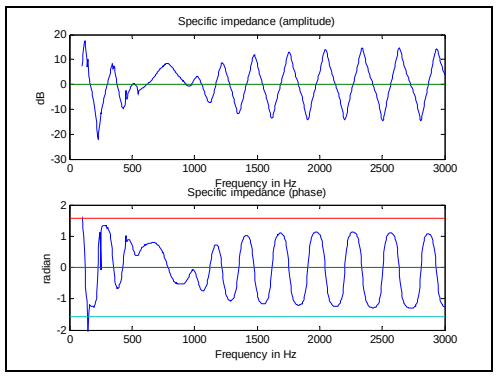

Figure 5.9: Magnitude and phase of a measured acoustic input impedance as a function of frequency in Hz.

The input impedance has been measured for three different static preloads: 0 N, 24 N and 40 N. They correspond to an extension of the rubber tube of 0 m, 0.03 m (that is 6% of the length) and 0.06 m (11%), respectively. Three input impedances have been measured. The corresponding $(kL)_{eq}$ are calculated (Figure 5.10a) as explained in

subsection 2.4. These should be compared with the theoretical results displayed in Figure 5.4. As previously explained, the functions do not monotically increase as a function of the frequency ("unwrapped" arctangent). After having unwrapped the functions, the equivalent wavenumbers multiplied by the length are obtained (Figure 5.10b), and then the equivalent wave speeds c_{eq} are obtained using equation (5.16) and are displayed in Figure 5.11.

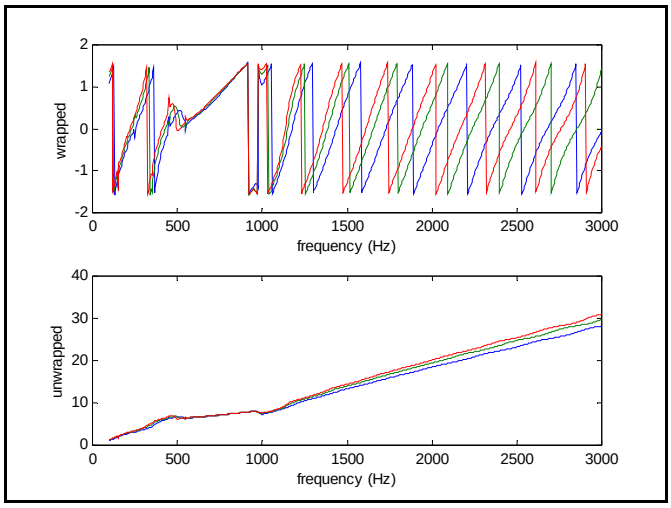

Figure 5.10: Not unwrapped (high) and unwrapped (low) variables $(kL)_{eq}$ associated with 3 measured input impedances.

For the lower and the higher frequency range, the effect of the tension is clearly visible in $(kL)_{eq}$. Conversely, the effect disappears, when the equivalent wave speed is calculated. This indicates that the effect of tension is essentially to increase the length of the tube. On the other hand, for the medium frequency range, the effect of tension is not visible in $(kL)_{eq}$. This means that the tension has no significant influence on the mechanical characteristics of the tube. Naturally, in the medium frequency range, an effect on the equivalent wave speed can be seen but, as in this range, the waves are evanescent, the length of the pipe may not influence the impedance. In conclusion, it can be said that for the tension considered, which corresponds to an extension of the length of the tube by as much as 10%, this does not significantly influence the mechanical properties of the tube. A much higher tension is necessary in order to obtain a significant effect.

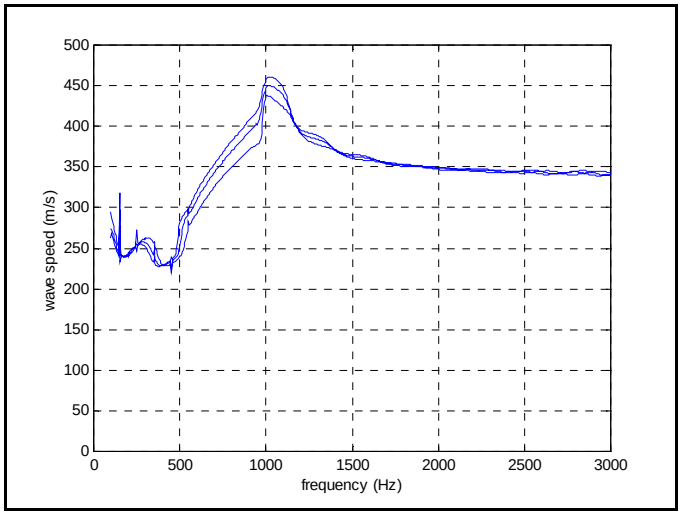

Figure 5.11: Equivalent wave speeds from the 3 measured impedances.

5.4. Conclusion

Wave propagation inside a stretched elastic cylindrical tube has been studied under plane wave approximation. Two models have been used. The first one is the Korteweg's model, in which the walls are characterised by their locally reacting impedance. In this model, two waves propagate: one propagates mainly in the fluid and is called Korteweg's wave, the second, which propagates in the structure, is the longitudinal wave. The Korteweg's wave exhibits a different behaviour according to the frequency. Three frequency ranges are emphasised. The wave is subsonic for the lower frequency range. For the medium range, the wave is evanescent, and for the higher frequency range the wave is supersonic and the wave speed tends toward the speed of sound in air.

A second, more sophisticated model has been produced, which leads to three propagating waves: two of these are very close to those previously described. The third one is triggered by the tension of the tube and corresponds to a string wave. The acoustic input impedance of the tube is calculated in order to compare the results with those arising from the Korteweg's model and also with those stemming from the experiments. An equivalent wave speed has been defined from the input impedance with the assumption that a unique wave is propagating, and through using the analogy of the rigid tube. For the three waves model, the results are similar to those obtained using the Korteweg's model, proving that this model is a good approximation for the calculation of the acoustic inner field. Indeed, if three different waves contribute to the field, one wave, which can be assimilated to the Korteweg's wave dominates and the contribution of the other waves might be negligible in the case of the rubber tube being investigated. This result is in accordance with [GT96], [Dal01].

Theoretical results have been compared with the measured input impedances of a stretched rubber tube membrane. The measured input impedances displayed exhibit the same three frequency ranges as described in the theoretical results. Moreover, the equivalent wave speed has been derived from the measured input impedances, revealing a satisfactory agreement between the theoretical and experimental equivalent celerities.

This demonstrates that the inner acoustic field is mainly dominated by the Korteweg's wave for which the propagation is subsonic within a low frequency range and supersonic in the high frequency range tending toward the speed of sound in air.

Appendix 5.A: motion equations of the stretched membrane

The membrane operator can be obtained from the Donnell's shell operator, as given in [Mar91], [Lei73], assuming that the thickness parameter $\frac{h^2}{12a^2}$ is set to zero. Such an operator can be modified in order to take into account the static preload effect. In this appendix, we recall the useful relationships which lead to the motion equations (5.1), assuming the membrane hypothesis and the axisymmetry of the vibratory field.

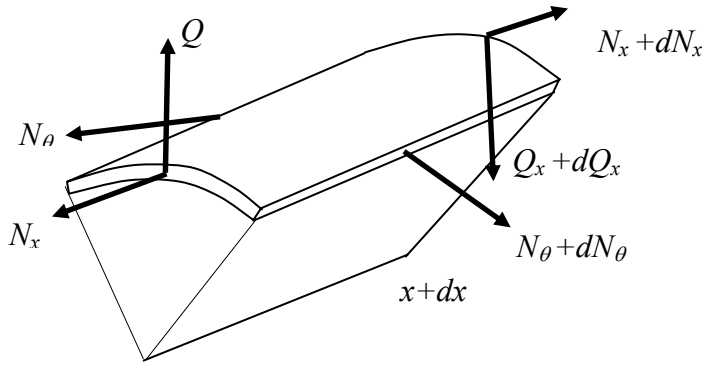

Figure A1: Forces applied to a membrane element

The forces applied to a membrane element of size (*dx*, *adθ)* are given in Figure A1. The projections of the equations of motion in the axial and radial directions are written as

$$\rho h \frac{\partial^2 u}{\partial t^2} = \frac{\partial N_x}{\partial x}, \tag{A1}$$

$$\rho h \frac{\partial^2 w}{\partial t^2} = -N_\theta - \frac{\partial Q}{\partial x} + P, \tag{A2}$$

The normal stresses in the axial and circumferential directions σ_{xx} and $\sigma_{\theta\theta}$ and the shear stress $\sigma_{x\theta}$ are related to strains ε_{xx}, ε_{xx}, ε_{xx} by

$$\sigma_{xx} = \frac{E}{1-\nu^2}(\varepsilon_{xx} + \nu\varepsilon_{\theta\theta}), \qquad \sigma_{\theta\theta} = \frac{E}{1-\nu^2}(\varepsilon_{\theta\theta} + \nu\varepsilon_{xx}), \qquad \sigma_{x\theta} = \frac{E}{1+\nu}\varepsilon_{x\theta}. \tag{A3}$$

The relationships between stresses and displacements are given by

$$\varepsilon_{xx} = \frac{\partial u}{\partial x}, \qquad \varepsilon_{\theta\theta} = \frac{w}{a}, \qquad \varepsilon_{x\theta} = 0. \tag{A4}$$

In order to take the static preload into account, we assume that static stresses in the membrane are $\sigma_{xx}{}^s = \frac{T}{A}$, and $\sigma_{\theta\theta}{}^s = \sigma_{x\theta}{}^s = 0$ (this is valid for the points which are sufficiently removed from the boundary conditions). From (A3), the static strains are

obtained as $\varepsilon^s{}_{xx} = \frac{T}{AE}, \varepsilon^s{}_{\theta\theta} = \frac{-\nu T}{EA}$, $\varepsilon^s{}_{x\theta} = 0$ and from relation (A4), the static displacements are established in the form of $u^s = \frac{T}{AE}x$ and $w^s = \frac{-\nu T}{EA}$.

Since the kinematic membrane hypothesis is retained, displacements u and w are supposed to be independent from the radial co-ordinate and are written as the sum of the static terms (u_s, w_s) and the dynamic terms (u_0, w_0) :

$$u = u^s + u^0, \qquad w = w^s + w^0. \tag{A5}$$

Taking the displacement fields (A5), where the static displacements are known, as a starting point, the strains are obtained from (A4), the stresses from (A3), and when the stresses are integrated with the membrane thickness this leads to the resulting forces

$$N_x = \int_{-h/2}^{h/2} \sigma_{xx} dz = \frac{Th}{A} + \frac{Eh}{(1-\nu^2)}\left[\frac{\partial u^0}{\partial x} + \nu\frac{w^0}{a}\right], \tag{A6}$$

$$N_\theta = \int_{-h/2}^{h/2} \sigma_{\theta\theta} dz = \frac{Eh}{(1-\nu^2)}\left[\frac{w^0}{a} + \nu\frac{\partial u^0}{\partial x}\right], \tag{A7}$$

$$Q_x = -N_x\frac{\partial w}{\partial x} = -\frac{Th}{A}\frac{\partial w^0}{\partial x}. \tag{A8}$$

Reporting (A6), (A7) and (A8) into the motion equations (A1) and (A2) results in the final form of the motion equation (5.1).

Capítulo 6

Conclusión general

El conjunto de trabajos presentados en esta memoria constituye una contribución a la comprensión del efecto de vibración de pared en el funcionamiento de los instrumentos de música de viento. En la actualidad, éste es un efecto que no está bien comprendido, y su cuantificación experimental y teórica es particularmente delicada debido a las múltiples interacciones que tienen lugar. Este documento ofrece una respuesta a esta problemática por medio del estudio de un modelo vibroacústico de instrumento simplificado, que permite un análisis detallado de los mecanismos de acoplamiento subyacentes. El objetivo central del trabajo es cuantificar la importancia de las vibraciones de las paredes sobre el sonido producido por un instrumento con perfil cilíndrico.

Los instrumentos de música de viento, bien sean de lengüeta simple (clarinete por ejemplo), lengüeta doble (trombón) o embocadura de flauta (tubo de órgano), están compuestos por un resonador cilíndrico acoplado a un mecanismo de excitación. Conservamos como modelo simple del resonador el de una estructura cilíndrica delgada apoyada en sus dos extremidades. El modelo de excitador utilizado es el de una lengüeta simple que permite el cálculo en el dominio temporal de las autooscilaciones del instrumento.

En lo que se refiere al resonador que constituye el tubo vibrante, éste puede ser caracterizado desde un punto de vista acústico por su matriz de impedancia de entrada. El modo acústico plano juega un papel esencial en las auto-oscilaciones del instrumento; la impedancia de entrada escalar asociada a este modo es esencial en el funcionamiento del instrumento. El estudio muestra que el papel de los defectos de ovalización del tubo es de gran importancia para tratar el acoplamiento entre la estructura y el fluido interno. Se ha estudiado la impedancia de entrada de tubos vibrantes que presentan una ligera ovalización y la de tubos de sección perfectamente cilíndrica. En ambos casos, la impedancia perturbada por las vibraciones se expresa a partir de la impedancia del tubo rígido mediante un factor de corrección adimensional. El análisis del modelo de impedancia de tubo vibrante conduce a las siguientes conclusiones.

6.1. Tubo de sección circular: resultados

En el caso de una sección perfectamente circular (capítulo 2), el estudio muestra que la perturbación debida a las vibraciones es, en general, pequeña y está asociada a los acoplamientos entre modos acústicos y de estructura que presentan la misma simetría o el mismo índice circunferencial. Los modos de respiración de la estructura son, por tanto, los únicos que están acoplados al modo acústico plano.

Esta interacción se pone de manifiesto en tres efectos: una resonancia mecánica, un efecto de coincidencia y un refuerzo de los picos de resonancia acústica. Estos efectos causan divergencias en la corrección de la impedancia debida a la vibración de las paredes en un sistema conservativo. Sin embargo, la introducción de mecanismos disipativos en la estructura (amortiguación estructural) o en el fluido (disipación viscotérmica en la capa límite) limita estos efectos y en ciertos casos hace que sean despreciables.

Sólo en el caso en que la primera frecuencia de respiración de la estructura está situada próxima a una frecuencia de resonancia acústica, la impedancia de entrada se ve perturbada. Esto sólo es posible para valores del módulo de Young (E) y de la densidad (ρ) especialmente pequeños, que son característicos de materiales de tipo caucho o polímero, evidentemente inutilizables para fabricar resonadores de instrumentos de música reales.

Las impedancias de entrada del tubo vibrante de sección perfectamente circular son utilizadas como datos de entrada en un modelo que acopla el excitador al resonador. Este modelo permite la obtención de simulaciones en el dominio temporal del sonido producido por el instrumento (más precisamente de la presión acústica en la boquilla). Estas simulaciones evidencian que mientras la impedancia de entrada del instrumento se encuentra perturbada por las vibraciones de las paredes, como es el caso de los tubos construidos con materiales de tipo polímero o caucho, se pueden observar modificaciones importantes del transitorio de ataque y del régimen permanente. Éste último está caracterizado de manera simple por dos parámetros objetivos: centro de gravedad espectral y frecuencia de ejecución, lo que permite cuantificar la importancia de las vibraciones de las paredes. La facilidad de interpretación (ligada al transitorio) y el timbre del instrumento son entonces afectados por la vibración de las paredes. En particular, se observan regímenes de autooscilaciones que presentan batidos ("nota del lobo"). La expresión "nota del lobo" se utiliza para describir una nota de características particulares, emitida en circunstancias específicas por ciertos instrumentos de cuerda (el violonchelo en especial). Esta nota, a menudo difícil de tocar, corresponde a un régimen multifónico y se asocia a un acoplamiento particularmente intenso entre la tabla de armonía y la cavidad. Por este motivo, el uso de la expresión "nota del lobo" en el contexto de los instrumentos de viento parece adecuada.

El análisis de las simulaciones temporales muestra que las perturbaciones de la impedancia acústica del modo plano relacionadas con las vibraciones de la estructura no son significativas para una estructura de sección perfectamente circular para todos los materiales utilizables en el ámbito de la construcción de instrumentos.

6.2. Tubo deformado: resultados

El caso de una estructura ligeramente ovalizada es muy diferente (capítulo 3) del de una estructura de sección perfectamente circular. En efecto, en este caso, existen acoplamientos entre modos acústicos y modos de estructura que presenten índices circunferenciales diferentes. Estos acoplamientos adicionales están inducidos por la imperfección de simetría del cilindro. En particular, el estudio de la impedancia de entrada del conducto deformado vibrante conduce a las siguientes conclusiones.

Los modos de menor frecuencia de la estructura no están, en general, asociados a los valores menores de los índices modales. Para los valores de los parámetros de estructura que utilizamos, el primer modo de estructura es, o bien un modo de flexión (orden circunferencial m=1), o bien un modo oval (orden circunferencial m=2). Este resultado implica que las frecuencias propias de los modos de respiración (orden circunferencial m=0) son superiores a estas últimas (m=1 y m=2). La presencia de un defecto origina un acoplamiento entre el modo plano y el primer modo oval de la estructura. Este acoplamiento es importante porque su frecuencia propia está próxima a las primeras frecuencias acústicas del tubo.

La perturbación de la impedancia de entrada del modo plano por el modo oval está vinculada a tres efectos muy similares a los descritos en el caso de una sección perfectamente circular: efecto de resonancia, efecto de coincidencia y efecto de refuerzo de las resonancias acústicas. Puesto que la frecuencia del modo de ovalización coincide o está próximo a una de las primeras frecuencias de resonancia acústica, se observa una perturbación importante de la impedancia cercana a la resonancia. Esta perturbación es más importante cuanto más amortiguado esté el modo oval.

Se han realizado simulaciones temporales de sonidos producidos por tubos sonoros deformados (complemento 4.5) que ponen en evidencia los efectos mencionados con anterioridad para los tubos de sección circular: modificación del transitorio de ataque y del régimen estacionario. También se obtienen notas del lobo. Estos resultados son válidos para tubos cuyos materiales y geometría han sido elegidos de manera que el primer modo oval coincida con primeras resonancias acústicas. En este caso, el régimen autooscilante del sistema está perturbado por las vibraciones del tubo debido al cambio importante de la impedancia de entrada inducida por sus vibraciones. Éstas ya no provocan correcciones menores, sino que perturban de manera significativa el funcionamiento del instrumento y causan regímenes de oscilación complejos (multifónicos).

6.3. Discusión sobre el estudio experimental [ND04]

Las conclusiones relativas a los modelos de impedancia de entrada y a las simulaciones temporales de tubos de sección circular o deformada nos llevan a formular una interpretación de una experiencia publicada en [ND04]. Hay que tener en cuenta que son raras las publicaciones en las que se estudia de manera precisa un efecto importante relacionado con las vibraciones de paredes. La interpretación propuesta constituye una síntesis de los resultados de este trabajo, y la presentamos en esta sección de conclusión: en [ND04], los autores estudian las autooscilaciones de un tubo de

órgano con embocadura de flauta. El tubo tiene las paredes delgadas de estaño. Se observan fuertes inestabilidades de tipo batido al hacer sonar el tubo. Esta perturbación muy importante se atribuye a las vibraciones de la pared. Los autores observan que la sección transversal del tubo de órgano es ligeramente elíptica y que la estructura vibra esencialmente sobre su primer modo oval. Formulan un modelo fenomenológico simple. A tenor del modelo explicado en el capítulo 3, se propone la interpretación física siguiente: el modo de estructura ovalizante no presenta la misma simetría que el modo acústico plano. El acoplamiento entre el modo plano (del que depende de manera fundamental la autooscilación) y ese modo de estructura no se puede explicar mediante un modelo vibroacústico de una estructura perfectamente cilíndrica. Los defectos de ovalización, que existen siempre en la práctica, juegan aquí un papel crucial, permitiendo un acoplamiento entre dos tipos de modos que estarían desacoplados en el caso de ausencia de defectos. Es la fuerte perturbación de la impedancia del modo plano resultante lo que provoca los regímenes de autooscilación particularmente inestables que se observan.

6.4. Resultados experimentales sobre una guía de onda de membrana

Se ha llevado a cabo un estudio experimental del acoplamiento del tubo con el fluido interno para el caso de un tubo membranoso de caucho. Este estudio no constituye una validación experimental propiamente dicha del modelo multimodal desarrollado en el capítulo 2. En la configuración elegida, el gran número de modos *in vacuo* de la membrana hace que el análisis mediante el método modal no resulte adecuado. Otro tipo de modelo, basado en un desarrollo en las ondas naturales del sistema acoplado, ha sido desarrollado y da cuenta de las medidas de impedancia de entrada efectuadas. Este modelo sencillo de interacción del fluido con el tubo consiste en describir la interacción mediante una admitancia de pared, que constituye un modelo de reacción local. Formular este tipo de hipótesis conduce a describir las ondas acústicas dentro del tubo a través de una velocidad aparente que depende de la admitancia de la pared. Esta celeridad es la celeridad de la onda llamada de Korteweg. Si se descarta la hipótesis de reacción local, hay que describir el movimiento del tubo a través de un operador de membrana que puede depender de una tensión axial aplicada sobre el mismo. Cuando la membrana está en tensión existen tres ondas acopladas en el medio y la resolución de una ecuación de dispersión permite el cálculo de la impedancia de entrada acústica del sistema. La teoría y el modelo coinciden.

Los resultados obtenidos sobre el tubo de caucho parecen estar lejos de las aplicaciones musicales. Sin embargo, el trabajo realizado en esta dirección constituye el primer paso para la validación experimental de este tipo de fenómenos.

6.5. Limitaciones del estudio

Los modelos analíticos desarrollados se basan en numerosas hipótesis simplificadoras. Aunque estas hipótesis estén justificadas en el marco de nuestro estudio, limitan la validez y el alcance de los resultados obtenidos. Por este motivo, la transposición de las conclusiones a un instrumento real se deberá realizar con prudencia:

- La interacción de la estructura con el fluido interno se describe en el marco de la aproximación “fluido ligero”. Esta aproximación es legítima mientras la densidad de la estructura y del fluido sean diferentes. Esta aproximación es más valida cuanto mayor sea la diferencia entre las densidades de la estructura y el fluido.
- Se ignora la radiación por la extremidad abierta del instrumento y se aplica la condición de Dirichlet $p=0$. Se podría tener en cuenta la radiación de la abertura introduciendo una matriz de impedancia de radiación. Esta condición se ha llevado a cabo en [Gau97] y causa acoplamientos intermodales acústicos, que se pueden despreciar.
- Se ha ignorado la radiación lateral de la estructura. Se ha tenido en cuenta en [Gau97] sin que se pueda mostrar que su influencia sea importante para el sonido musical producido.
- La fuente de excitación del tubo es acústica. La lengüeta que golpea la boquilla en cada periodo constituye una fuente de excitación mecánica cuya influencia ha sido ignorada en este estudio. Se propuso un modelo de este tipo en [Gau97], pero no da cuenta de la perturbación de la autooscilación del sistema.

El límite esencial del modelo de estructura deformada vibrante reside en la hipótesis que los modos de las estructuras cilíndrica y deformada son muy similares si la ovalización es pequeña. Esta hipótesis es discutible y debería ser objeto de una validación mediante un cálculo por elementos finitos, por ejemplo. Permite desarrollar el campo vibratorio sobre una base funcional conocida (la de los modos *in vacuo* de la estructura circular) y llevar a cabo un cálculo de la impedancia de entrada acústica de la estructura deformada teniendo sólo en cuenta el efecto de la deformación a través de un solo término de acoplamiento presente en el segundo miembro de la ecuación de movimiento de la estructura. Esta hipótesis, ya formulada por Yousri y F. Fahy y validada experimentalmente en [YF77], es la más restrictiva del modelo aquí propuesto.

6.6. Perspectivas

Los resultados obtenidos en este estudio se pueden proyectar en diferentes líneas de trabajo futuras:

- Los modelos de impedancia desarrollados y la implementación de simulaciones temporales se pueden utilizar para llevar a cabo tests auditivos en condiciones controladas. Se puede intentar, por ejemplo, variar las frecuencias de resonancias mecánicas del resonador y determinar mediante estos tests los umbrales de percepción de la diferencia entre los sonidos emitidos por instrumentos con tubos rígidos y vibrantes.

- Se puede complicar la geometría del instrumento por medio de métodos numéricos (como el método de los elementos finitos, por ejemplo). La obtención de la impedancia de entrada del tubo vibrante mediante el cálculo numérico de los primeros modos de la estructura se puede enfocar de dos manera: a) a través de un método analítico como el que se ha presentado en este documento (se trataría entonces de un método híbrido, en el que la base de representación se encontraría por vía numérica y el acoplamiento estaría descrito a través del método integromodal implementado de manera semianalítica) y b) a través de un método puramente numérico (utilización de un método numérico para describir las oscilaciones de la columna de fluido interno y

las vibraciones de la estructura). Una primera configuración para esta aplicación podría ser el tubo de órgano estudiado en [ND04]. La introducción de la ovalización de la sección debe permitir un cálculo numérico exacto de los modos *in vacuo* deformado. Solamente mediante un método numérico se pueden calcular los modos de estructura de un cuerpo de instrumento con agujeros laterales. Hay que tener en cuenta que la implementación de un método puramente numérico no permitiría analizar los mecanismos físicos que engendran el fenómeno de vibración de pared como permite hacerlo un método analítico.

- En artículos anteriores, se describen numerosos modelos de embocadura de flauta (ver por ejemplo [FH00]. Éstos se podrían implementar para simular la respuesta temporal de un tubo de órgano vibrante. El estudio experimental del mismo ha mostrado que podría ser sensible a las vibraciones de las paredes. En un modelo de estas características, el resonador se describe a través de su impedancia acústica como en el enfoque desarrollado en las simulaciones de sonidos emitidos por instrumentos con lengüeta simple.

- El capítulo 5 presenta un experimento llevado a cabo sobre una guía de membrana. La relación entre este estudio y los capítulos 2 a 4 no es directa en la medida en que no se presenta como una validación experimental del modelo multimodal. Sin embargo, dos prolongaciones de este capítulo 5 podrían precisar este vínculo: a) la primera es de naturaleza teórica y consiste en una comparación entre los dos métodos de representación del campo acústico en el interior del tubo vibrante, es decir, el desarrollo multimodal de los campos acústicos y vibratorios y la representación de los campos bajo la forma de la superposición de ondas naturales. b) La segunda prolongación al capítulo 5 sería de naturaleza experimental. Los modelos desarrollados en los capítulos 2 a 4 permiten definir las características de un material y una geometría de tubo que da lugar a un primer modo oval cuya frecuencia coincida con una de las primeras resonancias acústicas. Para un tubo de estas características, que habría que fabricar (cosa que puede presentar dificultades prácticas), se efectuarían medidas de impedancia de entrada como las presentadas en el capítulo 5. Así, se puede efectuar una validación de los modelos de impedancia perturbada descrita en los capítulos 2 y 4.

Conclusion générale

L’ensemble de travaux présentés dans ce mémoire constitue une contribution à la compréhension de l’effet de vibration de paroi sur le fonctionnement des instruments de musique à vent. Cet effet est aujourd’hui mal compris et sa quantification tant expérimentale que théorique est particulièrement délicate du fait des multiples interactions mises en jeu. Une réponse est apportée dans ce document grâce à l’étude d’un modèle vibroacoustique d’instrument simplifié, qui permet une analyse fine des mécanismes de couplage sous-jacents. L'objectif central du travail est de quantifier

l'importance des vibrations de parois sur le son produit par un instrument de perce cylindrique.

Les instruments de musique à vent que nous considérons, qu'ils soient à anche simple (clarinette par exemple), à anches lipales (trombone) ou à embouchure de flûte (tuyau d'orgue) sont composés d'un résonateur cylindrique couplé à un mécanisme d'excitation. Nous retenons comme modèle simple du résonateur celui d'une coque mince cylindrique appuyée à ses deux extrémités. Le modèle d'excitateur retenu est celui d'une anche simple, qui permet le calcul dans le domaine temporel des auto-oscillations de l'instrument.
En ce qui concerne le résonateur que constitue le tuyau vibrant, celui-ci peut être caractérisé d'un point de vue acoustique par sa matrice impédance d'entrée. Le mode acoustique plan jouant un rôle essentiel pour la mise en place des auto-oscillations, l'impédance d'entrée scalaire associée à ce mode est de toute première importance dans le fonctionnement de l'instrument. L'étude montre que le rôle des défauts d'ovalisation, encore appelé distorsion du tuyau est de toute première importance pour traiter le couplage coque/fluide interne. L'impédance d'entrée de tuyaux vibrants, présentant ou non une faible ovalisation a été étudiée. Dans tous les cas, l'impédance perturbée par les vibrations est exprimée à partir de l'impédance du tuyau rigide au moyen d'un facteur de correction adimensionnelle. L'examen du modèle d'impédance de tuyau vibrant fait apparaître les conclusions suivantes.

6.1. Tube de section circulaire : résultats

Dans le cas d'une section parfaitement circulaire (chapitres 2), l'étude montre que la perturbation due aux vibrations est en général faible et met en jeu des couplages entre modes acoustiques et de structure présentant la même symétrie ou encore le même indice circonférentiel. Les modes de respiration de la coque sont donc les seuls à être couplés au mode acoustique plan.

Plus précisément, cette interaction met en évidence trois effets : une résonance mécanique, un effet de coïncidence et un renforcement des pics de résonance acoustique. Le facteur de correction pour l'impédance présente des maximums au voisinage des fréquences de résonance de la structure, aux fréquences pour lesquelles des conditions de coïncidence spatiale entre les modes de structure et acoustiques est satisfaite, et aux fréquences de résonance acoustique. Ces effets donnent lieu à des divergences du facteur correctif pour un système conservatif. Cependant, l'introduction de mécanismes dissipatifs dans la structure (amortissement structural) ou dans le fluide (dissipation visco-thermique dans les couches limites) limite ces effets et dans certains cas les rend négligeables.

Une perturbation notable de l'impédance d'entrée n'est possible que si la première fréquence de respiration de la coque est située au voisinage d'une fréquence de résonance acoustique. Ceci n'est possible que pour des valeurs du module de Young (E) et de la masse volumique (ρ) particulièrement faibles, et caractéristiques de matériau de type caoutchouc ou polymère, évidement inutilisable pour fabriquer des résonateurs d'instruments de musique réels.

Les impédances d'entrée du tuyau vibrant de section parfaitement circulaires sont utilisées comme données d'entrée dans un modèle couplant excitateur et résonateur. Ce

modèle conduit à des simulations dans le domaine temporel du son produit par l'instrument (plus précisément de la pression acoustique dans le bec). Ces simulations mettent en évidence que lorsque l'impédance d'entrée de l'instrument est fortement perturbée par les vibrations de parois, comme c'est le cas des tuyaux constitués de matériaux de type polymères ou caoutchouc, il est possible d'observer des modifications importantes du transitoire d'attaque et du régime permanent. Ce dernier, est caractérisé de façon simple par deux paramètres objectifs (centre de gravité spectral et fréquence de jeu) permettant de quantifier l'importance des vibrations des parois. La facilité de jeu (lié au transitoire) et le timbre de l'instrument sont alors affectés par la vibration des parois. En particulier des régimes d'auto-oscillations présentant des battements et pouvant être qualifiés de 'note du loup' peuvent être observés. L'expression 'note du loup' est utilisée pour décrire une note d'émission particulière, présente dans certains instruments à cordes (le violoncelle en particulier). Cette note, souvent délicate à jouer et correspondant à un régime multiphonique (sensation de 'note qui roule') est associée à un couplage particulièrement fort entre la table d'harmonie et la cavité. Pour cette raison, l'emploi de l'expression 'note du loup' dans le contexte lié aux instruments à vent semble donc approprié.
L'analyse des simulations temporelles montre que les perturbations de l'impédance d'entrée acoustique du mode plan liées aux vibrations de la coque ne sont pas significatives pour une coque de section parfaitement circulaire pour tous les matériaux utilisables en lutherie.

6.2 Tube distordu : résultats

Le cas d'une coque légèrement ovalisée est très différent (chapitre 3) de celui d'une coque de section parfaitement circulaire. En effet, dans ce cas des couplages entre modes acoustiques et modes de structure présentant des indices circonférenciels différents existent. Ces couplages additionnels sont induits par la brisure de symétrie du cylindre. En particulier l'étude de l'impédance d'entrée du conduit distordu vibrant permet de lister les conclusions suivantes.

Les premiers modes d'une coque ne sont en général pas associés aux valeurs les plus faibles prises par les indices modaux. Pour les valeurs des paramètres de coque que nous utilisons, le premier mode de coque est soit un mode de flexion (ordre circonférentiel m=1) soit un mode ovalisant (ordre circonférentiel m=2). Ce résultat implique que les fréquences propres des modes de respiration (ordre circonférentiel m=0) soient supérieures à ces dernières. La présence d'un défaut induit un couplage entre le mode plan et le premier mode d'ovalisation de la coque. Ce couplage, qui est alors important du fait de la faible valeur de sa fréquence propre et la proximité des premières fréquences acoustiques du tuyau.

La perturbation de l'impédance d'entrée du mode plan par le mode ovalisant est liée à trois effets très similaires à ceux décrits dans le cas d'une section parfaitement circulaire : effet de résonance, effet de coïncidence et effet de renforcement des résonances acoustiques. Lorsque la fréquence du mode d'ovalisation coïncide ou est proche d'une des premières fréquences de résonance acoustique, une perturbation importante de l'impédance au voisinage du pic de résonance peut être observée. Cette perturbation est d'autant plus importante que le mode ovalisant est faiblement amorti.

Les simulations temporelles de sons produits par des tuyaux sonores distordus (complément 4.5) ont pu être mises en œuvre et permettent de mettre en évidence des effets déjà mentionnés pour les tuyaux de section circulaire : modification du transitoire d'attaque et du régime stationnaire. Des notes du loup peuvent également être obtenues. Ces résultats sont valides pour des tuyaux pour lesquels le matériau et la géométrie ont été choisis de telle sorte que le premier mode ovalisant coïncide avec des premières résonances acoustiques. Dans ce cas c'est très clairement le régime auto-oscillant du système qui est perturbé par les vibrations du tube, du fait du changement important de l'impédance d'entrée induit par ses vibrations. Celles-ci ne donnent plus lieu à des corrections mineures, mais perturbent fondamentalement le fonctionnement de l'auto-oscillateur et donnent lieu à des régimes d'oscillation complexes (multiphoniques).

6.3 Discussion sur l'étude expérimentale [ND04]

Les conclusions relatives aux modèles d'impédance d'entrée et aux simulations temporelles de tuyaux de sections circulaires ou distordues nous amènent à faire formuler une interprétation d'une expérience publiée dans [ND04]. Notons que les publications dans lesquelles un effet majeur lié aux vibrations de parois est rapporté de façon précise sont rares. L'interprétation proposée constituant une synthèse des résultats de ce travail, nous la présentons dans cette partie conclusive : dans [ND04], les auteurs étudient les auto-oscillations d'un tuyau d'orgue à embouchure de flûte. Le tuyau est à parois minces en étain. De fortes instabilités de type roulement ou battement sont observées lorsque l'on fait sonner le tuyau. Cette perturbation très importante est attribuée aux vibrations de paroi. Les auteurs observent que la section transversale du tuyau d'orgue est légèrement elliptique et que la coque vibre essentiellement sur son premier mode ovalisant et formulent un modèle phénoménologique simple. Nous proposons l'interprétation physique suivante : le mode de coque ovalisant ne présente pas la même symétrie que le mode acoustique plan. Le couplage fort observé entre le mode plan (dont dépend de façon essentielle l'auto-oscillation) et ce mode de structure ne peut s'expliquer au moyen d'un modèle vibroacoustique impliquant une structure parfaitement cylindrique. Les défauts d'ovalisation, qui existent toujours en pratique, jouent donc ici un rôle majeur en permettant un couplage entre deux types de modes qui seraient découplées en l'absence de défauts. C'est la forte perturbation de l'impédance du mode plan qui en résulte qui donne lieu aux régimes d'auto-oscillations particulièrement instables qui sont observés.

6.4 Résultats expérimentaux sur un guide d'onde membranaire

Une étude expérimentale du couplage tube/fluide interne a été effectuée dans le cas simple d'un tuyau membranaire en caoutchouc. Cette étude ne constitue pas à proprement parler une validation expérimentale du modèle multimodal développé dans le chapitre 2. En effet, dans la configuration retenue, le grand nombre de modes *in vacuo* de la membrane gène la mise en place de la méthode modale. Un autre type de modèle, basé sur un développement en ondes naturelles du système couplé a donc été développé et rend compte des mesures d'impédance d'entrée effectuées. Les conclusions de l'étude portent essentiellement sur la mise en évidence de l'insuffisance de l'hypothèse dite de 'réaction locale'. En effet, un modèle simple d'interaction fluide/tube consiste à décrire l'interaction au moyen d'une admittance de paroi, constituant un modèle de réaction locale. Formuler cette hypothèse conduit à décrire les

ondes acoustiques dans le tuyau à l'aide d'une célérité apparente, dépendant de l'admittance de paroi. Cette célérité est la célérité de l'onde dite de Korteweg. Si l'hypothèse de réaction locale n'est pas retenue, le mouvement du tuyau doit être décrit à l'aide d'un opérateur de membrane, qui dans le cadre de l'étude peut dépendre d'une tension axiale appliquée. Quand la membrane est sous tension, trois ondes couplées existent dans le milieu et la résolution d'une équation de dispersion permet le calcul de l'impédance d'entrée acoustique du système. Théorie et modèle sont en bon accord.

Les résultats obtenus sur le tuyau en caoutchouc semblent éloignés des applications musicales. Cependant, le travail réalisé dans cette direction constitue le premier pas dans la validation expérimentale de ce type de phénomène.

6.5 Limites de l'étude

Plusieurs hypothèses simplificatrices sont à la base des modèles analytiques développés. Bien que ces hypothèses soient justifiées dans le cadre de notre étude, elles en limitent la portée. Nous les listons ci-après : la géométrie de l'instrument simplifié ainsi que les conditions aux limites d'appuis imposés permettent de définir une configuration sur laquelle un modèle analytique peut être développé. La transposition des conclusions à un instrument réel doit donc être conduite avec prudence :

- L'interaction coque/fluide interne est décrite dans le cadre de l'approximation 'fluide léger'. Cette approximation est d'autant plus légitime que les masses volumiques de la structure et du fluide sont différentes.
- Le rayonnement par l'extrémité ouverte de l'instrument est ignoré et on suppose que la condition de Dirichlet $p=0$ s'applique. Une prise en compte du rayonnement de l'ouverture pourrait être effectuée en introduisant une matrice impédance de rayonnement. Cette condition a été mise en œuvre dans [Gau97] et induit des couplages intermodaux acoustiques, souvent faibles.
- Le rayonnement latéral de la coque a été ignoré. Sa prise en compte est effectuée dans [Gau97] sans que l'on puisse montrer que son influence est importante pour le son musical produit.
- La source d'excitation du tuyau est ici acoustique. L'anche qui frappe le bec à chaque période constitue une source d'excitation mécanique, dont l'influence a été ignorée dans cette étude. Un modèle d'une telle source a été proposé dans [Gau97], mais ne permet pas de rendre compte de perturbation majeure de l'auto-oscillation du système.

La limite essentielle du modèle de coque distordue vibrante réside dans l'hypothèse que les modes des coques circulaire et distordue sont très proches si l'ovalisation est faible. Cette hypothèse est discutable et devrait faire l'objet d'une validation à l'aide d'un calcul par élément finis par exemple. Elle permet de développer le champ vibratoire sur une base fonctionnelle connue (celle des modes *in vacuo* de la coque circulaire). Ceci permet de mener un calcul d'impédance d'entrée acoustique de coque distordue en ne prenant en compte l'effet de cette distorsion que par l'intermédiaire d'un seul terme de couplage présent au second membre de l'équation de mouvement de la coque. Cette hypothèse, déjà formulée par Yousri et F.Fahy et validée expérimentalement dans [YF77] est la plus restrictive du modèle proposé ici.

6.6 Perspectives

Les résultats obtenus au cours de cette étude permettent d'envisager plusieurs prolongements :

- Les modèles d'impédance développés ainsi que l'implémentation de simulations temporelles permettent de mettre en place des tests auditifs dans des conditions bien maîtrisées. On peut imaginer en effet de faire varier les fréquences de résonances mécaniques du résonateur (qui sont les paramètres pertinents dont dépendent les termes de couplages) et de déterminer au moyen de ces tests les seuils pour lesquels une différence est perceptible entre les sons des tuyaux rigides et vibrants.

- La prise en compte d'une géométrie plus complète de l'instrument peut être effectuée à l'aide d'une méthode numérique appropriée (méthode des éléments finis par exemple). Le calcul numérique des premiers modes de la structure doit permettre la détermination de l'impédance d'entrée du tuyau vibrant, soit à l'aide d'une méthode analytique présentée dans ce document (il s'agirait alors d'une méthode hybride, la base de représentation étant trouvée par voie numérique et le couplage étant décrit à l'aide de la méthode intégro-modale implémentée de façon semi-analytique), soit à l'aide d'une méthode purement numérique (élément finis de volume pour décrire les oscillations de la colonne de fluide interne et les vibrations de la structure). Un première configuration pour cette application pourrait être le tuyau d'orgue étudié dans [ND04]. L'introduction de l'ovalisation de la section doit permettre un calcul numérique exact des modes *in vacuo* distordu. De façon similaire le calcul des modes de structure d'un corps d'instrument possédant des trous latéraux qui brisent la symétrie de révolution est possible uniquement à l'aide de méthode numérique. Notons que la mise en œuvre d'une méthode purement numérique ne permettrait pas d'analyser les mécanismes physiques qu'engendrent le phénomène de vibration de paroi comme permet de le faire une méthode analytique.

- Des modèles d'embouchure de flûte sont décrits dans la littérature (voir par exemple [FH00] et pourraient être implémentés dans le but de simuler la réponse temporelle d'un tuyau d'orgue vibrant, dont l'étude expérimentale a montré qu'elle pouvait être sensible aux vibrations de parois. Dans un tel modèle, le résonateur est décrit à l'aide de son impédance acoustique tout comme dans l'approche développée dans les simulations de sons d'anche battantes.

- Le chapitre 5 présente une expérimentation menée sur un guide membranaire. Le lien entre cette étude et les chapitres 2 à 4 n'est pas direct dans la mesure où il n'est pas présenté de validation expérimentale du modèle multimodal. Cependant, deux prolongements au chapitre 5 pourraient préciser ce lien. Le premier prolongement est de nature théorique et concerne une comparaison entre deux méthodes de représentation du champ acoustique à l'intérieur d'un tuyau vibrant : La première méthode (mise en œuvre dans les chapitres 2 à 4) repose sur un développement multi-modal des champs acoustiques et vibratoires utilisant des bases fonctionnelles découplées : les modes in vacuo de la structure et les modes acoustiques transverses du tuyau rigide. La seconde méthode (mise en œuvre dans le chapitre 5) est basée sur une représentation des champs sous la forme de la superposition d'ondes naturelles associées au problème couplé tuyau/fluide interne. Une comparaison de ces deux méthodes de représentation des champs dans le but de tester leur efficacité constitue une perspective à ce travail. Le second prolongement au chapitre 5 est de nature

expérimentale. Les modèles développés dans les chapitres 2 à 4 permettent de définir les caractéristiques d'un matériau et une géométrie du tube donnant lieu à un premier mode ovalisant dont la fréquence coïncide avec l'une des premières résonances acoustiques. Pour un tel tuyau, qu'il convient de fabriquer (ce qui peut poser des difficultés pratiques), des mesures d'impédance d'entrée peuvent être effectuées comme celles présentées dans le chapitre 5. Une validation des modèles d'impédance perturbée décrit dans les chapitres 2 et 4 peut alors être effectuée.

Anexo A

Study of the input acoustic impedance of a vibrating cylindrical shell: consequences on clarinet-like instruments

Este anexo A reproduce una comunicación redactada en inglés, extraída de las actas del 7º Congreso Francés de Acústica junto con el 30º Congreso Alemán de Acústica (22-25 de marzo de 2004, Estrasburgo, Francia)

Cette annexe A reproduit une communication rédigée en anglais, extraite des actes du 7ième Congrès Français d'Acoustique joint au 30ième Congrès Allemand d'Acoustique (22-25 mars 2004, Strasbourg, France)

Study of the input acoustic impedance of a vibrating cylindrical shell: consequences on clarinet-like instrument

R. Pico Vila[1], F. Gautier[2], J. Gilbert[2]
[1]*Escuela Politécnica Superior de Gandia (EPSG). Departamento de Física, Universidad Politécnica de Valencia (UPV). c/ Nazaret-Oliva s/n, 46700 Gandia, Spain*
[2]*Laboratoire d'Acoustique de l'Université du Maine - UMR CNRS 6613, Université du Maine, avenue Olivier Messiaen, 72085 Le Mans cedex 9, France*
rpico@fis.upv.es

Introduction

The influence of the wall vibrations on the acoustic behaviour of wind instruments is a widely debated matter, although no clear results have been obtained. Musicians and manufacturers of wind instruments often state that the construction materials play an essential role in the acoustic quality of the instrument. Many scientific studies have aimed to address all phenomena related to wall vibration effect, but there are many difficulties to evaluate and quantify the role played by the instrument's material on its acoustic response. In this work, a vibroacoustic model of a clarinet-like instrument is proposed to evaluate the wall vibration effect on the acoustic behaviour of a wind instrument.

Vibroacoustic model

The body of the instrument is assimilated to a simply supported thin-walled cylindrical shell. The coupling between the shell modes of the body of the instrument and the acoustic modes of the air column (see figure 1) is deduced with an analytical vibroacoustic multimodal model [1].

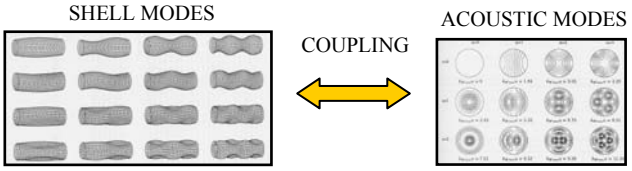

Figure 1: Vibroacoustic coupling between shell modes and acoustic modes

The acoustic behaviour of the body of the instrument (resonator) can be described by its input acoustic impedance considering only the interaction between the first breathing mode and the plane mode. Wall vibration effect can be evaluated as a correction (C) of the acoustic input impedance of a non-vibrating resonator (Z^r):

$$Z = Z^r (1 + C)$$

Note that for a perfectly circular cylinder, acoustic impedance is affected only by shell modes having the same symmetry as the plane mode. When considering the usual materials of woodwind construction, the wall vibration effect is negligible (all the curves in figure 2a are nearby the same).

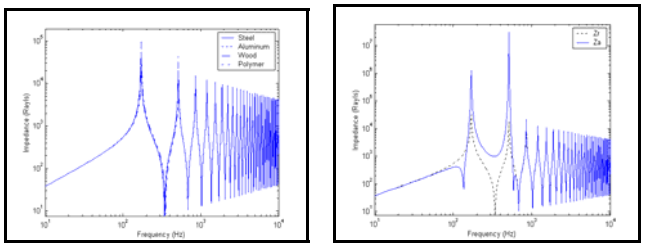

Figure 2: ***a)*** *Acoustic input impedance of 4 vibrating shells made of steel, aluminium, wood and polymer. Only the breathing shell mode has been considered. Differences are very small.* ***b)*** *Acoustic input impedance of a rigid cylinder (Zr) and a wall vibrating cylinder (Za) made of wood (E= $0.212 \cdot 10^9 N/m^2$ and density $\rho = 300 kg/m^3$). For Z^a, the materials are chosen in a way that the second acoustic resonance and the first mechanical resonance coincide. Tube length l=0.5; radius: 0.5mm and thickness: 14.5mm*

For a fixed value of the geometrical parameters of the cylinder, it is shown that for low enough values of Young's modulus (E) and density (ρ) the wall vibration effect can be much important. As a consequence, acoustic input impedance can be strongly affected as shown in figure 3. Three phenomena underlay this singular behaviour: a mechanical resonance, a spatial coincidence effect and an acoustic resonance. When two of these phenomena take place simultaneously, the perturbation effect becomes significant and the

acoustic resonances and antiresonances of the tube can be significantly altered.

Numerical simulations

Simulations in the time domain provide the periodic oscillations corresponding to the main oscillation regime of the instrument. The implementation of this method [2,3] enables us to obtain a numerical solution in the time domain of the inner pressure field of the instrument when oscillating. Through the simulations in the time domain, the behaviour of instruments made of different materials is analysed.

Main wall vibration effects

Change of timbre

The spectral envelope is an important feature of timbre perception. Steady state spectra of the simulated signals of vibrating resonators made of several materials are different from the rigid case only when E and ρ are low enough.

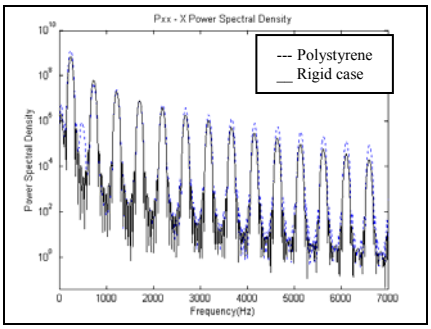

Figure 3: Spectra of steady state inner pressure simulated by polystyrene and rigid resonators.

Modification of the attack time

The starting transient is substantial in discrimination of musical sounds. Wall vibrations may alter the formation of stationary waves inside the instrument, and its oscillation regime. When E and ρ are small enough, this effect can be observed (figure 5).

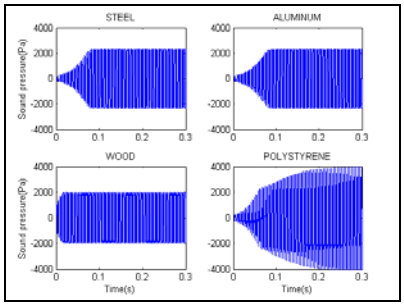

Figure 4: Transients simulated with steel and aluminium resonators are the same but differ from wood and polystyrene resonators

Wolf note

In some circumstances, the instrument may emit sounds in quasi-periodic regime called Wolf notes by analogy to bowed strings (cello). Transition through Wolf note has been observed in organ tube with flute mouthpiece and the interaction between ovaling shell modes and plane acoustic mode [4]. Numerical simulations of some vibrating resonators present the same behaviour. Therefore, wall vibration effect could explain this change of oscillation regime of the instrument.

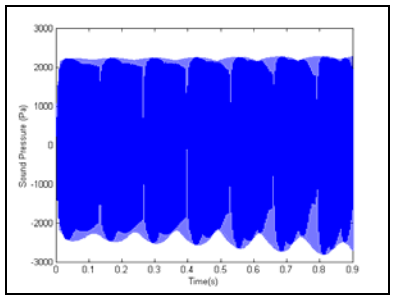

Figure 5: Simulation in the time domain of an instrument emitting a Wolf note

Conclusion

Wall vibration effect is only visible in simulations in the time domain when E and ρ are low enough

References

[1] F. GAUTIER and TAHANI 1998 Journal of Sound and Vibration **213**, 107-125. Vibroacoustic behavior of a simplified musical wind instrument.
[2] R. T. SCHUMACHER 1981 Acustica **48**(2), 73-84. Ab initio calculations of the oscillations of a clarinet.
[3] C. J. NEDERVEEN, J. P. DALMONT Mars 2004 Journal of Sound and Vibration **27**(1-2) 227-239 Pitch level changes in organ pipes due to wall resonances.

Anexo B

Relationship between the multimodal approach, and the membrane approach

Este anexo establece la relación entre el desarrollo multimodal desarrollado en el capítulo 2 y el modelo de membrana adoptado en el capítulo 5.

Cette annexe établit le rapport entre le développement multimodal développé dans le chapitre 2 et le model membranaire retenue dans le chapitre 5.

Comparison of two models

Let us consider the mechanical behaviour of the shell with the shell equation:

$$\rho_s h\left(\omega_a^2 L + \omega^2\right)\mathbf{X}(M) = -p(M)\mathbf{n} \tag{B1}$$

where L is the Donnell operator defined by:

$$L = \begin{pmatrix} a^2\dfrac{\partial^2}{\partial z^2} + \dfrac{1-\nu}{2}\dfrac{\partial^2}{\partial \theta^2} & \dfrac{1+\nu}{2}\dfrac{\partial^2}{\partial z \partial \theta} & \nu a\dfrac{\partial}{\partial z} \\ \dfrac{1+\nu}{2}\dfrac{\partial^2}{\partial z \partial \theta} & \dfrac{\partial^2}{\partial \theta^2} + \dfrac{1-\nu}{2}a^2\dfrac{\partial^2}{\partial z^2} & \dfrac{\partial}{\partial \theta} \\ -\nu a\dfrac{\partial}{\partial z} & -\dfrac{\partial}{\partial \theta} & -1-\beta\left(a^2\dfrac{\partial^2}{\partial z^2} + \dfrac{\partial^2}{\partial \theta^2}\right) \end{pmatrix} \tag{B2}$$

The hypothesis of the membrane consists of:

- Neglecting the angular dependency in the Donnell operator.
- Supposing that the thickness of the shell is much smaller than its radius, and as such, $\beta = 0$.
- Neglecting the torsion wave associated to v_0, we have:

With these approximations, the membrane operator can be expressed as:

$$L = \begin{pmatrix} a^2\dfrac{\partial^2}{\partial z^2} & 0 & \nu a\dfrac{\partial}{\partial z} \\ 0 & 0 & 0 \\ -\nu a\dfrac{\partial}{\partial z} & 0 & -1 \end{pmatrix} \tag{B3}$$

Tabla de figuras

Tablas

Referencias

[BA89] A. BARJAU, J. AGULLO 1989 *Acustica* **69**, 204-210. Calculation of the starting transients of a double reed conical woodwind.

[Bac87] J. BACKUS 1964, *Journal of the Acoustical Society of America* **36**(10), 1881-1887. Effect of wall material on the steady-state tone quality of woodwind instruments.

[BF93] B.J. BREVART, C.R. FULLER 1993 *Journal of the Acoustical Society of America* **94**(3), 1467-1475. Active control of coupled wave propagation in fluid-filled elastic cylindrical shells.

[BH66] J. BACKUS and T.C. HUNDLEY 1966 *Journal of the Acoustical Society of America* **39**(5), 936-945. Wall vibration in flue organ pipes and their effect on tone.

[BK88] A. H. BENADE and S. N. KOUZOUPIS 1988 *Journal of the Acoustical Society of America* **83**, 292. The clarinet spectrum: Theory and experiment

[BN40] BONER and NEWMAN 1940 *Journal of the Acoustical Society of America* **12**, 83-89. The effect of wall materials on the steady-state acoustic spectrum of flue pipes.

[Bru98] M. BRUNEAU 1998 *Manuel d'Acoustique fondamentale*, Editions Hermes, Paris.

[Cal89] CALIOPE 1989 *La parole et son traitement automatique*, Collection technique et Scientifique des Télécommunications, Masson editor.

[CC96] B.V. CHAPNIK, I. G. CURRIE 1996 *Internoise Congress Proceedings*, Liverpool, U.K., p.1011-1014. The effect of finite length flexible segments on acoustic wave propagation in piping systems.

[Col71] COLTMAN 1971 *Journal of the Acoustical Society of America* **49**(2), 520-523. Effect of material on flute tone quality.

[Dal01] J.P. DALMONT 2001 *Journal of Sound Vibration* **243**(3), 441-459. Acoustic impedance measurements Part II: a new calibration method.

[DB92] J.P. DALMONT, A. M. BRUNEAU 1992 *Journal of the Acoustical Society of America* **91**(5), 3026-3033. Acoustic impedance measurements: plane-wave mode and first helical mode contributions.

[DGO03] J. P. DALMONT, J. GILBERT, S. OLLIVIER 2003 *Journal of the Acoustical Society of America*, Vol. **114**, Nº4, Pt1. Nonlinear characteristics of single-reed instruments: Quasistatic volume flow and reed opening measurements.

[Duc90] E. DUCASSE 1990, *Premier Congrès Français d'Acoustique, Lyon*, suplemento en *J. de Physique* II, **C2**, 837-840. Modélisation d'instruments de musique pour la synthèse sonore: application aux instruments à vent.

[Ele93] J-Y. ELEGOET 1993 *Vibrations des coques distordues*, Mémoire de DEA, INSA de Lyon.

[Fen94] L. FENG 1994 *Journal of sound and Vibration,* **176**(3), 1994, 399-413. Acoustic Properties of Fluid-filled elastic pipes.

[FEN96] C. FULLER, S. ELLIOTT, P.A. NELSON 1996. *Active control of vibration*, Academic Press.

[FF82] C. R. FULLER and F. J. FAHY 1982 *Journal of Sound and Vibration* **81**(4), 501-518. Characteristics of wave propagation and energy distributions in cylindrical elastic shells filled with fluid.

[FH00] B. Fabre, A. Hirschberg 2000 Physical modelling of flute instruments : a review of lumped models, Acustica, 86(4), p.599-610.

[Fil94] P.J.T. FILIPPI 1994 *Acoustique générale*, SFA, Collection d'Acoustique, Les Editions de Physique.

[Fir78] I. M. FIRTH 1978 *Acustica* **39**, 252-263. The action of the cello at Wolf tone.

[Flu60] W. FLUGGE 1960 Stresses in shells, Springer-Verlag.

[Flu73] W.FLÜGGE 1973 *Stresses in shells*, 2ª Ed., Springer Verlag, Berlin, Heidelberg, New York.

[For64] K. FORSBERG 1964 A. I. A. A., **2**(12), 2150-2157, Influence of Boundary Conditions on the modal characteristics of thin cylindrical shells

[Fre81] J. J. FREDBERG 1981 *Annals of Biomedical Engineering* **9**, 463-473. Acoustic determinants of respiratory system properties.

[Ful83] C.R. FULLER 1983 *Journal of Sound and Vibration* **87**(3), 409-427. The input mobility of an infinite circular cylindrical elastic shell filled with fluid.

[Ful84] C. R. FULLER 1984 *Journal of sound and vibration* **96**(1), 101-110. Monopole excitation of vibrations in an infinite cylindrical elastic shell filled with fluid.

[FWG80] J.J. FREDBERG, M. E. B. WOHL, G. M. GLASS, H. I. DORKIN 1980 *Journal of Applied Physiology* **48**, 749-758. Airway Area by Acoustic Reflections measured at the mouth.

[Gau97] F. GAUTIER 1997 *Contribution à l'étude du comportement vibroacoustique des instruments de musique à vent*, Thèse Doctorale, Université du Maine, Le Mans, France.

[GB81] R.W. GUELKE, A.E. BUNN 1981 *Acustica* **48**, 101-106. Transmission line theory applied to sound wave propagation in tubes with compliant walls.

[GBP97] V. GIBIAT, M. BOUCHE-PILLON, S. PERROT, T. VANDENBOGAERDE, J. ROUMAIRE 1997 *Proceedings of the Fourth Congress on Acoustics*, *Marseille*, 585-588. Influence des résonances mécaniques sur l'émission acoustique d'un instrument à vent simplifié.

[GGA95] B. GAZENGEL, J. GILBERT and N. AMIR 1995 *Acustica* **3**, 445-472. Time domain simulation of single reed wind instrument. From the measured input impedance to the synthesis signal. Where are the tramps?

[GL94] J.L. GUYADER, B. LAULAGNET 1994 *Applied Acoustics* **43**, 247-269, Structural Acoustic radiation prediction: expanding the vibratory response on a functional basis.

[GR92] M. GÉRADIN, D. RIXEN 1992 *Théorie des vibrations. Application à la dynamique des structures*. Ed. Masson.

[GT96] F. GAUTIER, N. TAHANI 1996 *Internoise Congress Proceedings*, Existence of two longitudinal guided waves in a fluid-filled cylindrical duct with vibrating walls.

[GT98a] F. GAUTIER, TAHANI 1998 *Journal of Sound and Vibration* **213**, 107-125. Vibroacoustic behavior of a simplified musical wind instrument.

[GT98b] F. GAUTIER, TAHANI 1998 *Journal of Sound and Vibration* **215**(5)**,** 1165-1179. Vibroacoustics of cylindrical pipes: internal radiation modal coupling.

[HKW95] A. HIRSCHBERG., J. KERGOMARD, AND G. WEINREICH 1995 *Mechanics of musical instruments: Courses and lectures* 355, CISM

(International Center of Mechanical Sciences), Udine, Italy, Springer-Verlag, Wien-New York.

[HL02] C. M. HURTGEN, D. T. LAWSON 2002 *Journal of the Acoustical Society of America* **112**, 2292. Body vibrational spectra of metal flute models.

[IYK84] T. IRIE, G. YAMADA, Y. KOBAYASHI 1984 *Journal of Sound and Vibration* **96**(1), 133-142. Free vibrations of non-circular cylindrical shells with longitudinal interior partitions.

[JF86] M. JUNGER, D. FEIT 1986 *Sound structures and their interactions* (MIT Cambridge, MA), 2ª ed., p. 166-173, p.289-294.

[JF93] M.C. JUNGER, D. FEIT 1993 *Sound structure and their interaction*, The Acoustical Society of America and the American Institute of Physics.

[Kee92] D. H. KEEFE 1992 *Computer music journal* **6**, 57-73 Physical modelling of wind instruments.

[KK90] T. KAMAKURA, Y. KUMAMOTO 1990 *Frontiers of non linear acoustics: Proceedings of the 12th ISNA,* 333-338. Waveform distortions of finite amplitude acoustic wave in an elastic tube, ed. M. F. Hamilton y D. T. Blackstock, Elsevier Science Publishers Ltd, London

[KMW94] J. KRIMPHOFF, S. MCADAMS; S. WINSBERG 1994 *Journal de Physique* **IV** (C5), 625–628. Characterization of the timber of complex sounds. Acoustic analysis and psychophysical quantification.

[Kob00] M. KOB 2000 *Acta Acustica* **86**, 642-648. Influence of wall vibrations on the transient sound of a flue organ pipe.

[Kum72] R. KUMAR 1972 *Acustica* **27,** 317-329. Dispersion of axially symmetric waves in empty and fluid-filled cylindrical shell.

[KY41] KNAUSS, YEAGER 1941 *Journal of the Acoustical Society of America*, Vol. **13**. Vibration of the walls of a cornet.

[Lam98] H. LAMB 1898 *Memoirs and proceedings. Manchester literary and philosophical society*, vol. **42** n°9, 1-16. On the velocity of sound in a tube, as affected by the elasticity of the walls.

[Lau93] B. LAULAGNET 1993, *Proceedings of the Institute of Acoustics*, Vol. **15** part. 3, 731-738. Rayonnement acoustique extérieur des coques infinies présentant des petits défauts de circularité.

[Lau95] B. LAULAGNET 1995 *Euro-noise 95 proceedings,* 363-373. Modal method in sound radiation problems: academic and more complicated cases.

[Lei73] A. LEISSA 1973 *Vibrations of shells*. The Acoustical Society of America.

[Les88] C. LESUEUR 1988 *Rayonnement acoustique des structures*, Editions Eyrolles.

[LG89] B. LAULAGNET, J. L. GUYADER 1989 *Journal of Sound and Vibration* **131**(3), 397-415. Modal analysis of a shell's acoustic radiation in light and heavy fluids.

[Lig01] J. LIGHTHILL 2001 *Waves in fluids*, Cambridge University Press.

[LWR97] T. LOYAU, P. WEINACHTER, E. REBILLARD, J. L. GUYADER, 1997 *Journal of Sound and Vibration* **203**(5), 894-898. Experimental study of vibration response dispersion between structures.

[Mar88] V. MARTIN 1988 *C. R. Acad. Sci. Paris*, **306**(2), 1-4. Couplage fluide/structure : dispersion des ondes fluides guidées.

[Mar91] V. MARTIN 1991 *Journal of Sound and Vibration*, **144**(2), 331-353. Perturbation of fluid-guided waves induced by bending plates.

[Max95] L. MAXIT 1995 *Etude du rayonnement et de la transparence des coques distordues. Décomposition en série de Fourier selon théta de l'opérateur* Mémoire de DEA, INSA de Lyon.

[MI86] P. M. MORSE, K. U. INGARD 1986 *Theoretical acoustics*, Princeton University Press, Princeton.

[Mil09] D. C. MILLER 1909 *Science* Vol. **XXIX**, Nº 735. The influence of the material of wind instruments on the tone quality.

[Mou03] M.-H.MOULET 2003 *Caractérisation des jonctions en mécanique vibratoire*, Thèse de l'Université du Maine.

[MPT79] V.N. MERKULOV, V.Y.PRIKHOD'KO, V.V. TYUTEKIN 1979 *Sov. Phys. Acoust.* **25**(1), Normal modes in a thin cylindrical elastic shell filled with fluid and driven by forces specified in its surfaces.

[MWD95] S. McADAMS, S. WINSBERG, S. DONNADIEU, G. DE SOETE and J. KRIMPHOFF 1995 *Psychological Research*, **58**, 177-92. Perceptual scaling of synthesized musical timbres: common dimensions, specificities, and latent subject classes.

[ND04] C. N. NEDERVEEN, J. P. DALMONT 2004 Journal of Sound and Vibration **271**, 227-239. Pitch and level changes in organ pipes due to wall resonances.

[ND99] C. N. NEDERVEEN, J. P. DALMONT 1999 *Acta Acustica* Poster at FORUM ACUSTICUM. Abstract en *Acustica* **85**, Suppl. 1, S76. Experimental investigations of wall influences on woodwind instrument sound.

[OLG94] N. OUELAA, B. LAULAGNET, J. L. GUYADER 1994 *Acta Acustica* **2**, 275-289. Étude vibro-acoustique d'une coque cylindrique finie remplie de fluide en mouvement uniforme.

[PAK96] V. PAGNEUX, N. AMIR, J. KERGOMARD 1996 *Journal of Acoustical Society of America* **100**(4) 2034-2048. A study of wave propagation in varying cross-section waveguides by modal decomposition. Part I. Theory and validation.

[Par47] S. E. PARKER 1947 *Journal of the Acoustical Society of America* **19** (3), 415-419. Analyses of the tones of wooden and metal clarinets.

[PCG91] J. PUAUD, R. CAUSSE, V. GIBIAT 1991 *Journal d'Acoustique* **4**, 253-259. Quasi-périodicité et bifurcations dans la note de loup.

[Pes63] E.C. PESTEL, F. A. LECKIE 1963 *Matrix methods in elastomechanics*, McGraw Hill, New York

[PGG04] R. PICÓ VILA, J. GILBERT, F. GAUTIER. *Proceedings of the 7th CFA/DAGA*, Strasbourg, France, 22-25 March 2004. Study of the input acoustic impedance of a vibrating cylindrical shell: consequences on clarinet-like instrument.

[PGR04] R. PICO VILA, F. GAUTIER, J. REDONDO 2004 pendiente de publicación en *Journal of Sound and Vibration*. Acoustic input impedance of a vibrating cylindrical tube.

[RK78] S.I. RUBINOW, J. B. KELLER 1978 *Journal of Fluid Mechanics* Vol **8**, part 1, p. 181-203, Wave propagation in a viscoelastic tube containing a viscous fluid.

[Sch81] R. T. SCHUMACHER 1981 *Acustica* **48**(2),73-84. Ab initio calculations of the oscillations of a clarinet.

[SM82] K. SHIRAKAWA, M. MORITA 1982, *Journal of Sound and Vibration* **84**(1), 121-131, Vibration and buckling of cylinders with elliptical cross section.

[Smi86] R. SMITH 1986 *Proceedings of the Institute of Acoustics* **8**(1), p.91-96. The effect of material in brass instruments ; a review.

[Soe93] W. SOEDEL 1993 *Vibrations of shells and plates*, Hardcover, 2nd edition.

[Son74] M.M. SONDHI 1974 *Journal of the Acoustical Society of America*, **55**(5), 1070-1075. Model for wave propagation in a lossy vocal tract.

[Trd95] K. TRDAK 1995 *Intensités vibratoire et acoustique dans les tuyaux*, Thèse Doctoral, Université de Technologie de Compiègne, France.

[WN95] Z. WANG, A.N. NORRIS, 1995 *Journal of Sound and Vibration* 181(3), p.457-484. Waves in cylindrical shells with circumferential submembers: a matrix approach.

[YF77] S. N. YOUSRI, F. J. FAHY 1977 *Journal of Sound and Vibration* **52**(3), 441-452. Distorted cylindrical shell response to internal acoustic excitation below the cut-off frequency.

[YIT84] G. YAMADA, T. IRIE, Y. TAGWA 1984 *Journal of Sound and Vibration*, **95**(1),117-126. Free vibration of non-circular cylindrical shells with variable circumferential profile

[Zor73] W.E. ZORUMSKY 1973 *Journal of Acoustical Society of America* **154**(6), 1667-1673. Generalized radiation impedance and reflection coefficients of circular and annular ducts.

Resumen

El trabajo de tesis trata sobre el estudio de los fenómenos de vibraciones de paredes de los tubos, en el marco de las aplicaciones a los instrumentos de viento de lengüeta simple. Se propone un modelo vibroacústico con el objetivo de explicar el acoplamiento entre las paredes del cuerpo del instrumento y el fluido interno contenido en la columna de aire del tubo sonoro. En este modelo, el cuerpo del instrumento se simplifica mediante un cilindro simplemente apoyado. Las condiciones límite acústicas impuestas son una velocidad a la entrada del instrumento y presión nula en la otra extremidad. El campo de presión se describe por medio de un desarrollo multimodal y el campo vibratorio se rige por la ecuación de movimiento de la estructura. Este método ofrece una expresión analítica de la impedancia de entrada acústica del tubo, que tiene en cuenta los acoplamientos vibroacústicos por la presencia de un factor de corrección adimensional. Para un tubo perfectamente cilíndrico, la impedancia acústica sólo se ve alterada para los modos de estructura que tienen la misma simetría que el modo plano. Cuando consideramos los materiales habituales en la construcción de instrumentos de viento, el efecto de vibración de pared puede ser ignorado. Sin embargo, para las estructuras ligeramente deformadas, el modelo vibroacústico predice que aparecen acoplamientos adicionales asociados a modos de estructura y acústicos de órdenes circunferenciales diferentes. Se utilizan simulaciones en el dominio temporal para obtener una solución numérica del campo de presión interna de un instrumento con paredes vibrantes. Se analiza el comportamiento acústico de instrumentos vibrantes construidos con diferentes materiales. Se obtienen cambios de régimen de oscilaciones, cambios de timbre y de tiempo de ataque para condiciones muy particulares de la geometría de la estructura deformada y los parámetros físicos del material. Finalmente, se ha analizado las medidas obtenidas con un tubo de caucho y se han comparado con los resultados obtenidos por un modelo simplificado de propagación de ondas acústicas en tubo membranoso.

Palabras clave: acústica musical, instrumentos de viento, vibroacústica, efecto de vibración de las paredes

---

Résumé

Le travail de thèse concerne l'étude des phénomènes de vibrations de parois des tuyaux dans le cadre des applications aux instruments à vent à anche simple. Un modèle vibroacoustique est proposé dans le but d'expliquer le couplage entre les parois du corps de l'instrument et la colonne d'air interne au tuyau sonore. Dans ce modèle, la géométrie de l'instrument est simplifiée et est constituée d'un cylindre simplement appuyé. Les conditions limites acoustiques imposées sont une vitesse à l'entrée de l'instrument et une pression nulle à l'autre extrémité. Le champ de pression est décrit à l'aide d'un développement multimodal et le champ vibratoire est développé sur les modes *in vacuo* de la coque. La mise en œuvre de la méthode intégro-modale fournit une expression analytique de la matrice impédance d'entrée acoustique du tuyau et plus particulièrement de l'impédance du mode plan. Ces expressions tiennent compte des couplages vibroacoustiques par la présence d'un facteur de correction adimensionnel. Pour un tuyau parfaitement cylindrique, l'impédance acoustique est seulement altérée par les modes de coque ayant la même symétrie que le mode plan, et lorsque l'on considère les matériaux usuels de construction d'instruments à vent, l'effet de vibration

de paroi est négligeable. Pourtant, pour des coques faiblement distordues, le modèle vibroacoustique prédit que des couplages additionnels apparaissent associées à des modes de coque et acoustiques d'ordres circonférentiels différents. Des simulations dans le domaine temporel sont employées dans le but d'obtenir une solution numérique du champ de pression interne d'un instrument à parois vibrantes en situation de jeu. Le comportement acoustique d'instruments vibrants construits avec différents matériaux est analysé. Des changements de régime d'auto-oscillations, des changements de timbre et du temps d'attaque sont obtenus pour des conditions très particulières de la géométrie de la coque distordue et les paramètres physiques du matériau. Finalement, des mesures avec un tuyau en caoutchouc sont analysées et comparés aux résultats fournis par un modèle simplifié de propagation d'ondes acoustique en tube membranaire.
Mots clés : acoustique musicale, instruments à vent, vibroacoustique, effet de vibration de paroi

---

Summary:

The body of the thesis deals with the study of the phenomena of wall vibration /in tubes, within the framework of the applications to simgle-reed wind instruments. A vibroacoustic model is proposed in order to study the coupling of the walls of the body of the instrument and the internal fluid contained within the air column of the sound tube. In this model, the body of the instrument is simplified, and a simply supported cylinder is used. The acoustic limit conditions imposed are of a particular speed at the entrance of the instrument and null pressure at the other opening. The pressure field is described using a multimodal development and the vibratory field is determined by the movement equation of the structure. This method offers an analytical expression of the acoustic input impedance of the tube, which takes into account the vibroacoustic couplings resulting from the presence of an adimensional correction factor. For a perfectly cylindrical tube, the acoustic impedance is only altered for the structure modes that have the same symmetry as the plane mode. When the materials usually employed in the construction of wind instruments are considered, the wall vibration effect can be neglected. However, for slightly distorted structures, the vibroacoustic model predicts that there are additional couplings related to the structure and acoustic modes of different circumferential orders. Simulations in the time domain are used to obtain a numerical solution for the inner pressure field of an instrument with vibrating walls. The acoustic behaviour of vibrating instruments made of different materials is analysed. Here, changes in the oscillation regime, changes in timbre and attack time for very particular conditions in the geometry of the distorted structure are obtained together with the physical parameters of the material. Finally, the measurements acquired for a rubber tube have been analysed and compared with the results obtained when using a simplified model of acoustic wave propagation in a membranous tube.
Keywords: musical acoustics, reed woodwinds, vibroacoustics, wall vibration effect.